Mechanistic insights into the role of molecular and small chemical chaperones in the prion-like transmission via yeast prion amyloids

Sayanta Mahapatra

A thesis submitted for the partial fulfillment of the degree of

Doctor of Philosophy

Department of Biological Sciences

Indian Institute of Science Education and Research Mohali

Knowledge City, Sector 81, SAS Nagar, Manauli PO, Mohali

140306, Punjab, India

May 2023

Dedicated to my coworkers

Not all battles are fought for victory.
Some are fought simply to tell the world
that there was someone on the battlefield.

-Ravish Kumar

Declaration

The work presented in this thesis has been carried out by me under the guidance of Prof. Samrat Mukhopadhyay at the Indian Institute of Science Education and Research Mohali. This work has not been submitted in part or in full for a degree, a diploma, or a fellowship to any other university or institute. Wherever contributions of others are involved, every effort is made to indicate this clearly, with due acknowledgment of collaborative research and discussions. This thesis is a bona fide record of original work done by me and all sources listed within have been detailed in the bibliography.

Sayanta Mahapatra

Date:

Place:

In my capacity as the supervisor of the candidate's thesis work, I certify that the above statements by the candidate are true to the best of my knowledge.

Prof. Samrat Mukhopadhyay

Date:

Place:

Acknowledgments

This Ph.D. thesis was only possible with the support and contributions of several people. I want to thank every person directly and indirectly involved in this challenging yet beautiful journey.

I am immensely grateful to my Ph.D. advisor, Prof. Samrat Mukhopadhyay, for allowing me to be a part of this wonderful research group and work with him on fascinating research projects. I sincerely appreciate the enormous time and effort he invested in me, which enabled me to improve my presentation skills and develop scientific reasoning. I cannot thank him enough for allowing me to pursue the scientific questions that intrigued me during my Ph.D. I am incredibly thankful to him for the financial support he provided from project grants after the completion of my fellowship tenure.

I want to thank my thesis committee members, Prof. Anand Bachhawat and Dr. Shravan Kumar Mishra, for their insightful comments and yearly evaluation of my progress.

I express my sincere gratitude to my in-house collaborators, who made my journey easier by being my companion during the turbulent phases. I owe special thanks to Ashish, Anuja, Anamika, Anusha, Neha Punia, Priyanka Madhu, and Hema for their contributions to my thesis work. I would also like to thank Dr. Deepak Sharma and his lab members, Dr. Priyanka Singh and Dr. Abhishek Sharma, for their help in performing a critical assay in their lab at CSIR-IMTECH, Chandigarh, India.

I gratefully acknowledge the research culture created in the lab by the former members of Mukhopadhyay Lab. I appreciate the help of Dr. Neha Jain, Dr. Vijit Dalal, Dr. Dominic Narang, Dr. Shruti Arya, Dr. Karishma Bhasne, Dr. Hema Swasthi, Dr. Priyanka Dogra, Dr. Sourav Singha Roy, Dr. Priyanka Madhu, Dr. Aishwarya Agarwal, Dr. Debapriya Das, Dr. Swapnil Singh, Dr. Anupa Majumdar in different phases of my scientific voyage. I would like to thank Swastik P G for being one of the biggest supporters of my work.

I would especially like to thank Dr. Dominic Narang for creating the wild-type and several mutant Sup35 constructs and standardizing their purification, which hugely benefitted me. I sincerely thank Dr. Hema Swasthi, who mentored me in my initial years and introduced me to the beautiful world of protein aggregation and chaperones. I thoroughly enjoyed working with her, and her constructive criticism shaped my scientific mind. I thank both Hema and Dominic

for acknowledging my contribution as a coworker by providing co-authorship in scientific publications.

I want to acknowledge Dr. Debapriya Das for being a true well-wisher of mine. She extended her help in not only performing experiments and preparing manuscripts but also exploring various restaurants and cuisines in Chandigarh tri-city. I will cherish the memories we created together for my entire life. I am thankful to Dr. Aishwarya Agarwal and Dr. Priyanka Madhu for being friendly seniors and for always being there whenever I seek their suggestions on various aspects of research and beyond.

I gratefully acknowledge the research facilities at IISER Mohali that helped me immensely. I am grateful to DST-INSPIRE for providing me with fellowship during my research. I would like to thank Vidya bhaiya for taking care of the lab's cleanliness and making sure we performed our experiments without any problems. I am grateful to Taseen, who, as a technician, helped me to capture fluorescent images. I would also like to thank the workers in the hostels, academic blocks, administrative buildings, and library staff for making this journey better. I want to thank all the canteen and mess staff and all the people who ensured the adequate supply of glucose in my body to carry out prolonged experiments.

I feel blessed to be surrounded by some energetic souls in the lab whom I admire for their enthusiasm to help me out in difficult situations during the difficult days of RRR (**R**evision, **R**ejection, and **R**esubmission). I cannot thank enough the current lab mates Ashish, Sandeep, Anamika, Lisha, Anuja, Anusha, Roopali, Snehasis, Dr. Dipankar Bhowmik, Harshita, and Jyoti Swami from the bottom of my heart for a joyful environment in the lab that provided the perfect breeding ground for new ideas. Without them, this journey would have been even more difficult, especially during the pandemic days. I want to acknowledge Roopali and Sandeep for critically reading my thesis.

I want to convey my sincere gratitude to Dr. Karishma Bhasne, Dr. Aishwarya Agarwal, Ashish, and Roopali for taking care of the orders and purchases for the lab to ensure an adequate supply of resources required for my research.

I am thankful to Dhruva and Jyoti for their brief involvement with me in performing experiments.

I have no words to thank Anusha for being the perfect "Mr. Watson" for me in solving some scientific mysteries. She was the only person whom I mentored for more than 4 years during

my Ph.D., and I have no hesitation in acknowledging the fact that very few people are blessed to have such a coworker. I applied all my mentoring skills to her, which caused scattered incidents of disagreements, but that never hampered our work. She always provided support in surpassing the prolonged stressful periods during my Ph.D. Additionally, I would always be grateful to her for laughing at my poorest jokes and being my partner in restaurant hopping. I was fortunate enough to work with Neha Punia as her grand mentor. Neha's contribution to this thesis is disproportionate to her tenure of 1 year as an MS project student. I would like to appreciate her logical thinking and critical input in designing experiments and thoughtful suggestions during manuscript preparation.

I feel myself lucky to have my family and friends always there for me. My parents always encouraged me to travel the path according to my choice. They always kept me away from the day-to-day things so that I could concentrate on my work. I acknowledge my school friends Apu, Sayan, Ritankar, Subham, Samujjwal, Molay, Abhrajit, and Archisman for being my biggest cheerleaders. Chatting with them on various topics constantly refreshed my mind after harsh professional commitments. I am thankful to Rajshekhar, Mansi, Madhusudan, and Harsha at IISER, Mohali, for being my friends outside the lab.

Last but not least, I am indebted to the holy soil of Punjab that hosted me for several years and made these years memorable with its incredible culture, food, and music.

Sayanta Mahapatra

Mechanistic insights into the role of molecular and small chemical chaperones in the prion-like transmission via yeast prion amyloids

Name: Sayanta Mahapatra

Supervisor's name: Prof. Samrat Mukhopadhyay

Chapter 1. Introduction

Protein misfolding generates β-rich ordered aggregates known as amyloids, classically linked with neurodegenerative diseases. However, recent reports suggest the functional roles of amyloids. Prions are the sub-class of amyloids demonstrating self-perpetuating behavior for their distal invasion. The prion-like self-perpetuating conformational conversion is now extended to a variety of non-prion neurodegenerative and functional amyloids. The transmissibility of amyloids depends on several factors that regulate their number and seeding potential during autocatalytic amplification cycles. The amyloids generated from the prion determinant of *Saccharomyces cerevisiae* Sup35 (NM domain) is a reliable model to investigate the role of such critical molecular regulators via *in vitro* recapitulation. The disaggregase chaperone Hsp104 is an important regulator controlling prion propagation according to its concentration. Apart from the molecular chaperones, the biologically relevant polyanions such as glycosaminoglycans, RNA, and ATP also show their ability to control both amyloid formation and the disaggregation of existing aggregates. Therefore, these small molecules have recently emerged as the chemical chaperone to influence prion-like transmission. In this thesis, we study the sub-stoichiometric Hsp104, reminiscent of chaperone under-expression during aging. It accelerates the formation of prefibrillar species but also prolongs their persistence by introducing unusual kinetic halts and delaying their conversion into less transmissible matured fibrils. Biochemical studies and site-specific dynamic readouts reveal that Hsp104-created amyloids possess an altered, more ordered packing than the NM-only amyloids and also display an enhanced seeding ability that may promote prion-like amyloid propagation. On the other hand, our aggregation kinetics reveal that physiologically high concentrations of ATP molecules accelerate NM aggregation. Nevertheless, ATP also dose-independently disaggregates existing NM fibrils. However, the stable, compact, ATP-bound amyloids polymerized in the presence of high concentrations of ATP show nominal fragmentation by additional ATP or by Hsp104, which may restrict the prion-like transmission by limiting the number of seeds. Also, circular dichroism and Raman spectroscopic data

that trace amounts of ATP give rise to seeding-inefficient amyloids for their reduced β-sheet content, showing another anti-prion attribute of ATP. We also carry out seeding with the amyloids generated from seeded aggregation reactions of NM.In subsequent seeding cycles, we observe a variation in the seeding efficiency of the amyloids generated in seeded aggregations with different seed sizes.

Chapter 2. Sub-stoichiometric Hsp104 kinetically modulates the aggregation of a yeast prion determinant to regulate the genesis and persistence of sub-fibrillar seeds

Self-templated conformational conversion into amyloids is key for autocatalytic amyloid transmission in debilitating neurodegenerative diseases and the non-Mendelian inheritance of benign yeast prions. Molecular chaperones such as the disaggregase Hsp104 play an important role in the propagation of the prion phenotype [*PSI*$^{+}$], generated due to the aggregation of yeast

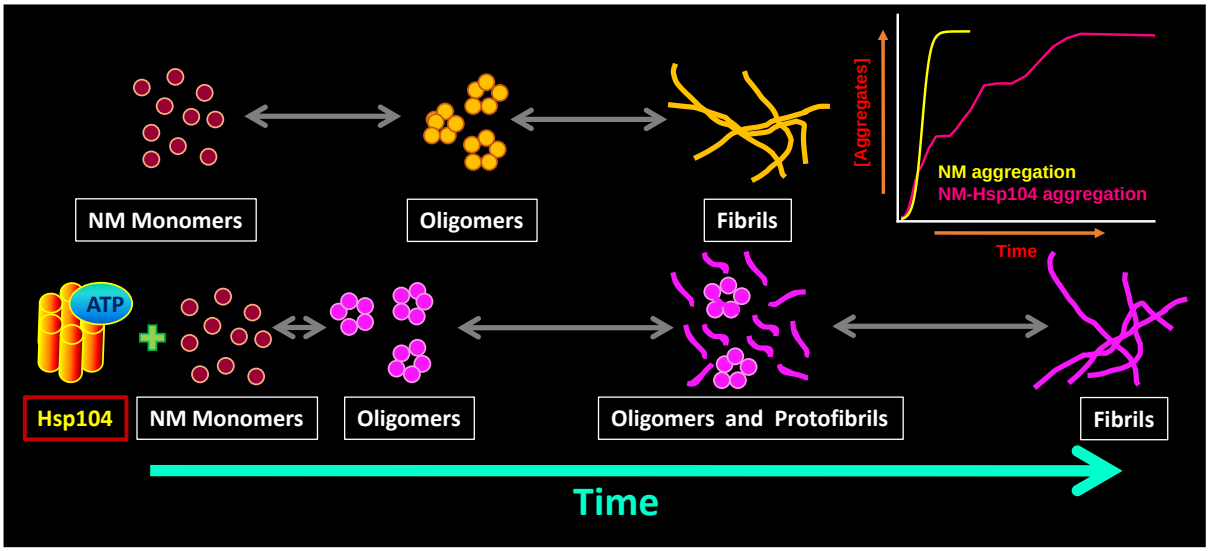

translational termination factor Sup35, in the subsequent generations by maintaining the adequate number of seeds. However, the underlying molecular connection behind the amount of seeds and the dose of Hsp104 remains elusive to us. In this *in vitro* recapitulation study, using the recombinantly purified prion determinant of *S. cerevisiae* Sup35 (NM domain) and Hsp104, we demonstrate that sub-stoichiometric concentrations of Hsp104 with ATP accelerate the amyloid formation of NM. It also delays the maturation of these amyloids by creating unusual kinetic halts resulting from a tug-of-war between the intrinsic aggregation propensity of the lower-order amyloids and the disaggregase activity of Hsp104. These unique kinetic features, which are sensitive to the absence of ATP or the presence of Hsp104-inhibitor GdmCl, not only promote the generation of amyloids but also increase their persistence before converting into fibrils. Thus, Hsp104, in sub-stoichiometric amounts, increases the abundance of ample, highly

transmissible prefibrillar aggregates as seeds over fewer matured fibrils that process limited seeding due to the fewer growth-competent ends. Taken together, our results demonstrate the pro-propagation activity of low concentrations of disaggregase chaperone Hsp104 via creating and maintaining efficient seeds that may unmask the link between the chaperone insufficiency in aged cells and the onset of amyloid transmission.

Chapter 3. Conformation alterations in yeast prion amyloids by sub-stoichiometricHsp104 to facilitate seeded aggregations

The formation of self-propagating amyloids via a templated conformational switch from the soluble proteins plays a pivotal role in the prion-like transmission of amyloids associatedwith biological functions and pathology. The disaggregase proteins, such as Hsp104, in sub-stoichiometric concentrations, might help in the propagation of amyloid-associated [*PSI*$^{+}$] phenotype by creating adequate prefibrillar amyloids of Sup35NM as seeds by modulating the aggregation kinetics. Apart from ensuring the quantity of seeds for prion-like propagation, the seeds are also required to effectively catalyze the fresh aggregation reactions promoting amyloid formation, which is critical for the seeded amyloid amplification cascades. Thereforeto investigate the self-templating potential of sub-stoichiometric Hsp104-modulated NM aggregates, we set up seeding reactions with NM-Hsp104 amyloids, which reveal that these display a better seeding capacity compared to the typical NM-only aggregates. Using biochemical and biophysical tools coupled with site-specific dynamic readouts, we discern the distinct structural and dynamical signatures of these amyloids. Furthermore, we reveal that Hsp104-remodeled amyloidogenic species are packed in a more ordered fashion compared to NM-only amyloids. Finally, we decipher that the enhanced autocatalytic self-templating ability of Hsp104-remodeled, conformationally distinct NM aggregates might be crucial for the transmission of prions. Taken together, our results demonstrate that sub-stoichiometric Hsp104 not only promotes compositional diversity but also leads to conformational modulations during amyloid formation, yielding effective seeds that are capable of driving prion-like propagation of [*PSI*$^{+}$] phenotype Our findings underscore the critical functional and pathological roles of sub-stoichiometric chaperones in prion-like propagation.

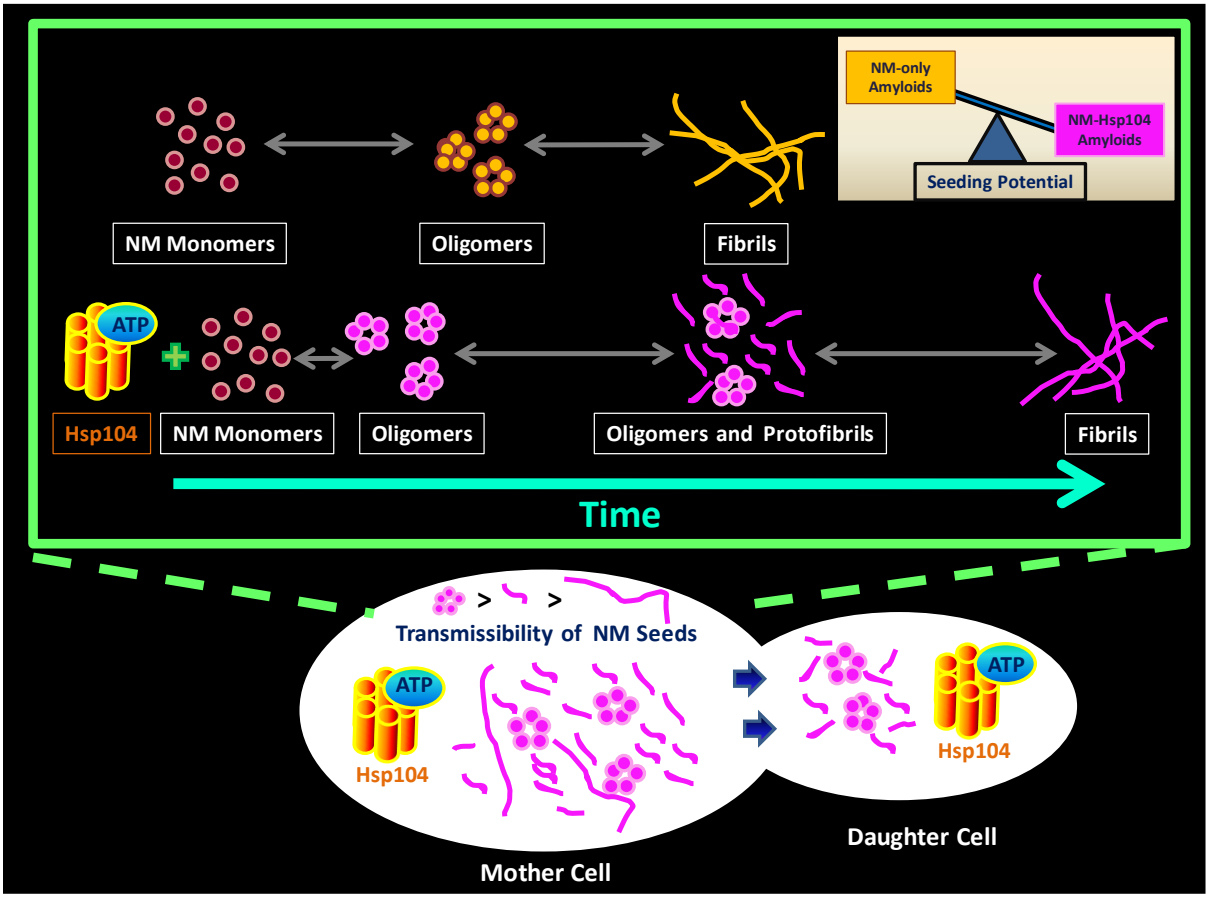

Chapter 4. ATP modulates self-perpetuating conformational conversion generating structurally distinct yeast prion amyloids that limit autocatalytic amplification

Prion-like self-perpetuating conformational conversion of proteins into amyloid aggregates is associated with both transmissible neurodegenerative diseases and non-Mendelian inheritance. The cellular energy currency ATP is known to indirectly regulate the formation, dissolution, or transmission of amyloid-like aggregates by providing energy to the molecular chaperones independent of any chaperones, modulate the formation and dissolution of amyloids from a yeast prion domain (NM domain of Saccharomyces cerevisiae Sup35) and restricts autocatalytic amplification by controlling the amount of fragmentable and seeding- competent aggregates. ATP, at (high) physiological concentrations in the presence of Mg^{2+}, kinetically accelerates NM aggregation. Interestingly, ATP also promotes phase-separation-mediated aggregation of a human protein that harbors a prion-like domain. We also show that ATP disaggregates preformed NM fibrils in a dose-independent manner. Our data indicate

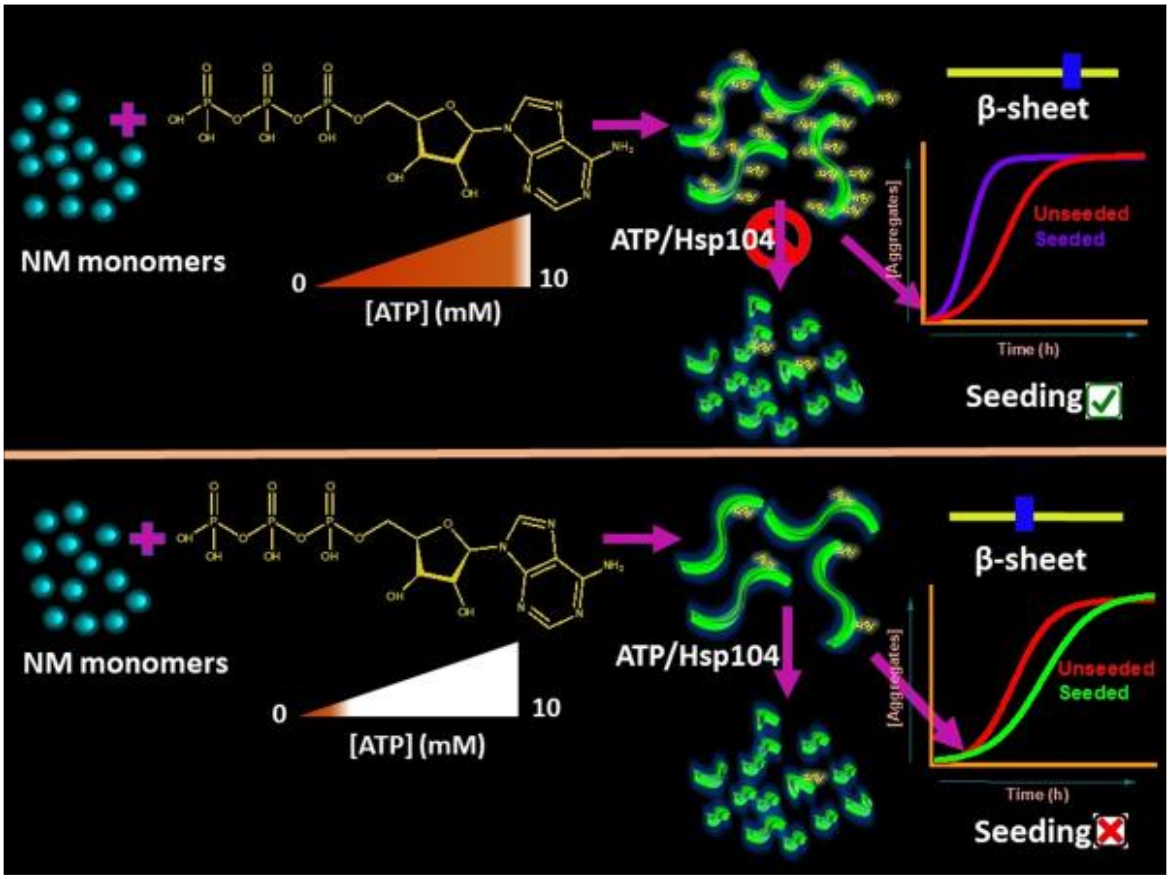

that ATP-mediated disaggregation, unlike the disaggregation by the disaggregase Hsp104, yields no oligomers that are considered one of the critical species for amyloid transmission. Furthermore, high concentrations of ATP delimit the number of seeds by giving rise to compact, ATP-bound NM fibrils that exhibit nominal fragmentation by either freeATP or Hsp104 disaggregase to generate lower molecular weight amyloids. Additionally, (low) pathologically relevant ATP concentrations restrict autocatalytic amplification by forming structurally distinct amyloids, which are found seeding-inefficient due to their reduced β-content. Our results provide key mechanistic underpinnings of concentration-dependent chemical chaperoning by ATP against prion-like transmissions of amyloids.

Chapter 5. Optimum seed size generates amyloids that ensure uninterrupted seeding cycles of yeast prion amyloids

Non-mendelian inheritance of phenotypic traits of yeast prions depends on the self-templated conformational switch to the prion form in consecutive generations. Acceleration of *de novo* aggregation by preformed amyloids or seeds is critical for prion-like propagation. However, apart from the kinetic profiling, the detailed characterization of amyloids formed from seeded

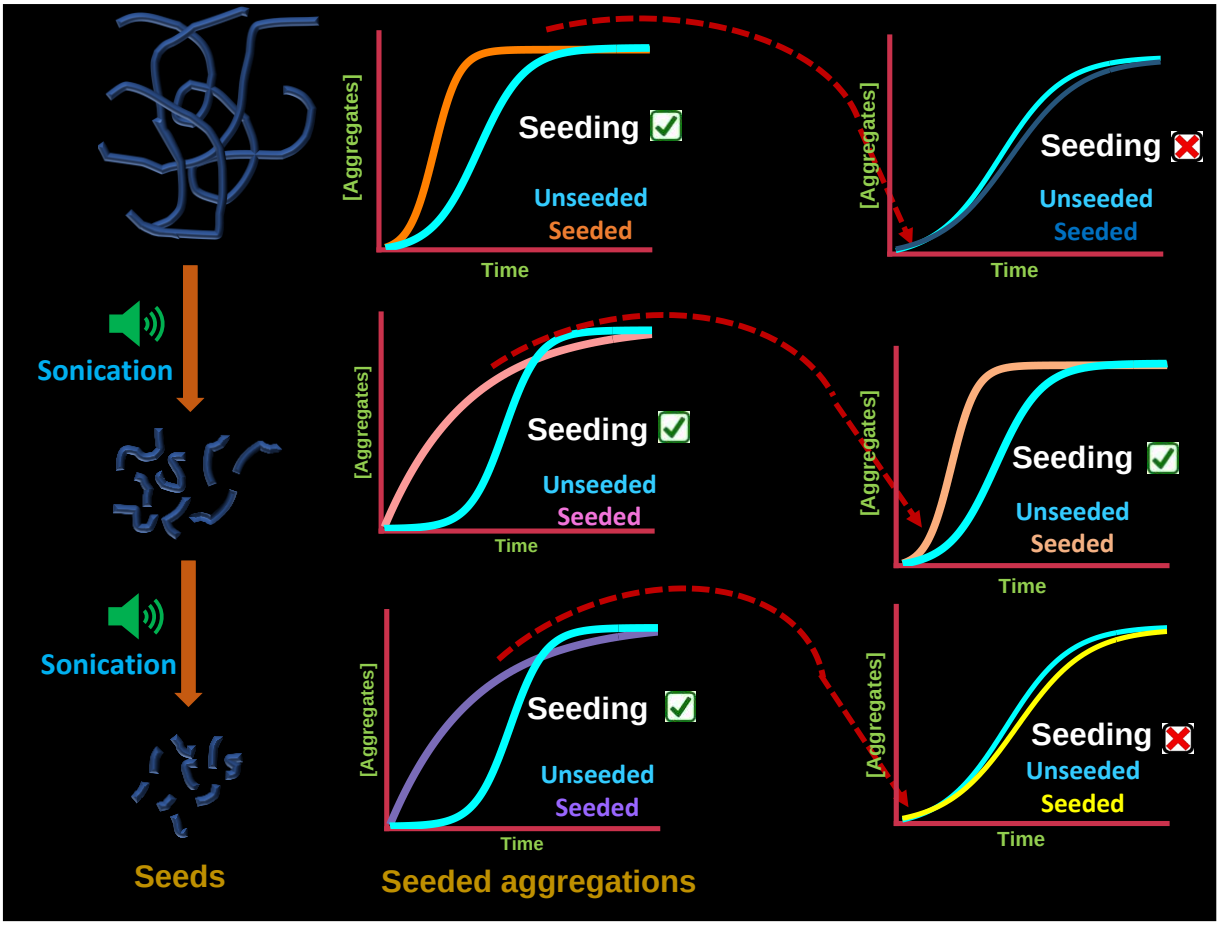

aggregations and their seeding ability in the successive self-templating cycles remains elusive. Using the yeast prion domain of *S. cerevisiae* Sup35 (NM domain), we carry out the sequential seeding with in *vitro* amyloids generated in seeded aggregation reactions with amyloids of different sizes. The subsequent seeding with the particles aliquoted from the saturated seeded aggregations unveils that only mildly sonicated fibrils give rise to theamyloid species that demonstrate further seeding ability. We speculated a seed size-dependent conformational change in the amyloids of seeded aggregations that may dictate their self-replicating ability. However, our Raman data suggests no significant conformational change in the amyloids derived from seeded aggregation reactions with respect to the de novo aggregation reactions. Interestingly, the sedimentation of saturated aggregation reactions reveals that the fraction of pelletable amyloids and soluble particles varies in the seeded aggregation reactions depending on the seeds used. This alteration in the amyloid composition, depending on the size of the seeds, may have implications in the subsequent seeding cycles. Taken together, our data suggest the requirement of optimum seed size to generate an amyloid composition in seeded aggregations, which can drive successive seeding cascades in the prion-like mechanism.

Chapter 6. Conclusions and future directions

In this thesis, we explored a number of molecular regulators of amyloid formation and the disaggregation of existing aggregates. Additionally, we unmasked the variation in the seeding ability of the amyloids generated in the seeded aggregation depending on the size of seeds used during polymerization. These factors regulate the amount and ability of seeds and either facilitate or hinder prion-like propagation of amyloids. In the future, it will be interesting to explore the role of other co-chaperones of disaggregase in the modulation of aggregation behavior, the multi-component phase separation of Sup35.

List of publications

- **Mahapatra, S.***, Sarbahi, A., Punia, N., Joshi, A., Avni, A., Walimbe, A., and Mukhopadhyay, S*. (2023) ATP molecules generate structurally-distinct amyloids to restrict seeded amplification of a yeast prion determinant. *J. Biol. Chem.* 299,104654**.*Co-corresponding authors**
- **Mahapatra, S.,** Sarbahi A., Madhu, P., Swasthi, H. M., Sharma, A., Singh, P., and Mukhopadhyay, S. (2022) Sub-stoichiometric Hsp104 regulates the genesis and persistence of self-replicable amyloid seeds of Sup35 prion domain. *J. Biol. Chem.* 298,102143.
- Swasthi, H. M., Bhasne, K., **Mahapatra, S.**, and Mukhopadhyay, S. (2018) Human Fibrinogen Inhibits Amyloid Assembly of Biofilm-Forming CsgA. *Biochemistry* 57, 6270–6273.
- Narang, D., Swasthi, H. M., **Mahapatra, S.**, and Mukhopadhyay, S. (2017) Site-Specific Fluorescence Depolarization Kinetics Distinguishes the Amyloid Folds Responsible for Distinct Yeast Prion Strains. *J. Phys. Chem. B.* 2017; 121: 8447-8453.
- **Mahapatra, S.*,** Sarbahi, A., Avni, A., Mukhopadhyay, S*. (2023) Optimum seed size generates amyloids that ensure uninterrupted seeding cycles of yeast prion amyloids. (Manuscript in preparation). ***Co-corresponding authors**

Presentations at Conferences

- **S. Mahapatra**, A. Sarbahi, N. Punia, A. Avni, S. Mukhopadhyay "Sub-stoichiometric Hsp104 and ATP molecules regulate the genesis, persistence and seeding potential of self□replicable amyloids of a yeast prion determinant" The Leuven Protein Aggregation Meeting (2022), Leuven, Belgium organized by Switch Laboratory at KU Leuven.

- **S. Mahapatra**, D. Narang, H. M. Swasthi, and S. Mukhopadhyay "Distinguishing the Amyloid Folds Responsible for Distinct Yeast Prion Strains" International Conference on Intrinsically Disordered Proteins: Forms, Functions, and Diseases (2017), Indian Institute of Science Education and Research (IISER) Mohali

Table of Contents

Introduction

1.1 Historical perspective

Amyloids are the ordered polymers of proteins connected to various neuropathological diseases and biological functions. Rudolph Virchow, one of the major contributors to the cell theory, coined the term 'amyloid' in 1854 to describe the interesting reaction of the corpora amylacea in the nerve tissues with iodine. He suggested that cerebral corpora amylacea are chemically carbohydrates in nature and form deposits during 'waxy' changes in the liver. Later, Friedreich and Kekule discovered that waxy spleen tissue contained no material that corresponded chemically to amylon (starch) or cellulose. These were the first attempts to investigate the chemical nature of amyloid deposits, which had been observed in organs since the 17th century. The proteinaceous character of amyloid entities was first reported by Astbury and Dickinson in 1935, where they observed a unique cross-β X-ray diffraction pattern of heat-denatured egg albumins. In the signature cross-β structure of amyloids, the individual strands of each β-sheet run perpendicular to the fibril axis (4.7 Å spacing), whereas the β-sheet (~10 Å spacing) are parallel to the fibril axis[1,2,3] (Figure 1.1a). The simplicity of the amyloid structures, their ability of templated replication of their own, and their role as catalysts to accelerate chemical reactions made these structures the potential primordial biomolecules of life[4,5,6]. With the recent advances in microscopic and spectroscopic tools, the detailed structural investigation of amyloids is possible to an atomic resolution that can detect the nanoscale variations in the universal cross-β structures of amyloids (Figure 1.1b). Intriguingly, structural variations are observed even in the amyloids formed from the same peptides under different polymerization conditions and in the presence of other proteins and small molecules. The structural diversity in amyloids gives rise to a spectrum of aggregated species that might exhibit different effects[7,8,9].

1.2 Amyloids in pathology and diseases

Amyloids are the ordered polymers of partially or fully unfolded, misfolded, and intrinsically disordered proteins (IDP) that are typically known for their association with fatal diseases such as Alzheimer's, Parkinson's, Huntington's, amyotrophic lateral sclerosis (ALS), frontotemporal dementia (FTD), prion diseases and so on[10,11]. The nascent polypeptide chain, right after its translation at ribosomes, explores a variety of folding intermediates in its rugged folding funnel to attain the native three-dimensional shapes. However, the IDPs in our proteome lack a global energy minima in the free energy landscape of protein folding to achieve a well-defined

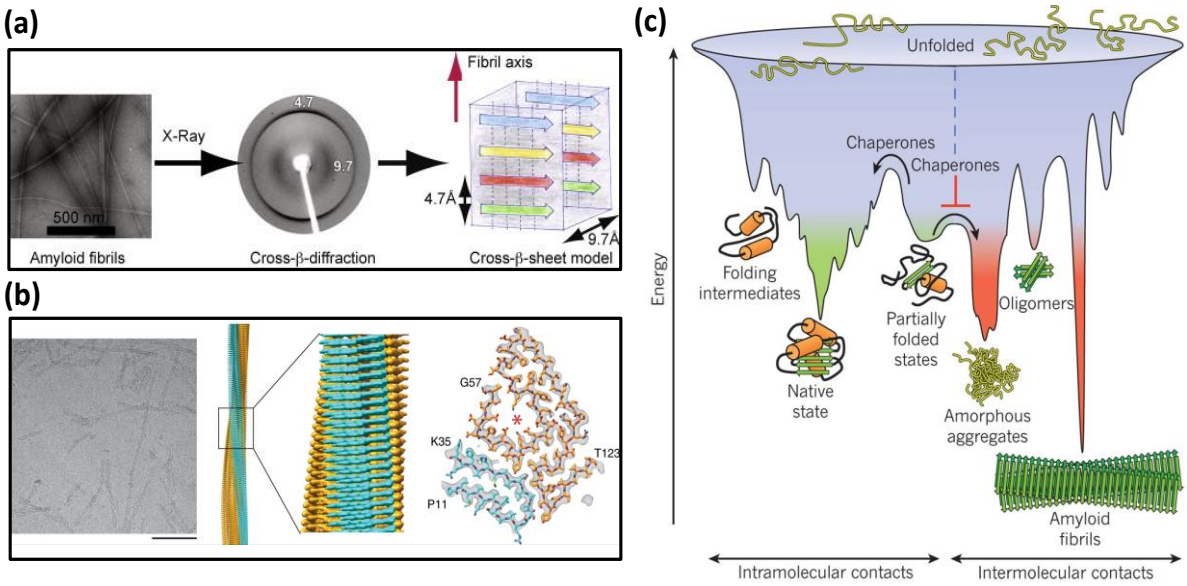

Figure 1.1 (a) Amyloid fibrils showing the fiber diffraction pattern. They show a meridional reflection at 4.7 Å and an equatorial reflection at around 8–11 Å, which suggest the presence of a cross-β-sheet structural motif as depicted in the drawing. Reproduced with permission from reference 3. (b) Cryo-EM reconstruction of the ATTR amyloid fibril. Cryo-EM image of the extracted fibrils. Scale bar = 200 nm. Side view of the reconstructed 3D map. N-terminal density: cyan; C-terminal density: orange. Cross-sectional view of the reconstructed 3D map (grey), superimposed with a molecular model of the N-terminal (cyan) and C-terminal peptide segment (orange). Terminal amino acids are indicated in the figure. The internal cavity is marked with an asterisk. Reproduced with permission from reference 9. (c) Scheme of the funnel-shaped free-energy surface that proteins explore as they move towards the native state (green) by forming intramolecular contacts.Reproduced with permission from reference 14.

shape[12,13]. The kinetically trapped folding intermediates, destabilized folded proteins, and natively unstructured IDPs with rapidly fluctuating conformations facilitate protein aggregation (Figure 1.1c). The occurrence of amyloidosis remains elusive despite having a protein quality control system involving molecular chaperones. The highly coordinated proteostasis network ensures tight regulation between protein synthesis and folding to their native shape, maintaining conformational stability, rescuing aggregated proteins, and protein degradation[14]. Aging is a pivotal factor that increases the onset of amyloid depositions, resulting in neurodegeneration. The statistics of Alzheimer's patients indicated that 52 % of the victims are over 75[15]. The age-dependent collapse in protein quality control is believed to be the reason behind amyloidogenesis[16,17]. Mutations in the amyloidogenic precursor proteins have been found to accelerate the generation of amyloids for α-synuclein, amyloid-β, or β_2-microglobulin. The expansion of the amyloidogenic sequences, similar to the case of poly-glutamine (poly-Q) repeats related to Hungtington disease, can facilitate detrimental amyloid diseases. Modifying the primary sequence of amyloidogenic proteins, such as proteolytic truncation or hyperphosphorylation, can control amyloid generation[1]. Moreover, the rate of

polymerization of amyloidogenic proteins also depends on the cellular microenvironment and the presence of metal ions, metabolites, glycosaminoglycans, or membranes during the aggregation. Additionally, the presence of another amyloidogenic protein to form hetero-amyloids via co-aggregation or regulation through chaperones plays a critical role in controlling protein aggregation[18]. The formation of liquid-liquid phase-separated droplets has recently emerged as the crucible for amyloid aggregation by increasing the local concentrations of monomeric proteins[19]. A subclass of amyloids is distinct from the others in its ability to self-propagate. These proteins are known as prions that are the self-perpetuating subclass of amyloids classically connected with some infamous neurodegenerative diseases such as Creutzfeldt-Jakob disease (CJD), kuru, and so on, which we have discussed in the subsequent section in detail.

1.3 Functional amyloids

Amyloids are traditionally known for their link with diseases; two more critical classes of amyloids gained our attention other than the pathological amyloids. Amyloids are recently being used as the next-generation nanomaterials that are *in vitro* polymerized and non-toxic in nature. These artificial amyloids are extensively used in optoelectronics, biosensing, tissue engineering using amyloid-based gels, adsorption of heavy metals from contaminated water, CO_2 absorption, and so on[20,21]. Another critical class of amyloids is called functional amyloids, which serve several biological functions inside cells. The existence of beneficial amyloids is evident in all eukaryotes, ranging from mammals to yeasts, and also in bacteria[22]. Pmel17 is one of the celebrated functional amyloids that function as a scaffold for melanin biosynthesis in mammals at melanosomal pH[23,24]. The bacterial protein curli forms amyloids that are the critical component of biofilms of bacteria such as *E. coli* and *Salmonella*. These biofilms protect the bacteria against the host immune defenses and antibiotics[25]. Amyloids formed from spidroins can increase the tensile strength of the spider web[26]. Aggregates also help in the storage of protein or peptide hormones, such as prolactin, in an inert state inside secretory granules of neuroendocrine cells[27]. The yeast pyruvate kinase Cdc19 is stored as amyloid within stress granules, and its re-solubilization ensures survival from stress[28]. A host of benign prions play biological roles in cells. Fungi harbor some of the most studied functional prions that play several biological roles in fungi. In addition, prions, especially the fungal prions and their self-perpetuating behavior, shed light on the crucial aspects of cell-to-cell amyloid transmission and serve as an excellent model for studying the spread of aggregates[29]. Therefore,

in the subsequent sections, we have focoused on the prions, the prion-like mechanism that is currently thought to be the principal mechanism of amyloid colonization, and also, on the fungal prions as a model to understand amyloid propagation.

1.4 Self-perpetuating prions in pathology and functionality

Prion diseases such as Creutzfeldt-Jakob disease (CJD), kuru, fatal familial insomnia in humans, scrapie in sheep, and mad cow disease are the sub-class of amyloid-associated neurodegenerative diseases having the unique property of self-propagation via an autocatalytic switch to the infectious conformations[30]. Stanley Pruisner discovered that, unlike viruses,

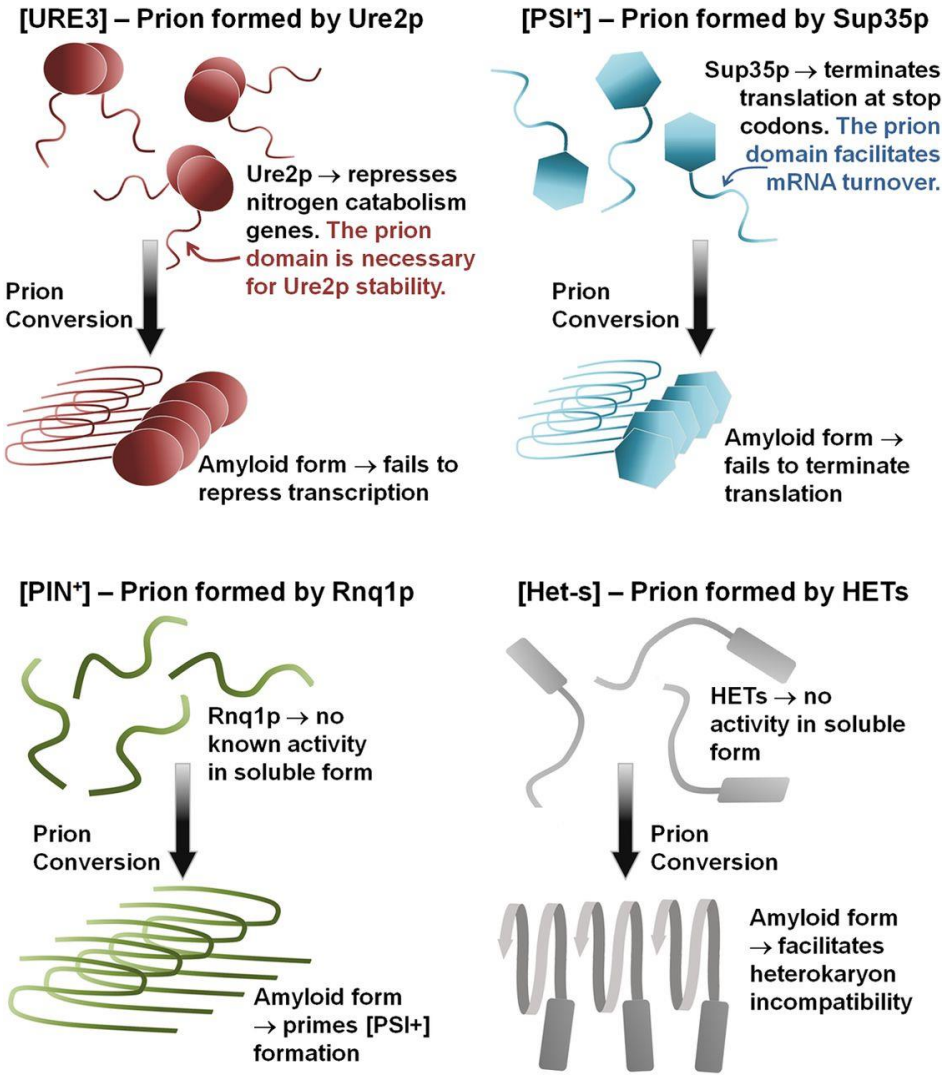

Figure 1.2 Prions [*URE3*], [*PSI*$^{+}$], and [*PIN*$^{+}$] of *S. cerevisiae* and [Het-s] of *Podospora anserina*. These prions are based on self-propagating amyloids of Ure2p, Sup35p, Rnq1p, and HET-s, respectively. Reproduced with permission from reference 41.

these infectious elements were devoid of nucleic acids. Eventually, seminal research by Prusiner and others indicated that prion diseases are caused by a self-templating amyloidogenic form of a normal cellular protein: PrP. Therefore, it is evident that the same PrP protein has two different faces, like Dr. Jekyll and Mr. Hyde. One is the monomeric, benign PrP^{c} state that serves certain biological functions, and the other is the aggregated state PrP^{sc}, which is associated with diseases[31]. PrP is a glycoprotein having an evolutionarily conserved amino acid sequence, and it is localized at the cell surface of neurons via the C-terminal, glycosyl-phosphatidylinositol (GPI) anchor. However, the exact biological function of PrP^{c} remains largely unknown, and many reports suggest its connection with various biological processes such as cell adhesion, transmembrane signaling, cellular protection against stress, copper homeostasis, stem cell renewal, memory mechanism, and so on[32,33,34]. However, its conversion to the self-templating amyloid form PrP^{sc} is responsible for the pathogenicity of transmissible prion diseases, which show widespread transmission in the same mammalian species. Intriguingly, due to the phenomenon called species-barrier, the infection due to the prion particles of one mammalian species cannot transmit to the other mammalian species[35].

Classically, prions are connected with fatal diseases. However, there is a subset of prions that, even in their aggregated state, does not have any toxic effect on the cells. Instead, the amyloid form also has certain physiological functions that are distinct from its functions in its soluble form[36]. These functional prions exhibit similar biophysical properties to the disease-associated prions, but the generation of functional prions is tightly regulated. Unlike the cytotoxic amyloids, which arise due to mutation, truncation, modification, or processing-induced uncontrolled protein misfolding or unfolding, the aggregation to the functional prion state is regulated via specific extra or intra-cellular signals for multicellular organisms[31]. For unicellular organisms, environmental stresses trigger the aggregation to the prion state as a part of the stress response. For example, the mRNA-binding prion-like protein cytoplasmic polyadenylation element-binding (CPEB) protein has been identified as the functional prion that acts as the translational regulator in its aggregated state to control memory maintenance [37,38]. Another compelling evidence of a prion-like mechanism in the mammalian brain is the protein TIA-1, whose aggregates promote the assembly of stress granules during environmental stress in the mouse hippocampus. The formation of stress granules facilitates the sequestration of RNAs to save cellular energy required to translate proteins that are not involved in stress response [39].

The most prominent prions with well-identified biological significance are the fungal prions that control the protein-based inheritance traits without the help of any DNA or RNA. Wickner discovered this group of functional prions in yeasts. A common feature in all these non-chromosomal genetic elements is the phenotypic changes that resemble the loss-of-function phenotype of that gene upon switching to the amyloid conformation of that prion. [*URE3*] prion associated with the protein Ure2p is involved in the transcription of genes associated with nitrogen catabolism whose self-propagating, aggregated form failed to repress transcription. [PSI^+] prions arise from the assembly of a translation termination factor Sup35 protein which gives rise to a distinct yeast colony color as it could not terminate translation in its aggregated state. The prion [*Het-s*] of *Pseudospora anserina* drives the heterokaryon incompatibility in the aggregated state, but the protein's function is not yet known. For the protein Rnq1 in yeast, the function in the soluble form remains uncharacterized. However, this protein act as the primer for [PSI^+] prion formation in the amyloid form (Figure 1.2)[40,41].

Understanding prion biology becomes even more critical due to the mounting reports that suggest an extension of the prion-like phenomenon in non-prion amyloids. The template-induced misfolding of the normal isoform of the protein leading to the aggregation and their spread to the broader areas were observed in the case of almost all infamous non-prion disease-causing amyloids such as Aβ, α-synuclein, tau, p53, TDP-43, Huntingtin[42,43]. Seminal studies in cultured neurons and mouse models confirm that exogenous α-synuclein aggregates could induce misfolding and aggregation of native α-synuclein, and those aggregates may propagate in a prion-like manner within the nervous system. Similarly, using a transgenic mouse model, the prion behavior of Aβ aggregates isolated from the patients of Alzheimer's were detected, where they induce aggregate formation in healthy brain tissues[44,45]. Apart from the neurodegenerative amyloids, the aggregates of tumor suppressor protein p53 linked to cancer also demonstrate prion-like behavior[46]. Furthermore, the functional amyloids from CPEB that control the long-term memories in mammals also show selective synapse-specific prion-like transmission[47]. Taken together, it is clear from our discussion that the implication of prion-like templated conformational conversion is not exclusive to a handful of proteins. Instead, the prion mechanism has much broader implications in the transmissibility of various amyloids involved in cellular pathophysiology from yeast to multicellular mammals. In the following sections, we have tried to explore the intricate mechanistic details of the prion-like mechanism in light of the cytoplasmic inheritance of Sup35 related prion phenotype [PSI^+].

1.5 [*PSI*$^+$] prion as a model for prion-like amyloid transmission

Yeasts are the simplest eukaryotes that share many critical cellular factors and pathways that govern protein folding, misfolding, and amyloid formation and transmission in higher eukaryotes. The evolutionarily conserved processes such as chaperone networks, the ubiquitin-proteasome system, autophagy, and vesicular trafficking in yeasts enable us to utilize this organism as a reliable model for the amyloid and prion biology and several cellular or environmental factors that regulate their genesis and transmission[48]. Amongst all the yeast

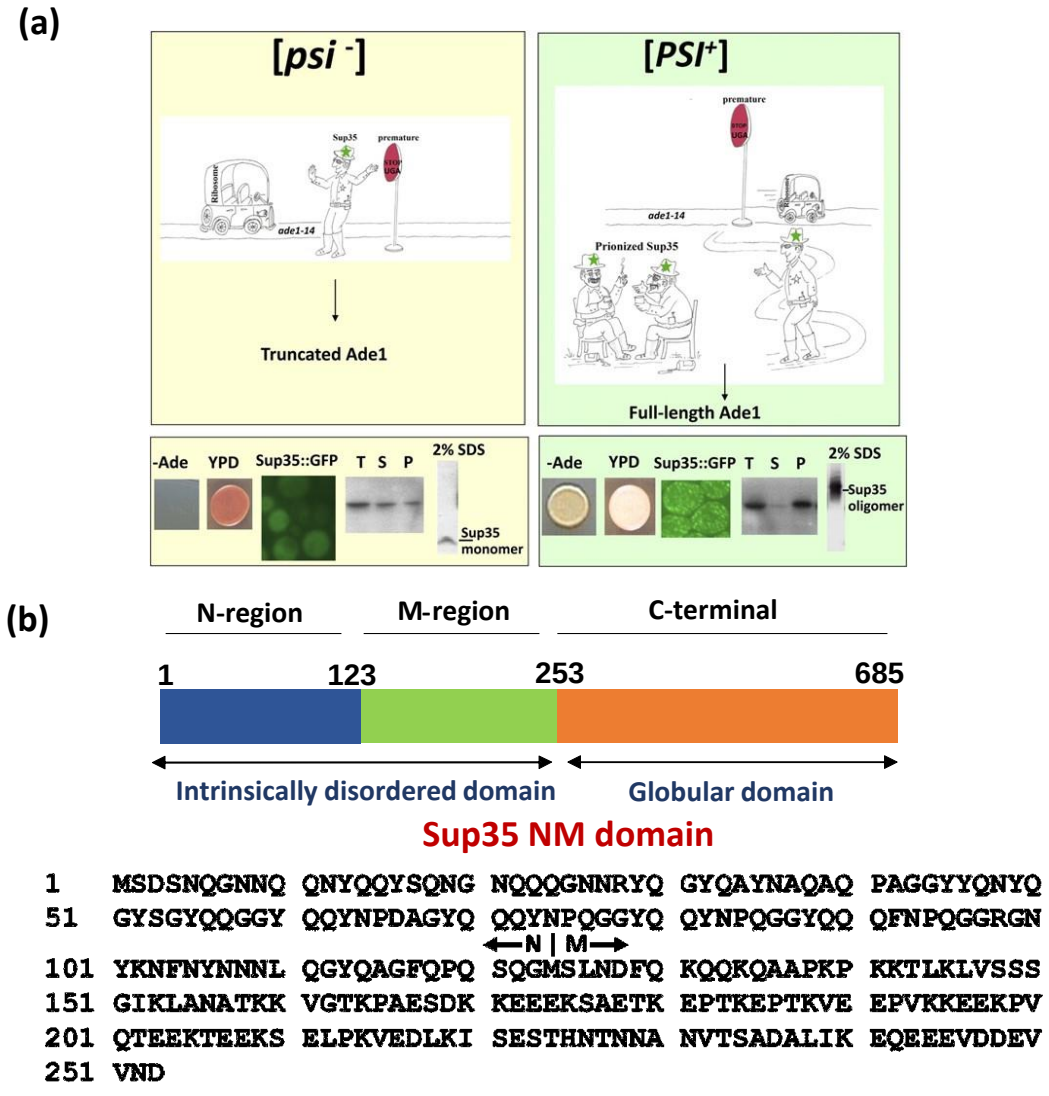

Figure 1.3 (a) [*PSI*$^+$] phenotypes. In the absence of the prion (left), the Sup35 release factor—shown as a conscientious cop—causes the ribosome to stop at the premature stop codon in the ade1-14 mutation. This leads to the release of a truncated Ade1 protein, preventing the cell from synthesizing adenine. In the presence of the [*PSI*$^+$] prion, shown as corrupted cops playing cards and drinking, the conscientious Sup35 is drawn into the party, and the ribosome can read through the stop codon, allowing cells to make some full-length Ade1. Thus, as shown below the cartoon, the [*psi*$^-$] cells cannot grow on –Ade plates and accumulate a red intermediate on complex YPD medium, while the [*PSI*$^+$] cells grow on –Ade and are white on YPD. Sup35 tagged with GFP is diffuse in [*psi*$^-$] cells but forms aggregates

(e.g., many small parties) in [*PSI*$^+$] cells. When total cell lysates (T) are separated into supernatant (S) and pellet (P) fractions and Western blots made of boiled SDS acrylamide gel separations are developed with Sup35 antibody, Sup35 is mainly found in the supernatant in [*psi*$^-$] lysates but mostly in the pellet in [*PSI*$^+$] lysates. When lysates are separated on agarose gels, following room temperature incubation with 2% SDS, Sup35 runs as a monomer in [*psi*$^-$] cells but primarily as oligomers in [*PSI*$^+$]cells. Reproduced with permission from reference 51. (b) Prion (NM) domain of Sup35 showing the putative boundary between N and M domain.

prions, the [*PSI*$^+$] prion adopted by the Sup35 protein, is one of the most suitable systems to investigate the prion phenomenon. Sup35 protein has 685 amino acids divided into three domains. For the TSEs, [*URE3*], [*PSI*$^+$], and [*Het-s*], a limited part of the corresponding protein is necessary and sufficient to transmit the prion *in vivo*. The N- and M-domain of Sup35 constitute the prion determinant that controls its switch to the prion conformation. On the other hand, the C-domain controls its GTP-binding ability and translational activity. The soluble Sup35 prematurely stops the translation by recognizing a stop codon of ade1-14 mRNA, yielding a truncated peptide. These peptides generate a red pigment upon complex biochemical conversion, which gives rise to red-colored colonies known as the [*psi*$^-$] phenotype. Moreover, these cells can not grow without adenine in the growth medium (Figure 1.3). Like other fungal prions, the conversion to the prion state [*PSI*$^+$] hinders its function as a translational terminator. This ensures the readthrough of ade1-14 mRNA, which gives rise to white-colored colonies instead of red color colonies that can grow even in the absence of adenine in the growth medium[49,50,51]. This easily observable phenotypic switch acts as the convenient marker of prion formation due to cellular or environmental factors, oxidative stress and mutants lacking antioxidants, overexpression of the protein, or receiving preformed amyloids known as seeds from its mother during budding. However, the frequency of the *de novo* appearance of prions are very low. Therefore, the formation of prion amyloids in yeasts depends mainly on the successful protein-based, non-Mendelian inheritance of self-templating seeds that can induce aggregation, leading to the [*PSI*$^+$] phenotype. Maintaining the number of sufficient self-propagating seeds is crucial for the cross-generational passage of the [*PSI*$^+$] prion phenotype that resembles the prion-like cell-to-cell transmission of detrimental aggregates. Therefore, a detailed understanding of the propagation of [*PSI*$^+$] is critical as it provides general insights into the amyloid transmission that follows typical nucleation, fragmentation-driven prion-like mechanism[52]. In the next part, we have talked about the seeds, several critical determinants of their transmissibility, and the mechanistic insights on how they regulate the propagation of prion phenotype in the light of the Sup35 protein.

1.6 The role of nucleation and fragmentation in seed genesis

The backbone of the prion-like mechanism is the formation of amyloids that typically follows sigmoidal kinetics called nucleation-dependent polymerization. The first step of this process is the lag or stationary phase, in which the formation of the critical nucleus of aggregation happens. This phase is followed by the log or exponential phase leading to an exponential increase in the amount of amyloids with time. This is followed by the saturation phase of

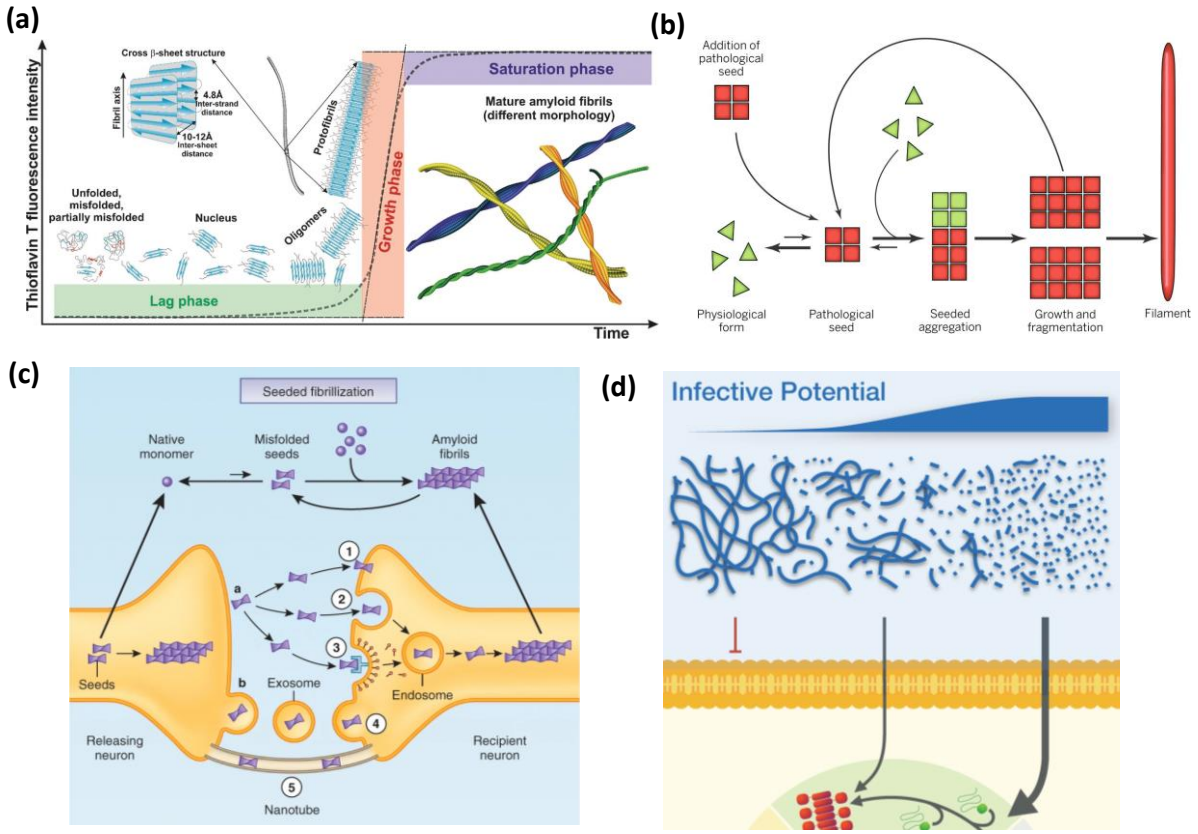

Figure 1.4 (a) Nucleation-dependent polymerization of unfolded or misfolded peptide chains into mature amyloid fibrils. Reproduced with permission from reference 53. (b) A pathological pathway leading from soluble proteins to insoluble filaments. Reproduced with permission from reference 43. (c) Hypothetical modes of prion-like transmission. Reproduced with permission from reference 55. (d) The physical dimensions of prion particles modulate their suprastructure and their infective potential. Reproduced with permission from reference 57.

where the matured fibrils appear. In the saturation phase, the fibrils, the lower molecular weight aggregates, and unrecruited monomers remain in equilibrium[53]. The polymerization process becomes faster by introducing preassembled amyloid entities named seeds, which can eliminate or shorten the lag phase, as noticed *in vitro* aggregation reactions. One such process is described as secondary nucleation, where the already-formed aggregates catalyze the formation of critical nuclei[54]. The amyloid diagnostic dye Thioflavin T (ThT) can be used to monitor these events in amyloid formation that showed a dramatic increase in the intensity at

480 nm in the amyloid-rich restricted environment (Figure 1.4a). ThT behaves as a molecular rotor. In the free state, it is non-fluorescent because its fluorescence is quenched due to twisted intramolecular charge transfer (TICT) in the excited state occurring because of the twisting of the C-C single bond. However, when bound to amyloid fibrils, this twisting is restricted, resulting in the enhancement of ThT fluorescence[55].

The nucleated formation of amyloids and their subsequent involvement in accelerating fresh aggregations are essential for the seeded amplification of amyloids and the prion-like spread (Figure 1.4b). In the prion-like transmission cycle, two properties of the seeds play a significant role. First, the quality of seeds is determined by their efficiency in promoting autocatalytic amyloid formation. The conformational characteristics, such as β-sheet content, often dictate the seeding potential of amyloids. Second, the quantity of seeds that provides sufficient growth-competent surface or end for the recruitment of monomers. The number of seeds is inversely proportional to the molecular weight, and the high molecular weight amyloids, such as fibrils, possess limited polymerization ends compared to the sub-fibrillar amyloids. Another characteristic of seeds that governs the prion-like transmission of seeds is their ability to invade the lipid bilayer. Recent studies unmasked various mechanisms by which neuron-to-neuron transmission of seeds occurs. Three such mechanisms have been discussed here briefly. First, the naked seeds invade the lipid layer of the neuron, and there are several mechanisms, such as direct invasion, endocytosis, or receptor-mediated endocytosis, by which the recipient neurons internalize them. Second, membrane-bound seeds emerge from the donor cells, fuse with the recipient cell's plasma membrane, and unload their cargo. Third, the intercellular passage of seeds forms a direct connection between the donor and recipient cell cytoplasm through nanotubes (Figure 1.4c)[56]. According to most of the mechanisms revealed to date, the neuronal transmission of seeds involves the passage of seeds through the lipid bilayer of donor and/or recipient cells. In recent work, it was noticed that the low molecular weight, Sup35 amyloids showed greater permeability through lipid bilayers than the matured fibrils (Figure 1.4d)[57]. However, the inheritance of [*PSI*$^{+}$] prions in budding yeasts do not involve lipid membrane invasion, as the transfer of Sup35 seeds happens through the continuous cytoplasmic connection between mother and daughter cells during budding. Intriguingly, the low molecular weight amyloids exhibit more diffusibility through the cytoplasmic stream connecting mother and daughter yeast cells[58]. Altogether, various studies point to the requirement of ample low molecular weight amyloids for a continued prion multiplication as opposed to fewer matured, high molecular weight fibrils demonstrating

limited transmissibility. In the next section, we have discussed some factors that regulate the amount and ability of autocatalytic seeds that drive seeded amyloid transmission.

1.7 The disaggregase Hsp104 in the transmission of [*PSI*$^+$] prions

The protein quality control system ensures the proper folding of proteins to their three-dimensional functional form using an exciting class of proteins that do not integrate with the final folded structure of the client proteins. These proteins, called molecular chaperones, not only help the newly translated polypeptide but are also involved in the conformational repair of misfolded proteins and the clearance of irreversibly misfolded or aggregated proteins via unfolded protein response or autophagy. The chaperones are also termed stress proteins or heat-shock proteins (HSPs), as their expression levels become upregulated under cellular stress to maintain proteostasis. Chaperones are named based on their molecular weight. Except for some of the low molecular weight heat shock proteins (small heat shock proteins or sHSPs), all chaperones depend on energy provided by ATP hydrolysis for substrate processing. In all domains of life, the highly coordinated network of chaperones is vital due to the marginal stability of the natively folded form of proteins from the folding intermediates. Moreover, one-third of our proteome consists of intrinsically disordered proteins or proteins that harbor intrinsically disordered domains. The metastability in proteins due to mutations or environmental factors or the natively unstructured proteins leads to aggregation often associated with neurodegenerative diseases[59]. Therefore, the requirement of a unique group of chaperones capable of disassembling a wide range of amyloids is essential for cellular and organismal well-being. Disaggregase chaperone machinery rescues proteins from aggregates that can either be channeled to degradation or reactivated to reduce the energetic burden of novel biosynthesis of proteins[60]. Disaggregases such as ClpB in bacteria, Hsp104 in yeasts, Hsp101 in plants, and Hsp110 in mammals are some of the disaggregases that several groups of researchers characterize to gain insight into the disaggregase activities on aggregate remodeling[61,62,63,64].

In yeasts, the disaggregation of protein aggregates is performed by the protein Hsp104, a chaperone from the group of chaperones known as AAA+ ATPase or Hsp100 in an ATP-dependent manner[65,66]. Interestingly, it is observed that the overexpression of Hsp104 in yeasts leads to the disappearance of the [*PSI*$^+$] phenotype in the daughter cells; this probably hints about the connection between the cross-generational inheritance of the prion phenotype associated with Sup35 and the disaggregase machinery Hsp104[67]. The loss of [*PSI*$^+$] during the budding of yeast cells or curing of [*PSI*$^+$] phenotype and its relation to the disaggregase

Hsp104 was further confirmed by using the specific small molecular inhibitor of this chaperone guanidinium hydrochloride (GdmCl) that can impair the propagation of [PSI^+] phenotype when it was introduced to the yeast growth medium[68]. Therefore, the role of disaggregase Hsp104 in the inheritance of [PSI^+] phenotype from mother to daughter yeast cells drew attention to the researchers as a model to study the neuronal transmission of aggregates via the prion-like mechanism. Hsp104 is a 908 amino acid-containing protein that forms a hexamer for substrate processing from its central pore. Each of the six Hsp104 protomers consists of an N-terminal domain (NTD), two nucleotide-binding domains (NBD1 and NBD2), with NBD1 flanked by a

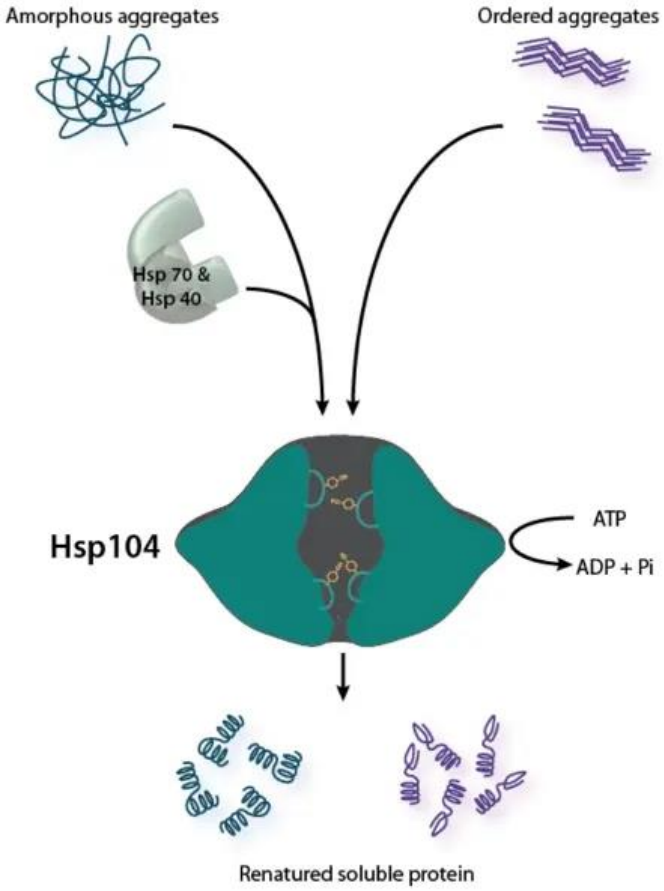

Figure 1.5 Disaggregation of disordered aggregates (shown on the left) requires the cooperation of the Hsp70 chaperone system (Hsp70 and Hsp40). Hsp104 remodels ordered amyloid aggregates (shown on the right) without the aid of Hsp70 and Hsp40 *in vitro*, but Hsp70 and Hsp40 can improve Hsp104 activity against amyloid. For both types of aggregated structures, Hsp104 couples ATP hydrolysis to substrate translocation through its central channel to promote disaggregation. Tyrosine-bearing pore loops engage and shuttle substrate through the central channel. Reproduced with permission from reference 66.

middle domain (MD), and a C-terminal domain (CTD). The two NBDs contain structural elements that bind and hydrolyze ATP. Despite details characterization, especially by cryo-EM

and mutational analysis, the domain-specific functions of Hsp104 remain controversial. The NTD is involved in hexamer cooperativity. NBD1 and NBD2 domains are reportedly involved in ATP hydrolysis coupled with substrate processing. NTD, NBD1, including the small linker region inside it, and MD residues are critical for intrinsic disaggregase activity and cooperation with other chaperones[65]. Hsp70 and Hsp40 assist Hsp104 in resolving the chemically or thermally denatured proteins and hold them to refold in their native functional structure. Hsp70 and Hsp40 also present aggregated substrates to Hsp104 for substrate refolding after rescuing the proteins from the aggregates (Figure 1.5). However, for disassembly, Hsp70 and Hsp40 are not absolutely required for many amyloids, although their presence with Hsp104 can increase the efficiency of amyloid remodeling. For example, Sis1, an Hsp40, was reported to deliver the substrate to Hsp104 for prion remodeling *in vivo*.Additionally, the cooperative interaction between Ssa1 (an Hsp70) and Hsp104 was found vital for processing prion fibers generated from various yeast prions[69,70]. Incorporating Hsp70 and Hsp40 into Sup35 prions converted them into better substrates for Hsp104 concentration-dependent remodeling of Sup35 prions *in vitro* [71]. The prion remodeling activity of Hsp104 is unique for Sup35NM amyloids as it does not require Hsp70 or Hsp40 *in vitro* to disassemble amyloids[72]. Several *in vivo* studies also suggested that Hsp104 alone is sufficient to control the propagation of [*PSI*$^+$][73,74].

In the context of [*PSI*$^+$] propagation, the role of Hsp104 is to create an adequate number of lower molecular weight seeds by disaggregating less transmissible matured fibrils. Furthermore, the dose of Hsp104 is critical for regulating the number of seeds. As we mentioned earlier, the overexpression of Hsp104 can cure the yeast cells from [*PSI*$^+$]. On the other hand, inactivation of Hsp104 by gene knockout, mutation, or by using chemical inhibitors impaired the transmission of the [*PSI*$^+$] phenotype. The underlying reason behind the Hsp104 dose-dependent regulation of [*PSI*$^+$] propagation remains largely elusive. *In vitro* studies using pure Hsp104 showed that high concentrations of Hsp104 inhibit the aggregation of the prion domain of Sup35[75]. Moreover, at very high concentrations, Hsp104 disaggregates the amyloids to such an extent that the resulting species do not display any seeding behavior, and there is an inhibition of the passage of prions in subsequent generations[67]. This view was challenged by another report where the asymmetric partition of seeds resulting the retention of high molecular weight seeds in the mother cells. This unequal disaggregation of amyloids leads to the transmission of only a small number of lower molecular weight seeds to the daughter yeast cells that, after a few generations, is insufficient for the cytoplasmic inheritance of [*PSI*$^+$] prion[76]. The curing of yeast cells from [*PSI*$^+$] prions also happens due to the presence of non-

denaturating, low concentrations of GdmCl in the growth medium of yeasts. GdmCl acts as the small molecule inhibitor of Hsp104 that binds with the nucleotide-binding domains of Hsp104. As an uncompetitive inhibitor of this enzyme, guanidinium ion binds with the ATP-bound Hsp104 forming a Hsp104-ATP-Gdm^+ complex and slows down the rate of ATP hydrolysis compared to the Hsp104-ATP which drives its prion remodeling[77]. The genetic inactivation of Hsp104 also demonstrated a distinct [*PSI*$^+$] curing kinetics showing more rapid prion loss via a distinct mechanism compared to the curing by GdmCl[78].The inactivation of Hsp104 leads to an increase in size and reduction in the number of seeds, which lowers the number of transmissible seeds required for prion propagation. Taken together, the dose of Hsp104 is pivotal for the cellular inheritance of [*PSI*$^+$] prions through regulating the number of seeds and severs as the model to study the role of disaggregases in amyloid transmission across cells.

1.8 Conformational diversity in Sup35 prions and the role of Hsp104

The amyloidogenic monomers assemble into the amyloids that are typically rich in β-sheet secondary structure. Despite the broader similarities in amyloid structure, the same monomeric building blocks lead to forming of a host of aggregates with distinct nanoscale architecture. In recent reports, this structural diversity shows its connection with the variation in the amyloid-associated pathological or functional outcomes in acute neurodegenerative disorders or biological processes. These structurally distinct amyloid conformers are reported to exhibit morphological differences in atomic force microscopy or electron microscopy for detrimental amyloids. These conformationally diverse amyloids of single proteins are known as polymorphs[79,80]. Amalgamation of *in vivo* and *in vitro* studies uncover that amyloid polymorphisms arise due to the presence of other proteins or polypeptides, the presence of small molecules, and aggregation conditions such as pH and salt concentrations[81,82]. This conformational diversity in the aggregates also implicates the differential infective potential and cytotoxicity, which complicates the identification of the culprit amyloid conformers and designing the conformation-based anti-amyloid compounds for therapeutics[83,84]. The conformational flexibility leading to the variation in the manifestation of diseases is also observed in prion diseases. It was first observed in goats that the same batch of scrapie agents exhibited two distinct clinical pathologies. To denote the structural diversity in the protein-based infectious particle prions, the term 'strain' was borrowed from the nucleic acid based infectious elements such as viruses[85]. This stain phenomenon of prions is also prevalent in functional yeast prions such as [*PSI*$^+$], Ure2p, and so on. Due to the relatively more straightforward detection of conformational conversion to prions through non-Mendelian

phenotypic alterations, yeast prions are widely utilized to understand the relationship between amyloid conformational dynamics and its outcome.

Sup35, upon aggregation, gives rise to [*PSI*$^{+}$] prions that demonstrate a distinct colony color compared to the phenotype associated with the soluble proteins. Various structural models of the monomer organization within Sup35NM fibril architecture have been proposed. For example, the parallel in-register structural model suggests that the amyloid assembly is primarily governed by intermolecular interactions whereby identical residues of different Sup35NM protein molecules are aligned and stacked on top[86,87,88] On the other hand, according to the alternative model known as the β-helix model, the combination of intra- and intermolecular contacts is necessary for prion formation[89]. In-depth structural analysis of Sup35 NM unmasked that the intermolecular contacts are formed between the top and bottom regions of adjacent Sup35NM proteins, and intramolecular contacts predominate in the central core region[89]. Recent studies have provided more substantial proof in favor of parallel in-register packing. When recombinantly purified Sup35NM were polymerized *in vitro* in three different temperatures and injected into the [*psi*$^{-}$] cells, the phenotypic outcomes were distinguishable. The structural distinction of these three amyloid variants composed of Sup35 NM proteins is established by seminal biochemical and spectroscopic characterizations by various groups. The polymerization temperature-dependent variants of Sup35NM amyloids (abbreviated as 'Sc' followed by the polymerization temperatures) shows a nanoscale structural variation in the multi-layered, cross-β parallel in register packing[90] . The intriguing question is how the altered architecture of the fibrils produces phenotypic differences. Since a host of previous studies pointed towards the concentration-dependent role of Hsp104 in the inheritance of [*PSI*$^{+}$] prion, it is speculated that the differential phenotypic outcomes are due to the strain-specific remodeling of NM amyloids by Hsp104. The most compelling evidence is shown by Shorter and co-workers, where the amyloid variants of Sup35, Sc4, Sc25, and Sc37 were fragmented to a different extent[72]. The unique nanoscopic arrangements in these amyloids govern their ability to interact with Hsp104 to regulate the number of seeds. Our and others' work on Sc4 and Sc37 suggest that the M-domain of NM retains its flexibility even in the amyloid form and does not contribute to constituting the amyloid core. Therefore, this dynamic solvent-exposed domain can act as the binding site for chaperones such as Hsp104 for amyloid severing. Interestingly, detailed conformational characterization reveals that the Sc37 amyloids are more structured than the Sc4 amyloid, and Sc4 shows more fragmentation by Hsp104 than the Sc25 and Sc37 irrespective of the presence of co-chaperones Ssa1 (an Hsp70) or Sis1 (an

Hsp40)[90,91]. The extensive fragmentation of Sc4 can generate more growth-competent fiber ends as seeds for self-templated Sup35 amyloid formation. The greater extent of severing mediated by Hsp104 of Sc4 owing to its nano-structural features possibly answers why Sc4 typically gives rise to strong [*PSI*$^{+}$] and why Sc25 and Sc37 prions generate weak [*PSI*$^{+}$] as confirmed by a host of *in vivo* studies[92,93].

1.9 Polyanions in amyloid formation and dissolution

A large number of proteins or peptides, such as chaperones, peptide neurotransmitters, Modulators of protein aggregations (MOAGs), or aggregation-prone proteins that form co-

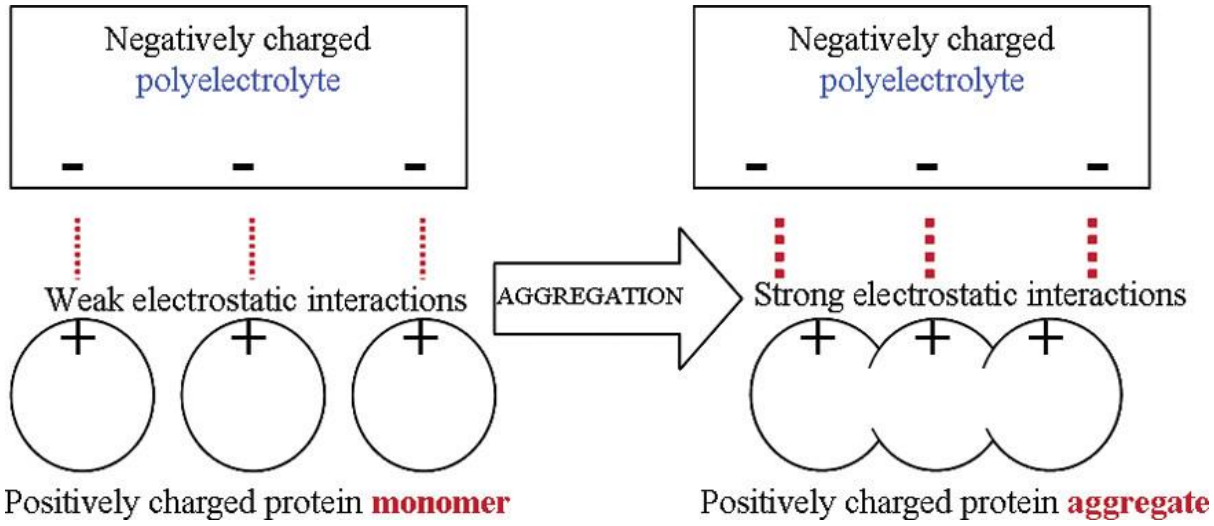

Figure 1.6 Schematic representation of the effects of protein aggregation on electrostatic interactions between two oppositely charged systems. Reproduced with permission from reference 99.

aggregates function as the regulator of protein aggregation by directly interacting with the amyloidogenic proteins and existing aggregates. However, apart from the proteins, other non-protein biopolymers and small molecules also influence several facets of amyloid formation and dissolution. The most popular class of such molecules are the molecules that are designed to combat amyloid infection. Designing small molecules as the inhibitor of amyloid formation is challenging due to the transient nature of these species. Identifying the culprit species is the most critical step against infectious detrimental amyloids. For several neurodegenerative amyloids, oligomers are believed to be more toxic than monomers or fibrils. Therefore, the small molecules that modulate aggregation may have several modes of action that may help in combating protein-misfolding disorders. The absence of a native three-dimensional structure of the intrinsically disordered monomers makes identifying the binding partner difficult, which

may block amyloidogenesis. However, several small molecules, such as vitamin A (retinoic acid) and YX-I-1, showed the potential to bind with the monomers of Aβ-42 and hIAPP, respectively, to inhibit the nucleation process that generates amyloids. The cell viability assay revealed that a curcumin derivative that binds with the hIAPP oligomers reduced its toxicity. Finally, some molecules that induce the fibril disassembly has been isolated. However, fibril disaggregation yielding toxic oligomers instead of non-toxic oligomers or other lower molecular weight species may create additional complications. In place of designing molecules that retard or block aggregation, the small molecules that accelerate the fibrillation and bypass the persistence of more toxic and highly transmissible oligomers or other intermediate amyloids have gained attention[94]. Apart from these modulators of amyloids that are identified for therapeutics, there are specific biologically relevant non-protein molecules that gained the attention of the researchers as the coexistence of these molecules was found with the proteinaceous amyloid plaques isolated from the infected tissues. Here we have discussed three crucial small molecular regulators that directly interact with the amyloids to influence their aggregation and disintegration.

1.9.1 Glycosaminoglycans

Upon careful biochemical characterizations of the amyloid deposits obtained from the victims, charged polyelectrolytes such as glycosaminoglycans, ATP, and so on were detected frequently. Glycosaminoglycans (GAGs) are the heteropolysaccharide composed of repetitive disaccharide units having a molecular weight of 10-100 kDa that are the major component of the extracellular matrix. GAGSs are known to favor aggregation. One of the most common GAG, heparan sulfate, is linked with various amyloid-related disorders such as Alzheimer's, light chain amyloidosis, type 2 diabetes, and prion diseases. The underlying mechanism behind facilitating the aggregation by GAG remains poorly understood. The data indicated that GAGs are the structural template for assembling amyloidogenic precursors (Figure 1.6). Studies suggest that electrostatic interactions is the predominant mode of interaction between these amyloidogenic proteins and highly charged polyelectrolytes[95]. Apart from accelerating *de novo* aggregation, heparin also exhibits its ability to drive templated growth of Tau amyloids by facilitating the interaction between seeds and monomers[96]. The LLPS-mediated aggregation of tau suggests an alternative mechanism of aberrant Tau aggregation that proceeded via phase separation and recruitment of heparin into the droplets[97].

1.9.2 ATP

The other important biologically relevant polyanion that has recently grabbed researchers' attention is the ATP. ATP is involved in protein homeostasis indirectly by providing energy to most of the chaperones of the protein quality control system. However, the concentration of ATP required for fueling molecular chaperone machinery is in micromolar concentrations. Still, why cells maintain multi-fold higher concentrations of ATP leads the researchers to hypothesize a direct role of these molecules in the solubility of proteins or aggregation [98]. *In vitro* studies by Dobson and co-workers uncovered the role of molecular ATP in promoting the fibrillation of human lysozyme and human muscle acyl phosphatase. The interaction between these proteins and polyanions is non-specific and primarily through electrostatic interactions as these interactions are sensitive to high concentrations of Mg^{2+} or Ca^{2+} salts[99]. These polyanions bind with the amino acids, such as lysine, that bear the positively charged side chains and minimize the electrostatic repulsion between monomeric building blocks facilitating aggregation. A similar mechanism of ATP-mediated facilitation is observed for the lysine-rich segment of Alzheimer associated tau protein known as tauK18. The dimerization of Tauk18 monomers promotes the dimer formation that induces fibrillation of this protein that otherwise does not aggregate[100]. The involvement of ATP in facilitating aggregation and its activity, such as inhibiting aggregation or solubilizing existing aggregates, make this nucleotide a potential small chemical chaperone. ATP is an amphipathic molecule that consists of the hydrophilic triphosphate moiety and the hydrophobic adenosine ring. ATP may behave as hydrotropes similar to the other amphipathic molecules, such as NaXS and NaTO, used to solubilize hydrophobic compounds. ATP, due to its hydrotropic properties, prevents the aggregation of FUS in physiologically relevant concentrations. Additionally, it is also capable of disaggregating preformed FUS fibres. In the same study, it is shown that ATP might inhibit the aggregation of synthetic Aβ42 peptides whose aggregation causes Alzheimer's disease and the prion domain of the functional yeast prion protein Mot3 (Mot3-PrD)[98].

1.9.3 RNA

RNA is also one of the crucial biological polyanions that modulate the aggregation of several amyloids. One of the most studied roles of RNA-induced genesis of amyloids was the aggregation of tau, which is associated with a host of neuropathological diseases such as Alzheimer's, Frontotemporal dementia, and so on, collectively known as tauopathies. The most compelling proof of RNA and Tau interaction was the *in vivo* studies in cell culture and mouse

brains that cytosolic and nuclear tau aggregates contain RNA, mainly small nuclear RNAs (snRNAs) and small nucleolar RNAs (snoRNAs)[101]. Towards uncovering the mechanistic insight, it is found that, like other polyanions, the principal interaction that governs the binding of RNA with Tau is electrostatic through the phosphate groups of RNA and the repeat domain of tau. RNA not only promoted the spontaneous unseeded aggregation of tau but also, like heparin, acted as a bridge between preformed tau aggregates and monomers for the auto-catalytic growth generating higher order Tau aggregates[96]. Furthermore, polyA RNA but not polyU and polyC induce a stable seeding-competent Tau strain whose seed ability was diminished after the treatment of RNase. This confirms the essentiality of RNA-Tau complexation in generating seeding-competent RNA[102]. The prionogenesis of murine Prion proteins (rRNA) is also reported to be affected by the RNA: rPrP ratio. Interestingly, the excess amount of rPrP with respect to RNA increased the aggregate formation rate. In the presence of more RNA than protein, the formation of seeding competent oligomers is noticed predominantly[103]. The modulation of heterotypic coacervates by RNA has now emerged as an essential regulatory mechanism for stress granule-associated protein TDP-43. At higher concentrations of RNA, the selective RNA interaction with one of the components of this system maintains it in a liquid-like state[104]. However, RNA is found in screening the interactions that facilitate aggregation in lower concentrations. Further studies have also described the pivotal role of RNA in spatiotemporally modulating the phase separation of several aggregation-prone prion-like proteins such as FUS and TDP-43. Numerous neuronal-associated proteins with PLDs exist in cytoplasmic inclusions that may mature into pathological aggregates, a hallmark of several neurodegenerative disorders.

1.10 Thesis motivation and perspective

Prion-like conformational switch to the self-perpetuating aggregates is classically believed as the phenomenon shown by a handful of amyloidogenic proteins. However, with passing days, more reports are coming where the non-prion amyloids demonstrate a prion-like mechanism for their distal invasion. Therefore, to gain insights into the mechanistic underpinning of prion-like propagation, we used the prion determinant of the yeast prion Sup35 for the *in vitro* investigation. Many molecular regulators control the prion-like mechanism by regulating the amount and ability of autocatalytic seeds. This thesis aims to decipher the role of two molecular regulators of prion-like propagation. The disaggregase Hsp104 is involved in the genesis of seeds for the cross-generational inheritance of [*PSI*$^{+}$] through Sup35 amyloids. Several *in vivo* and *in vitro* studies tried to decipher the dose-dependent role of this disaggregase in generating

sufficient seeds. However, many facets of aggregate remodeling by Hsp104 remain controversial. In chapter 2, we used sub-stoichiometric concentrations of Hsp104, which is reminiscent of chaperone insufficiency during aging, and monitored the alteration in NM fibrillation kinetics due to the presence of Hsp104. In chapter 3, we intended to probe the conformational characteristics of amyloids resulting from Hsp104-mediated NM aggregation using biochemical studies coupled with the site-specific dynamic readouts, which may control their seeding ability. In chapter 4, we aimed to decipher the role of free ATP molecules in prion-like propagation as it showed the potential to impact both protein aggregation and disintegration of existing aggregates directly. In this chapter, we focus on the influence of the binding of ATP to the amyloids in their seeding potential, stability, and fragility, which is critical for prion-like amyloid transmission. In chapter 5, we performed sequential seeding with NM amyloids. We observed that only an optimal seed size might form such amyloids that can demonstrate seeding ability in successive seeding cycles.

1.11 References

(1) Iadanza, M. G., Jackson, M. P., Hewitt, E. W., Ranson, N. A., and Radford, S. E. (2018) A new era for understanding amyloid structures and disease. *Nat. Rev. Mol. Cell Biol. 19*, 755–773.

(2) Sipe, J. D., and Cohen, A. S. (2000) Review: History of the amyloid fibril. *J. Struct. Biol. 130*, 88–98.

(3) Maji, S. K., Wang, L., Greenwald, J., and Riek, R. (2009) Structure-activity relationship of amyloid fibrils. *FEBS Lett. 583*, 2610–2617.

(4) Aumüller, T., and Fändrich, M. (2014) Protein chemistry: Catalytic amyloid fibrils. *Nat. Chem. 6*, 272–273.

(5) Al-Garawi, Z. S., McIntosh, B. A., Neill-Hall, D., Hatimy, A. A., Sweet, S. M., Bagley, M. C., and Serpell, L. C. (2017) The amyloid architecture provides a scaffold for enzyme-like catalysts. *Nanoscale 9*, 10773–10783.

(6) Greenwald, J., Friedmann, M. P., and Riek, R. (2016) Amyloid Aggregates Arise from Amino Acid Condensations under Prebiotic Conditions. *Angew. Chemie - Int. Ed. 55*, 11609–11613.

(7) Sidhu, A., Segers-Nolten, I., Raussens, V., Claessens, M. M. A. E., and Subramaniam, V. (2017) Distinct Mechanisms Determine α-Synuclein Fibril Morphology during Growth and Maturation. *ACS Chem. Neurosci. 8*, 538–547.

(8) Fitzpatrick, A. W. P., Falcon, B., He, S., Murzin, A. G., Murshudov, G., Garringer, H. J., Crowther, R. A., Ghetti, B., Goedert, M., and Scheres, S. H. W. (2017) Cryo-EM structures of tau filaments from Alzheimer's disease. *Nature 547*, 185–190.

(9) Schmidt, M., Wiese, S., Adak, V., Engler, J., Agarwal, S., Fritz, G., Westermark, P., Zacharias, M., and Fändrich, M. (2019) Cryo-EM structure of a transthyretin-derived amyloid fibril from a patient with hereditary ATTR amyloidosis. *Nat. Commun. 10*, 1–9.

(10) Ke, P. C., Zhou, R., Serpell, L. C., Riek, R., Knowles, T. P. J., Lashuel, H. A., Gazit, E., Hamley, I. W., Davis, T. P., Fändrich, M., Otzen, D. E., Chapman, M. R., Dobson, C. M., Eisenberg, D. S., and Mezzenga, R. (2020) Half a century of amyloids: Past, present and future. *Chem. Soc. Rev. 49*, 5473–5509.

(11) Uversky, V. N. (2017) Intrinsically disordered proteins in overcrowded milieu: Membrane-less organelles, phase separation, and intrinsic disorder. *Curr. Opin. Struct. Biol. 44*, 18–30.

(12) Dill, K. A., Maccallum, J. L., and Folding, P. (2012) The Protein-Folding Problem, 50 Years On 1042–1046.

(13) Cordeiro, Y., Macedo, B., Silva, J. L., and Gomes, M. P. B. (2014) Pathological implications of nucleic acid interactions with proteins associated with neurodegenerative diseases. *Biophys. Rev. 6*, 97–110.

(14) Hartl, F. U., Bracher, A., and Hayer-Hartl, M. (2011) Molecular chaperones in protein folding and proteostasis. *Nature 475*, 324–332.

(15) (2020) 2020 Alzheimer's disease facts and figures. *Alzheimer's Dement. 16*, 391–460.

(16) Kaushik, S., and Cuervo, A. M. (2015) Proteostasis and aging. *Nat. Med. 21*, 1406–1415.

(17) Klaips, C. L., Jayaraj, G. G., and Hartl, F. U. (2018) Pathways of cellular proteostasis in aging and disease. *J. Cell Biol. 217*, 51–63.

(18) Bhasne, K., and Mukhopadhyay, S. (2018) Formation of Heterotypic Amyloids: α-Synuclein in Co-Aggregation. *Proteomics 18*, 1–11.

(19) Agarwal, A., and Mukhopadhyay, S. (2022) Prion Protein Biology Through the Lens of Liquid-Liquid Phase Separation: Liquid-liquid phase separation of prion protein. *J. Mol. Biol. 434*, 167368.

(20) Wei, G., Su, Z., Reynolds, N. P., Arosio, P., Hamley, I. W., Gazit, E., and Mezzenga, R. (2017) Self-assembling peptide and protein amyloids: From structure to tailored function in nanotechnology. *Chem. Soc. Rev. 46*, 4661–4708.

(21) Hauser, C. A. E., Maurer-Stroh, S., and Martins, I. C. (2014) Amyloid-based nanosensors and nanodevices. *Chem. Soc. Rev. 43*, 5326–5345.

(22) Otzen, D., and Riek, R. (2019) Functional Amyloids. *Cold Spring Harb. Perspect. Biol.* a033860.

(23) McGlinchey, R. P., and Lee, J. C. (2018) Why Study Functional Amyloids? Lessons from the Repeat Domain of Pmel17. *J. Mol. Biol. 430*, 3696–3706.

(24) Dogra, P., Roy, S. S., Joshi, A., and Mukhopadhyay, S. (2020) Hofmeister Ions Modulate the Autocatalytic Amyloidogenesis of an Intrinsically Disordered Functional Amyloid Domain via Unusual Biphasic Kinetics. *J. Mol. Biol. 432*, 6173–6186.

(25) Jain, N., and Chapman, M. R. (2019) Bacterial functional amyloids: Order from disorder. *Biochim. Biophys. Acta - Proteins Proteomics 1867*, 954–960.

(26) Dai, B., Sargent, C. J., Gui, X., Liu, C., and Zhang, F. (2019) Fibril Self-Assembly of Amyloid-Spider Silk Block Polypeptides. *Biomacromolecules 20*, 2015–2023.

(27) Chatterjee, D., Jacob, R. S., Ray, S., Navalkar, A., Singh, N., Sengupta, S., Gadhe, L., Kadu, P., Datta, D., Paul, A., Sakunthala, A., Mehra, S., Pindi, C., Kumar, S., Singru, P. S., Senapati, S., and Maji, S. K. (2022) Co-aggregation and secondary nucleation in the life cycle of human prolactin/galanin functional amyloids. *Elife 11*, 1–29.

(28) Cereghetti, G., Wilson-Zbinden, C., Kissling, V. M., Diether, M., Arm, A., Yoo, H., Piazza, I., Saad, S., Picotti, P., Drummond, D. A., Sauer, U., Dechant, R., and Peter, M. (2021) Reversible amyloids of pyruvate kinase couple cell metabolism and stress granule disassembly. *Nat. Cell Biol. 23*, 1085–1094.

(29) Wickner, R. B. (2016) Yeast and fungal prions. *Cold Spring Harb. Perspect. Biol. 8*, 1–16.

(30) Prusiner, S. B. (1982) Science.6801762 *216*.

(31) Si, K. (2015) Prions: What Are They Good For? *Annu. Rev. Cell Dev. Biol. 31*, 149–169.

(32) Legname, G. (2017) Elucidating the function of the prion protein. *PLoS Pathog. 13*, 6–11.

(33) Westergard, L., Christensen, H. M., and Harris, D. A. (2007) The cellular prion protein (PrPC): Its physiological function and role in disease. *Biochim. Biophys. Acta - Mol. Basis Dis. 1772*, 629–644.

(34) Linden, R. (2017) The biological function of the prion protein: A cell surface scaffold of signaling modules. *Front. Mol. Neurosci. 10*, 1–19.

(35) Luers, L., Bannach, O., Stöhr, J., Wördehoff, M. M., Wolff, M., Nagel-Steger, L., Riesner, D., Willbold, D., and Birkmann, E. (2013) Seeded Fibrillation as Molecular Basis of the Species Barrier in Human Prion Diseases. *PLoS One 8*.

(36) Wickner, R. B., Edskes, H. K., Son, M., Bezsonov, E. E., Dewilde, M., and Ducatez, M. (2018) Yeast Prions Compared to Functional Prions and Amyloids. *J. Mol. Biol. 430*, 3707–3719.

(37) Reselammal, D. S., Pinhero, F., Sharma, R., Oliyantakath Hassan, M. S., Srinivasula, S. M., and Vijayan, V. (2021) Mapping the Fibril Core of the Prion Subdomain of the Mammalian CPEB3 that is Involved in Long Term Memory Retention. *J. Mol. Biol. 433*, 167084.

(38) Ivshina, M., Lasko, P., and Richter, J. D. (2014) Cytoplasmic polyadenylation element binding proteins in development, health, and disease. *Annu. Rev. Cell Dev. Biol. 30*, 393–415.

(39) Rayman, J. B., and Kandel, E. R. (2022) Functional Prions in the Brain.

(40) Wickner, R. B., Edskes, H. K., Shewmaker, F., and Nakayashiki, T. (2007) Prions of fungi: Inherited structures and biological roles. *Nat. Rev. Microbiol. 5*, 611–618.

(41) Wickner, R. B., Shewmaker, F. P., Bateman, D. A., Edskes, H. K., Gorkovskiy, A., Dayani, Y., and Bezsonov, E. E. (2015) Yeast Prions: Structure, Biology, and Prion-Handling Systems. *Microbiol. Mol. Biol. Rev. 79*, 1–17.

(42) Goedert, M., Clavaguera, F., and Tolnay, M. (2010) The propagation of prion-like protein inclusions in neurodegenerative diseases. *Trends Neurosci. 33*, 317–325.

(43) Goedert, M. (2015) Alzheimer's and Parkinson's diseases: The prion concept in relation

to assembled Aβ, tau, and α-synuclein. *Science 349*, 61–69.

(44) Gomez-Gutierrez, R., and Morales, R. (2020) The prion-like phenomenon in Alzheimer's disease: Evidence of pathology transmission in humans. *PLoS Pathog. 16*, 1–6.

(45) Tarutani, A., Suzuki, G., Shimozawa, A., Nonaka, T., Akiyama, H., Hisanaga, S. I., and Hasegawa, M. (2016) The effect of fragmented pathogenic α-synuclein seeds on prion-like propagation. *J. Biol. Chem. 291*, 18675–18688.

(46) Costa, D. C. F., de Oliveira, G. A. P., Cino, E. A., Soares, I. N., Rangel, L. P., and Silva, J. L. (2016) Aggregation and prion-like properties of misfolded tumor suppressors: Is cancer a prion disease? *Cold Spring Harb. Perspect. Biol. 8*, 1–22.

(47) Si, K., Lindquist, S., and Kandel, E. R. (2003) A Neuronal Isoform of the Aplysia CPEB Has Prion-Like Properties. *Cell 115*, 879–891.

(48) Chernova, T. A., Chernoff, Y. O., and Wilkinson, K. D. (2019) Yeast models for amyloids and prions: Environmental modulation and drug discovery. *Molecules 24*, 1–23.

(49) Glover, J. R., Kowal, A. S., Schirmer, E. C., Patino, M. M., Liu, J. J., and Lindquist, S. (1997) Self-seeded fibers formed by Sup35, the protein determinant of [PSI+], a heritable prion-like factor of S. cerevisiae. *Cell 89*, 811–819.

(50) Ter-Avanesyan, M. D., Dagkesamanskaya, A. R., Kushnirov, V. V., and Smirnov, V. N. (1994) The SUP35 omnipotent suppressor gene is involved in the maintenance of the non-Mendelian determinant [psi+] in the yeast Saccharomyces cerevisiae. *Genetics 137*, 671–676.

(51) Liebman, S. W., and Chernoff, Y. O. (2012) Prions in Yeast *191*, 1041–1072.

(52) Brundin, P., Melki, R., and Kopito, R. (2010) Prion-like transmission of protein aggregates in neurodegenerative diseases. *Nat. Rev. Mol. Cell Biol. 11*, 301–307.

(53) Adamcik, J., and Mezzenga, R. (2018) Amyloid Polymorphism in the Protein Folding and Aggregation Energy Landscape. *Angew. Chemie - Int. Ed. 57*, 8370–8382.

(54) Linse, S. (2017) Monomer-dependent secondary nucleation in amyloid formation. *Biophys. Rev. 9*, 329–338.

(55) Lakowicz, J. R. (2006) Principles of fluorescence spectroscopy. *Princ. Fluoresc. Spectrosc.*

(56) Guo, J. L., and Lee, V. M. Y. (2014) Cell-to-cell transmission of pathogenic proteins in neurodegenerative diseases. *Nat. Med. 20*, 130–138.

(57) Marchante, R., Beal, D. M., Koloteva-Levine, N., Purton, T. J., Tuite, M. F., and Xue, W. F. (2017) The physical dimensions of amyloid aggregates control their infective potential as prion particles. *Elife 6*, 1–20.

(58) Xue, W., Hellewell, A. L., Hewitt, E. W., Radford, S. E., Hellewell, A. L., Hewitt, E. W., Radford, S. E., Xue, W., Hellewell, A. L., Hewitt, E. W., and Radford, S. E. (2010) When size matters *6896*.

(59) Balchin, D., Hayer-Hartl, M., and Hartl, F. U. (2016) In vivo aspects of protein folding and quality control. *Science 353*.

(60) Saibil, H. (2013) Chaperone machines for protein folding, unfolding and disaggregation. *Nat. Rev. Mol. Cell Biol. 14*, 630–642.

(61) Barnett, M. E., Zolkiewska, A., and Zolkiewski, M. (2000) Structure and activity of ClpB from Escherichia coli. Role of the amino- and carboxyl-terminal domains. *J. Biol. Chem. 275*, 37565–37571.

(62) Kryndushkin, D. S., Engel, A., Edskes, H., and Wickner, R. B. (2011) Molecular chaperone Hsp104 can promote yeast prion generation. *Genetics 188*, 339–348.

(63) Taguchi, Y. V., Gorenberg, E. L., Nagy, M., Thrasher, D., Fenton, W. A., Volpicelli-Daley, L., Horwich, A. L., and Chandra, S. S. (2019) Hsp110 mitigates α-synuclein pathology in vivo. *Proc. Natl. Acad. Sci. U. S. A. 116*, 24310–24316.

(64) McLoughlin, F., Kim, M., Marshall, R. S., Vierstra, R. D., and Vierling, E. (2019) HSP101 interacts with the proteasome and promotes the clearance of ubiquitylated protein aggregates. *Plant Physiol. 180*, 1829–1847.

(65) Sweeny, E. A., Tariq, A., Gurpinar, E., Go, M. S., Sochor, M. A., Kan, Z. Y., Mayne, L., Englander, S. W., and Shorter, J. (2020) Structural and mechanistic insights into Hsp104 function revealed by synchrotron X-ray footprinting. *J. Biol. Chem. 295*, 1517–1538.

(66) Sweeny, E. A., Desantis, M. E., and Shorter, J. (2011) Purification of Hsp104, a protein disaggregase. *J. Vis. Exp.* 2–9.

(67) Greene, L. E., Zhao, X., and Eisenberg, E. (2018) Curing of [PSI+] by Hsp104

Overexpression: Clues to solving the puzzle. *Prion 12*, 9–15.

(68) Ness, F., Ferreira, P., Cox, B. S., and Tuite, M. F. (2002) Guanidine Hydrochloride Inhibits the Generation of Prion "Seeds" but Not Prion Protein Aggregation in Yeast. *Mol. Cell. Biol. 22*, 5593–5605.

(69) Higurashi, T., Hines, J. K., Sahi, C., Aron, R., and Craig, E. A. (2008) Specificity of the J-protein Sis1 in the propagation of 3 yeast prions. *Proc. Natl. Acad. Sci. U. S. A. 105*, 16596–16601.

(70) Winkler, J., Tyedmers, J., Bukau, B., and Mogk, A. (2012) Hsp70 targets Hsp100 chaperones to substrates for protein disaggregation and prion fragmentation. *J. Cell Biol. 198*, 387–404.

(71) Shorter, J., and Lindquist, S. (2008) Hsp104, Hsp70 and Hsp40 interplay regulates formation, growth and elimination of Sup35 prions. *EMBO J. 27*, 2712–2724.

(72) Desantis, M. E., and Shorter, J. (2012) Hsp104 drives "protein-only" positive selection of sup35 prion strains encoding strong [PSI+]. *Chem. Biol. 19*, 1400–1410.

(73) Klaips, C. L., Hochstrasser, M. L., Langlois, C. R., and Serio, T. R. (2014) Spatial quality control bypasses cell-based limitations on proteostasis to promote prion curing. *Elife 3*, 1–24.

(74) Serio, T. R., Cashikar, A. G., Kowal, A. S., Sawicki, G. J., Moslehi, J. J., Serpell, L., Arnsdorf, M. F., and Lindquist, S. L. (2000) Nucleated conformational conversion and the replication of conformational information by a prion determinant. *Science 289*, 1317–1321.

(75) Shorter, J., and Lindquist, S. (2004) Hsp104 catalyzes formation and elimination of self-replicating Sup35 prion conformers. *Science 304*, 1793–1797.

(76) Ness, F., Cox, B. S., Wongwigkarn, J., Naeimi, W. R., and Tuite, M. F. (2017) Over-expression of the molecular chaperone Hsp104 in Saccharomyces cerevisiae results in the malpartition of [PSI+] propagons. *Mol. Microbiol. 104*, 125–143.

(77) Grimminger, V., Richter, K., Imhof, A., Buchner, J., and Walter, S. (2004) The Prion Curing Agent Guanidinium Chloride Specifically Inhibits ATP Hydrolysis by Hsp104 * *279*, 7378–7383.

(78) Wegrzyn, R. D., Bapat, K., Newnam, G. P., Zink, A. D., and Chernoff, Y. O. (2001) Mechanism of Prion Loss after Hsp104 Inactivation in Yeast. *Mol. Cell. Biol. 21*, 4656–4669.

(79) Strohäker, T., Jung, B. C., Liou, S. H., Fernandez, C. O., Riedel, D., Becker, S., Halliday, G. M., Bennati, M., Kim, W. S., Lee, S. J., and Zweckstetter, M. (2019) Structural heterogeneity of α-synuclein fibrils amplified from patient brain extracts. *Nat. Commun. 10*, 1–12.

(80) Close, W., Neumann, M., Schmidt, A., Hora, M., Annamalai, K., Schmidt, M., Reif, B., Schmidt, V., Grigorieff, N., and Fändrich, M. (2018) Physical basis of amyloid fibril polymorphism. *Nat. Commun. 9*, 1–7.

(81) Klement, K., Wieligmann, K., Meinhardt, J., Hortschansky, P., Richter, W., and Fändrich, M. (2007) Effect of Different Salt Ions on the Propensity of Aggregation and on the Structure of Alzheimer's Aβ(1-40) Amyloid Fibrils. *J. Mol. Biol. 373*, 1321–1333.

(82) Kodali, R., Williams, A. D., Chemuru, S., and Wetzel, R. (2010) Aβ(1-40) forms five distinct amyloid structures whose β-sheet contents and fibril stabilities are correlated. *J. Mol. Biol. 401*, 503–517.

(83) Heilbronner, G., Eisele, Y. S., Langer, F., Kaeser, S. A., Novotny, R., Nagarathinam, A., Åslund, A., Hammarström, P., Nilsson, K. P. R., and Jucker, M. (2013) Seeded strain-like transmission of β-amyloid morphotypes in APP transgenic mice. *EMBO Rep. 14*, 1017–1022.

(84) Westermark, G. T., Fändrich, M., and Westermark, P. (2015) AA amyloidosis: Pathogenesis and targeted therapy. *Annu. Rev. Pathol. Mech. Dis. 10*, 321–344.

(85) Morales, R. (2017) Prion strains in mammals: Different conformations leading to disease. *PLoS Pathog. 13*, 1–5.

(86) Ross, E. D., Edskes, H. K., Terry, M. J., and Wickner, R. B. (2005) Primary sequence independence for prion formation *102*.

(87) Shewmaker, F., Ross, E. D., Tycko, R., and Wickner, R. B. (2008) Amyloids of shuffled prion domains that form prions have a parallel in-register β-sheet structure. *Biochemistry 47*, 4000–4007.

(88) Shewmaker, F., McGlinchey, R. P., and Wickner, R. B. (2011) Structural insights into functional and pathological amyloid. *J. Biol. Chem. 286*, 16533–16540.

(89) Krishnan, R., and Lindquist, S. L. (2005) Structural insights into a yeast prion illuminate nucleation and strain diversity. *Nature 435*, 765–772.

(90) Narang, D., Swasthi, H. M., Mahapatra, S., and Mukhopadhyay, S. (2017) Site-Specific Fluorescence Depolarization Kinetics Distinguishes the Amyloid Folds Responsible for Distinct Yeast Prion Strains. *J. Phys. Chem. B 121*, 8447–8453.

(91) Desantis, M. E., and Shorter, J. (2012) Hsp104 drives "protein-only" positive selection of sup35 prion strains encoding strong [PSI+]. *Chem. Biol. 19*, 1400–1410.

(92) Tanaka, M., Chien, P., Naber, N., Cooke, R., and Weissman, J. S. (2004) Conformational variations in an infectious protein determine prion strain differences. *Nature 428*, 323–328.

(93) Tanaka, M., Collins, S. R., Toyama, B. H., and Weissman, J. S. (2006) The physical basis of how prion conformations determine strain phenotypes. *Nature 442*, 585–589.

(94) Xu, Y., Maya-Martinez, R., and Radford, S. E. (2022) Controlling amyloid formation of intrinsically disordered proteins and peptides: slowing down or speeding up? *Essays Biochem.* 1–17.

(95) Iannuzzi, C., Irace, G., and Sirangelo, I. (2015) The effect of glycosaminoglycans (GAGs) on amyloid aggregation and toxicity. *Molecules 20*, 2510–2528.

(96) Dinkel, P. D., Holden, M. R., Matin, N., and Margittai, M. (2015) RNA Binds to Tau Fibrils and Sustains Template-Assisted Growth.

(97) Ambadipudi, S., Biernat, J., Riedel, D., Mandelkow, E., and Zweckstetter, M. (2017) Liquid-liquid phase separation of the microtubule-binding repeats of the Alzheimer-related protein tau. *Nat. Commun. 8*, 1–13.

(98) Patel, A., Malinovska, L., Saha, S., Wang, J., Alberti, S., Krishnan, Y., and Hyman, A. A. (2017) Biochemistry: ATP as a biological hydrotrope. *Science 356*, 753–756.

(99) Calamai, M., Kumita, J. R., Mifsud, J., Parrini, C., Ramazzotti, M., Ramponi, G., Taddei, N., Chiti, F., and Dobson, C. M. (2006) Nature and significance of the interactions between amyloid fibrils and biological polyelectrolytes. *Biochemistry 45*, 12806–12815.

(100) Kim, H. I., Heo, C. E., Han, J. Y., Lim, S., Lee, J., Im, D., Lee, M. J., and Kim, Y. K. (2020) ATP kinetically modulates pathogenic tau fibrillations. *ACS Chem. Neurosci. 11*, 3144–3152.

(101) Lester, E., Ooi, F. K., Bakkar, N., Ayers, J., Woerman, A. L., Wheeler, J., Bowser, R., Carlson, G. A., Prusiner, S. B., and Parker, R. (2021) Tau aggregates are RNA-protein

assemblies that mislocalize multiple nuclear speckle components. *Neuron 109*, 1675-1691.e9.

(102) Zwierzchowski-Zarate, A. N., Mendoza-Oliva, A., Kashmer, O. M., Collazo-Lopez, J. E., White, C. L., and Diamond, M. I. (2022) RNA induces unique tau strains and stabilizes Alzheimer's disease seeds. *J. Biol. Chem. 298*, 102132.

(103) Kovachev, P. S., Gomes, M. P. B., Cordeiro, Y., Ferreira, N. C., Valadão, L. P. F., Ascari, L. M., Rangel, L. P., Silva, J. L., and Sanyal, S. (2019) RNA modulates aggregation of the recombinant mammalian prion protein by direct interaction. *Sci. Rep. 9*, 1–12.

(104) Grese, Z. R., Bastos, A. C., Mamede, L. D., French, R. L., Miller, T. M., and Ayala, Y. M. (2021) Specific RNA interactions promote TDP-43 multivalent phase separation and maintain liquid properties. *EMBO Rep. 22*, 1–17.

Sub-stoichiometric Hsp104 kinetically modulates the aggregation of a yeast prion determinant to regulate the genesis and persistence of sub-fibrillar seeds

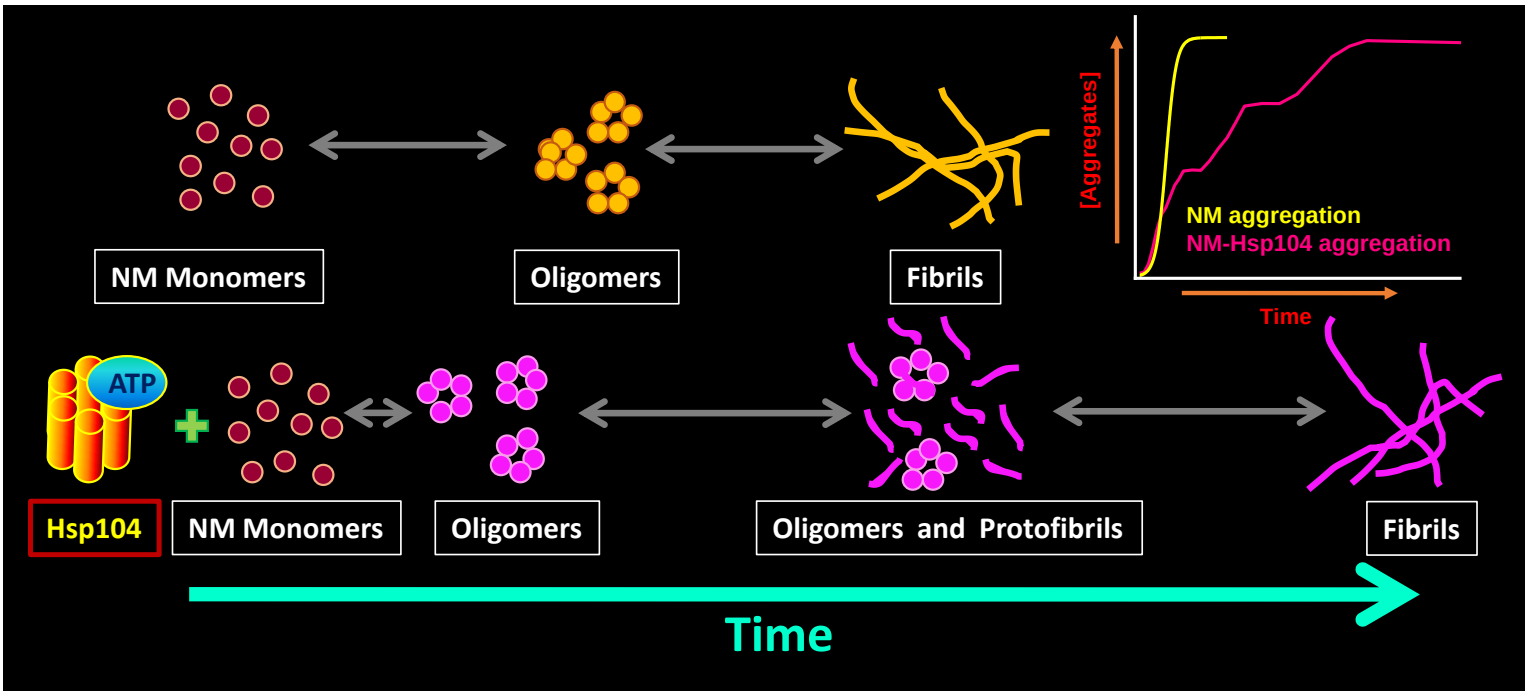

Reference: **Mahapatra, S.**, Sarbahi A., Madhu, P., Swasthi, H. M., Sharma, A., Singh, P., and Mukhopadhyay, S. (2022) Sub-stoichiometric Hsp104 regulates the genesis and persistence of self-replicable amyloid seeds of Sup35 prion domain. *J. Biol. Chem*. 298 ,102143.

2.1 Introduction

Protein misfolding results in the deposition of proteinaceous β-rich amyloid aggregates and is associated with a range of fatal neurodegenerative diseases[1,2]. Prions belong to one of the sub-classes of amyloids that can exhibit a self-perpetuating conformational conversion[3]. They can migrate from a small infected patch to the distal parts of the neuronal tissues resulting in adverse cellular consequences leading to neurodegeneration. The prion-like mechanism has also been proposed for other amyloidogenic proteins such as α-synuclein, tau, amyloid β (Aβ), Huntingtin, p53, and so forth[4,5,6,7,8]. The prion-like spreading in the brain is thought to involve the preformed self-replicable amyloid entities called the propagons or seeds that are considered the minimum units of amyloid infections. Aging increases the frequency of these events as the protein quality control (PQC) system faces challenges[9]. The PQC system comprising a sophisticated network of proteins, called the chaperones, is devoted to the proper folding of nascent polypeptide chains but also guides the unfolded and misfolded proteins to attain the native three-dimensional shape by inhibiting their aberrant aggregation and eliminating irreversibly aggregated proteins[10,11,12]. Disaggregases (Hsp110 in higher eukaryotes; ClpB in *Escherichia coli*; Hsp104 in yeast) belong to an important class of chaperones that are involved in the ATP-dependent and cochaperone-regulated disassembly of aggregated proteins that bypass the other surveillance of the PQC system[13,14,15]. In aged neurons, however, one of the critical manifestations of the PQC dysfunction is the lower expression of these disaggregases, such as Hsp110, Hsp70, and so forth[16]. The insufficiency of the disaggregases has been linked with the amyloid-promoting propensity and its fatal consequence[17].

A functional prion protein (Sup35) that is beneficial to yeast serves as an excellent model to develop the prion concept as well as to elucidate the role of disaggregases in the prion-like transmission of several disease-associated amyloids. This is due to the following reason[18]. Firstly, due to its superstructural resemblance with disease-linked amyloids that exhibit a prion-like propagation. Secondly, the distinct prion phenotypes [PSI^+ and psi^-] and the prion strains can be recapitulated by protein-only transmission using *in vitro*-generated amyloids. Interestingly, these traits exhibit a dose-dependence with respect to the cellular disaggregase machinery of yeasts, namely, Hsp104, a hexameric AAA+ ATPase that controls the cross-generational non-Mendelian inheritance of [PSI^+] phenotype and is reminiscent of the neuron-to-neuron transmission of self-replicable amyloid seeds[19,20,21]. A concerted activity of co-chaperones such as Hsp70 or Hsp40 with Hsp104 is shown to be important for the amyloid remodeling activity *in vivo* and *in vitro*. However, Hsp104 alone can autonomously

disaggregate Sup35 amyloids *in vitro*[13,22]. Additionally, *in vivo* studies showed that the overexpression of Hsp104 alone was sufficient to remodel Sup35 aggregates[23,24]. Whereas, in the case of other yeast prions such as Ure2p, the role of Hsp70 and Hsp40 is considered important for prion propagation[25,13,26]. Therefore, at least for Sup35 amyloids, Hsp104 is believed to be the principal chaperone that governs prion propagation. At higher concentrations, Hsp104 dissolves the aggregates up to the non-infectious level and impairs the passage of the prion phenotype resulting in the curing of the [*PSI*$^+$] phenotype[27]. Also, the genetic or chemical inactivation of Hsp104 hinders the propagation of the [*PSI*$^+$] phenotype due to the unavailability of enough prefibrillar seeds that are generated from matured fibrils by Hsp104[28,29]. Though generation and persistence of prefibrillar amyloids as the seeds for the successful prion-like infection are critical as matured amyloid fibrils show limited infective potential due to their fewer ends of polymerization and lower cytoplasmic diffusibility[30,31]. Understanding the underlying mechanism of prion formation and propagation at low concentrations of Hsp104 is important for the studies related to the disaggregase under-expression during aging and its link with the elevated risk of prion-like amyloid colonization. The studies have suggested that the sub-stoichiometric Hsp104 accelerates the fibrillation that minimizes the existence of prefibrillar aggregates resulting in less efficient fibrillar seeds[32]. Also, the chance of generating prefibrillar seeds indirectly through disaggregating fibrils by Hsp104 in such low concentrations is very nominal[22]. Therefore, collectively these observations do not fully explain the critical aspect of the abundance of prefibrillar amyloid species in the presence of low concentrations of Hsp104, which is crucial in the self-templating cascade of prions.

In this work, we aim at deciphering the molecular mechanism behind the feasible generation of prefibrillar amyloids as effective seeds by only Hsp104 at low concentrations, in the absence of Hsp70 or Hsp40, through *in vitro* recapitulation of the cellular scenario of yeasts in a minimalistic approach. We used the NM domain of the *Saccharomyces cerevisiae* translation termination factor, Sup35. The NM domain is intrinsically disordered in the (monomeric) non-prion form and comprises the N-terminal part abundant in polar uncharged amino acids (glutamine, asparagine, and tyrosine) and a highly charged middle region (M) (Figure 2.1a). The NM domain of Sup35 is necessary and sufficient to recapitulate all the characteristics of the prion state, and therefore, represents a prion determinant in yeast. Using sub-stoichiometric ratios of Hsp104, we detected a pronounced kinetic alteration of the NM aggregation behaviour that supported not only the rapid generation of seeding-competent prefibrillar amyloids but also ensured the prolonged persistence of these species before their

recruitment into matured amyloid fibres. Additionally, we were also able to capture conformationally distinct, Hsp104- remodelled NM species that exhibit a much higher seeding potential.

2.2 Experimental procedures

2.2.1 Materials

HEPES, magnesium chloride hexahydrate, sodium phosphate dibasic dihydrate, tris (hydroxymethyl) aminomethane (Tris), β-mercaptoethanol, ATP disodium salt hydrate, DTT, and ThT were bought from Sigma. GdmCl, proteinase K, and urea were procured from Amresco. Ammonium sulfate, imidazole, lysozyme, SDS, EDTA, and potassium chloride was bought from HIMEDIA. Potassium hydroxide, sodium chloride, sodium hydroxide, glycerol, A-11 anti-amyloid oligomer antibody, methanol, horseradish peroxide (HRP)–conjugated goat anti-rabbit antibody was procured from Merck. IPTG and antibiotics (chloramphenicol and ampicillin) were purchased from Gold Biocom. Enhanced chemiluminescence kit, HRP-conjugated rabbit anti-mouse antibody, was obtained from Thermo Fisher Scientific. Nickel-nitriloacetic acid (Ni-NTA) column and Q-Sepharose were from GE Healthcare Life sciences. Phosphoenolpyruvate (PEP) and pyruvate kinase (PK) were procured from Roche Diagnostics

2.2.2 Expression and purification of Sup35NM

C-terminal hexa-histidine recombinant Sup35NM proteins were overexpressed in BL21 (DE3)/pLysS cells using IPTG and then from the harvested cells proteins were extracted; the extracted proteins were subjected to first Ni-NTA purification in the gradient of imidazole and further from a Q-sepharose column using the gradient of sodium chloride. The detailed protocol is described by us.[33]

2.2.3 Expression and purification of Hsp104

A modification of a previous protocol was used [34]. N-terminal His_6-tag recombinant Hsp104 pPROEX-HTb Hsp104 of *S. cerevisiae* were overexpressed in BL21(DE3) RIL E. coli cells using 1 mM IPTG as inducer at 15 C for 14 h. Harvested cells suspended in chilled 10 ml lysis buffer (40 mM HEPES–KOH pH 7.4, 500 mM KCl, 20 mM $MgCl_2$, 2.5% (w/v) glycerol, 20 mM imidazole) were incubated in 4 C with lysozyme (2 mg/ml) followed by sonication. The cell debris was removed by centrifugation at 11,500 rpm for 30 min, and the supernatant was subject to Ni-NTA purification using the gradient of imidazole. After Ni-NTA purification, the eluant was buffer exchanged with the (20 mM Tris–HCl pH 8, 0.5 mM EDTA, 5 mM $MgCl_2$,

50 mM NaCl) using MWCO 30,000 Amicon Ultra (Millipore) 15 ml centrifugal concentrator units. The protein further purified using the Q-sepharose column using the gradient of NaCl, and the eluant was further buffer exchanged with the cleavage buffer (20 mM HEPES–KOH pH 7.4, 140 mM KCl, and 10 mM $MgCl_2$) using the concentrator unit mentioned previously. Recombinant Tobacco Etch virus (TEV) protease carrying a hexa-histidine tag was used at a ratio His_6- Hsp104: TEV protease (15:1) to cleave the histidine (His_6) tag of the Hsp104 at 30 ^oC for 1 h. The cleaved His_6 tags of Hsp104, the uncleaved His_6-Hsp104, and the histidine-tagged TEV protease were removed by binding them with the Ni-NTA resin, and in the flow-through, the pure Hsp104 with no histidine tags were collected and stored in a storage buffer (20 mM HEPES–KOH pH 7.4, 140 mM KCl, and 10 mM $MgCl_2$, 1 mM DTT, 0.5 mM EDTA) at −80 ^{o} C until further use. The luciferase reactivation assay confirmed the activity of Hsp104. Luciferase (80 nM) in Tris–HCl buffer, pH 7.4, was denatured at 45 ^oC for 7 min, chemiluminescence were recorded before and after denaturation. The chemiluminescence was also recorded for denatured luciferase without or with bi-chaperone (Ssa1 1 μM, Ydj1 1 μM) or tri-chaperone preparations (Ssa1 1 μM, Ydj1 1 μM, Hsp104 6 μM) in the presence of the Luciferase assay reagent, 1 mM ATP, 1 mM DTT, and ATP-regeneration system in Tris–HCl buffer, pH 7.4. The extent of recovery of luciferase was calculated by the percentage of chemiluminescence generated with respect to the native luciferase, which was more in the case of tri-chaperone machinery compared to the bi-chaperone machinery. This validated the activity of Hsp104 used in this study.

2.2.4 Amyloid aggregation reactions

For the setting up of aggregation reactions, methanol precipitated NM was dissolved in 8 M urea (20 mM Tris–HCl buffer, pH 7.4) for 3 h at RT. Monomerized protein was first passed through a 100 kDa filter to remove any preexisting aggregates if present, and subsequently, the filtrate was concentrated using a 3 kDa filter before the aggregation reaction. The concentrated monomers of NM were further centrifuged at 13,000 rpm for 15 min at RT, after which the supernatant was added such that, its final concentration is 2.5 μM in assembly buffer (40 mM HEPES–KOH pH 7.4, 150 mM KCl, 20 mM $MgCl_2$, 1 mM DTT, 10 μM ThT) without or with Hsp104 and 5 mM ATP and ATP-regeneration system (20 mM PEP and PK (15 μg/ml) at RT under stirring at 80 rpm using the magnetic beads. ThT fluorescence was monitored RT by exciting at 450 nm, and the fluorescence emission was recorded at 480 nm. Hsp104 influenced NM aggregation reactions were also carried out under the same aggregation conditions and

assembly buffer independently with ATP, ATP-regeneration system, and 3 mM GdmCl in the assembly buffer and also in the absence of ATP and ATP-regeneration system.

2.2.5 Dot-blot assays

Monomeric NM (2.5 μM) was aggregated in the assembly buffer (40 mM HEPES–KOH pH 7.4, 150 mM KCl, 20 mM $MgCl_2$, 1 mM DTT) in the presence of Hsp104 (0.025 μM), ATP (5 mM), and ATP-regeneration system (20 mM PEP and 15 μg/ml PK) at RT under stirring at 80 rpm, and after 7 h and 30 h from the commencement of the reaction, the aliquots (2 μl) were spotted on the nitrocellulose membrane. NM monomers (2.5 μM) were also aggregated in the absence of Hsp104 and ATP for 7 h under the same conditions in the same assembly buffer and spotted (2 μl) on the nitrocellulose membrane. The blots were blocked using 3% bovine serum albumin in PBS with Tween-20 (PBST) (0.05 % Tween-20) for 1 h at RT and then probed with the primary antibody. (A11; 1:500) and (anti-His; 1:10,000) overnight at 4 C. The blots were washed six times with PBST and incubated with an appropriate HRP-conjugated secondary antibody for 1 h at RT. Again, the blots were washed thrice using PBST and subsequently developed using an ECL kit.

2.2.6 Estimation of the Sup35NM monomers recruited in the amyloids

Monomeric NM (2.5 μ M) was aggregated in the assembly buffer (40 mM HEPES–KOH PH 7.4, 150 mM KCl, 20 mM $MgCl_2$, 1 mM DTT) without or with Hsp104 (0.025 μ M), ATP (5 mM), and the ATP-regeneration system (20 mM PEP and 15 μg/ml PK) for 6 h or 30 h, respectively, at RT under stirring at 80 rpm, and the amyloids generated in the reactions were pelleted down at 16,400 rpm for 30 min. The pellets were resuspended in 8 M urea (20 mM Tris–HCl, pH 7.4) overnight to monomerize the amyloids, and SDS-PAGE was performed. The Coomassie-stained monomeric NM band intensities were relatively estimated using the ImageJ software (www.imagej. nih.gov) concerning the band corresponding to the monomers of a known NM concentration in 8 M urea (20 mM Tris– HCl, pH 7.4)[35]. To validate the occurrence of secondary nucleation, aliquots were taken from the Hsp104-mediated NM aggregation reaction after 6 h and 30 h, respectively, from the commencement of the aggregation reactions. The amyloids so formed were retrieved and then monomerized in 8 M urea (20 mM Tris–HCl, pH 7.4) following the protocol mentioned previously, and after the SDS-PAGE, the fraction of monomers recruited in the amyloids were compared in both the samples by comparing the Coomassie band intensities of the NM monomers using the ImageJ software. NM monomers (2.5 μM) were aggregated without or with 0.05 μM Hsp104 at RT

and stirred at 80 rpm for 6 h or 30 h, respectively. Then, the generated NM or NM-Hsp104 fibrils were precipitated by centrifugation at 16,400 rpm for 30 min. The retrieved pellets were resuspended in 8 M urea (20 mM sodium phosphate, pH 7.4) and kept overnight before the SDS-PAGE analysis.

2.2.7 Atomic Force Microscopy

Monomeric NM (2.5 μμ M) was aggregated in the assembly buffer (40 mM HEPES–KOH pH 7.4, 150 mM KCl, 20 mM $MgCl_2$, 1 mM DTT) without or with Hsp104 (0.025 μμ M), ATP (5 mM), and the ATP-regeneration system (20 mM PEP and 15 μg/ml PK), and samples were aliquoted after different time points from the commencement of the reactions for imaging. For some samples for AFM, Hsp104, and ATP were introduced after 1 h from the commencement of the reaction, and samples were aliquoted after indicated time points after. For AFM imaging, the mica was freshly cleaved and washed with filtered water. Twenty microliters of the sample was deposited on mica. The sample was incubated for 5 min. The mica was washed with 100 μl of filtered water twice, followed by drying under a gentle nitrogen stream. The AFM images were acquired on Innova atomic force microscope (Bruker) using the NanoDrive (v8.03) software (www.bruker.com). The images were processed and analyzed using the WSxM 5.0 Develop software (www.wsxm.eu)[36]. The height profiles were plotted using Origin 9.65 (www.originlab.com).

2.2.8 Statistical analysis

All the experiments were repeated at least three times, and the data are represented as mean ± SD showing the scattered data points from independent experimental replicates. The statistical significance analysis was performed by one-way ANOVA tests, and the *p*-values were reported in the figure legends. All the data analysis, data fitting (adjusted $R^2 > 0.95$), and data plotting were performed using Origin 9.6.

2.3 Results

2.3.1 Hsp104 modulates the NM assembly kinetics

As a prelude to the aggregation studies, we confirmed by luciferase reactivation assay that the Hsp104 used by us were functionally active (Figure 2.1b). We first carried out the amyloid formation kinetics at a low micromolar protein concentration in the absence of Hsp104 using a well-known amyloid reporter, namely, thioflavin-T (ThT). The aggregation of NM (2.5 μM) proceeded via typical nucleation-dependent polymerization kinetics possessing a lag phase of approximately 50 min, an assembly phase, and a saturation phase (Figure 2.1c)[37,38] . In order to investigate the effect of the low concentrations of Hsp104 in NM assembly, we performed the aggregation kinetics in the presence of Hsp104 at several sub-stoichiometric ratios

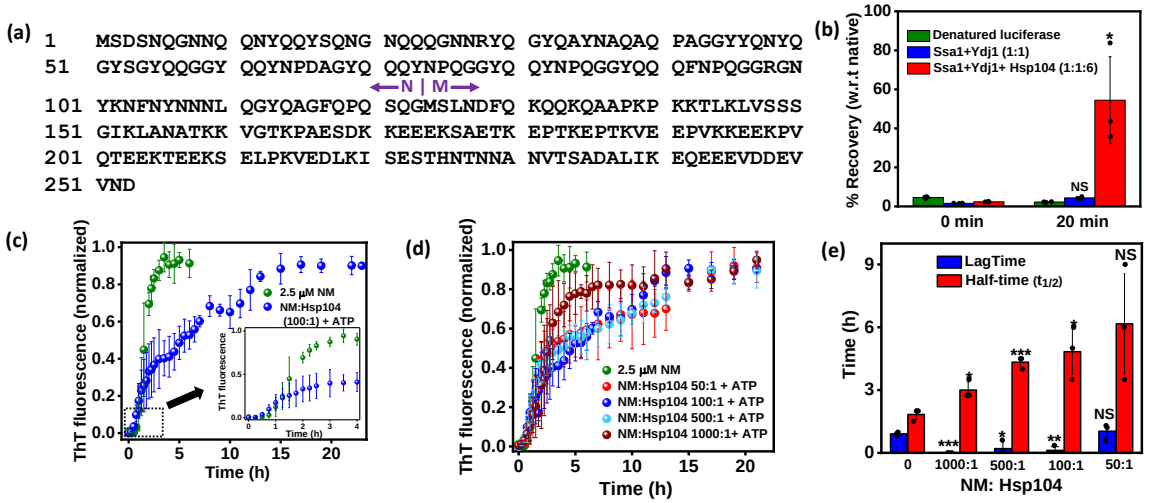

Figure 2.1. (a) The amino acid sequence of Sup35NM showing the putative boundary between the N- and M-domain. (b) Luciferase reactivation assay using denatured luciferase (80 nM) in the absence or presence of Ssa1 (1 μM) and Ydj1 (1 μM), also in the presence of Ssa1 (1 μM) , Ydj1 (1 μM) and Hsp104 (6 μM) with ATP (1 mM) and ATP regeneration system. The extent of recovery of luciferase was calculated by the percentage of chemiluminescence with respect to native luciferase. Standard deviations were estimated using three independent replicates (n = 3). NS for Ssa1-Ydj1, *P < 0.05 for Ssa1-Ydj1-Hsp104 with respect to denatured luciferase. (One-way ANOVA) (c) Normalized thioflavin-T (ThT) fluorescence kinetics of NM (2.5 μM) without or with Hsp104 (0.025 μM) and ATP (5 mM) during amyloid formation (stirred at 80 rpm at room temperature). The kinetics of the first 5 h from the commencement of the reactions are shown in the inset. (d) Normalized ThT fluorescence kinetics of NM (2.5 μM) without or with Hsp104 and ATP (5 mM) during amyloid formation at room temperature and 80 rpm showing the 20 h of aggregation. Standard deviations were estimated from three independent experiments (n = 3) (e) The lag time and $t_{1/2}$ of the NM aggregations without or with various sub-stoichiometric ratios of Hsp104. The lag times were retrieved by fitting the first 6 h fluorescence intensities to sigmoidal function, and $t_{1/2}$ were determined from the time points when the normalized fluorescence intensities reached 0.5. The SDs were calculated from three independent experiments (n = 3). $***p < 0.001$, $*p < 0.05$, $**p < 0.01$, NS (not significant) for NM: Hsp104 1000:1, 500:1, 100:1, 50:1, respectively, compared to the lag time of aggregation reactions without Hsp104. $*p < 0.05$, $***p <$

0.001, $*p < 0.05$, NS for NM: Hsp104 1000:1, 500:1, 100:1, 50:1, respectively, compared to the half-time of the aggregation reactions without Hsp104 (One-way ANOVA).

containing ATP and an ATP regeneration system. We observed rapid oligomerization of NM and shortening of the lag phase in the presence of Hsp104, an observation that is consistent with the previous study. At the lowest concentration of Hsp104 (NM: Hsp104 = 1000:1), the lag phase is almost abolished. Interestingly, the shortening of the lag phase in the presence of a low concentration of Hsp104 is associated with a delay in the assembly phase. This observation indicated that the assembly and maturation of Hsp104-induced early species get retarded in a dose-dependent manner (Figure 2.1d,e). Next, in order to directly visualize the nanoscale morphology, we carried out atomic force microscopy (AFM) imaging. In the Hsp104-mediated NM aggregation reaction, a mixture of spherical oligomers and protofibrils were observed that matured into longer fibrils after 30 h from the commencement of the reaction. In contrast, in the absence of Hsp104, we observed primarily matured fibrils at a much earlier time point (7 h) (Figure 2.2a-c). We validated the early oligomerization by Hsp104 by probing both the aggregation reactions at the early time points by an oligomer-specific antibody such as the A11 antibody[39,40]. More intense signals from the spots corresponding to the Hsp104-mediated aggregation reaction confirmed an increased oligomerization in the early time points compared to the NM-only aggregation reaction (Figure 2.2d,e). Next, we wanted to test if the observed spherical aggregates formed after 7 h Modulation of amyloidogenesis of a yeast prion by Hsp104 during the NM-Hsp104 reaction retained the characteristics of amyloid oligomers. We were able to detect the A11- positive signal, albeit weaker, indicating the existence of a smaller fraction of the oligomeric species in the presence of Hsp104 but not in its absence. This weak A11-reactivity in the presence of sub-stoichiometric Hsp104 disappeared after 30 h, presumably due to the complete conversion of the oligomeric species into matured fibrils (Figure 2.2f,g). Therefore, early spherical oligomers and/or short (submicron) protofibrils can possibly represent crucial prefibrillar species. Together, this set of results showed that Hsp104, at a sub-stoichiometric concentration, accelerates the early

oligomerization events but decelerates the growth kinetics allowing a prolonged persistence of prefibrillar species (oligomers and protofibrils) before they mature into amyloid fibres.

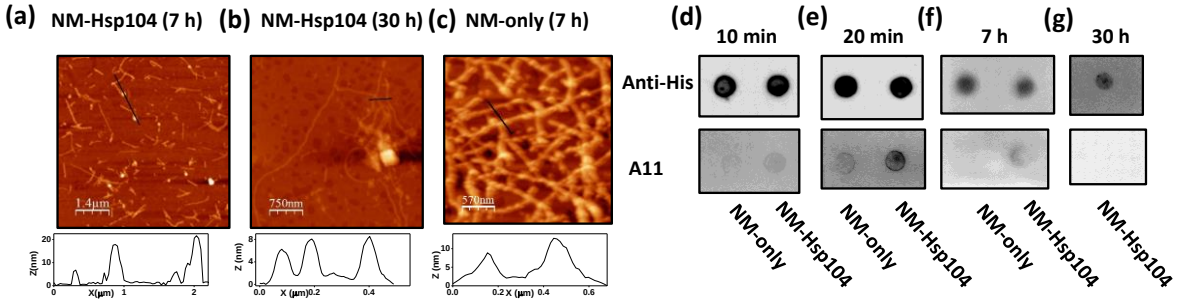

Figure 2.2 (a,b) AFM images of NM amyloids (2.5 μM monomers) showing the oligomers and protofibrils with the height of ~20 nm and 7 nm, respectively, in the presence of Hsp104 (0.025 μM), plus ATP after 7 h (a) and fibrils with the height ~7 nm after 30 h (b). (c) AFM image of NM fibrils (2.5 μM monomers) formed after 7 h of aggregation in the absence of Hsp104 with the height ~9 nm. (d-g) Samples from the NM aggregation reactions without or with Hsp104 (NM:Hsp104 100:1) and ATP were spotted on nitrocellulose membrane after (d) 10 min, (e) 20 min, (f) 7 h, and after (g) 30 h for NM-Hsp104 aggregation only, from the commencement of the reactions and dot-blotted with the anti-His and A11 antibodies.

2.3.2 The role of Hsp104-mediated disaggregation in the NM assembly kinetics

Next, we asked whether the modulation in the aggregation kinetics by Hsp104 is due to its specific disaggregase activity or a passive perturbation in the NM polymerization by this chaperone. In order to distinguish between these two possibilities, the aggregation reaction of NM monomers with Hsp104 was set up in the absence of ATP, as Hsp104 is ATP-dependent amyloid disassembling machinery, and we did not observe any measurable change in the aggregation kinetics (Figure 2.3a). We also performed NM aggregation with Hsp104 and ATP but in the presence of a millimolar concentration of guanidinium hydrochloride (GdmCl) that acts as a potent inhibitor of Hsp104 by preventing its ATP hydrolysis-dependent disaggregase activity[41,42]. In this case, we did not observe any changes in the aggregation profile, suggesting a coordinated role of ATPase and disaggregase activities of Hsp104 in altering the NM aggregation behavior (Figure 2.3b). On this basis, we further tested if there was a different extent of monomer recruitment in amyloids in NM-only and Hsp104-mediated NM assembly due to their pronounced kinetic dissimilarities. However, when we retrieved the high molecular weight aggregates in the pellet fraction after the completion of aggregation reactions by high-speed centrifugation and monomerized them using the denaturant, we observed similar band intensities of the NM band on SDS-PAGE for NM-only and Hsp104-mediated NM aggregations. This indicates the recruitment of nearly the same fraction of NM monomers into

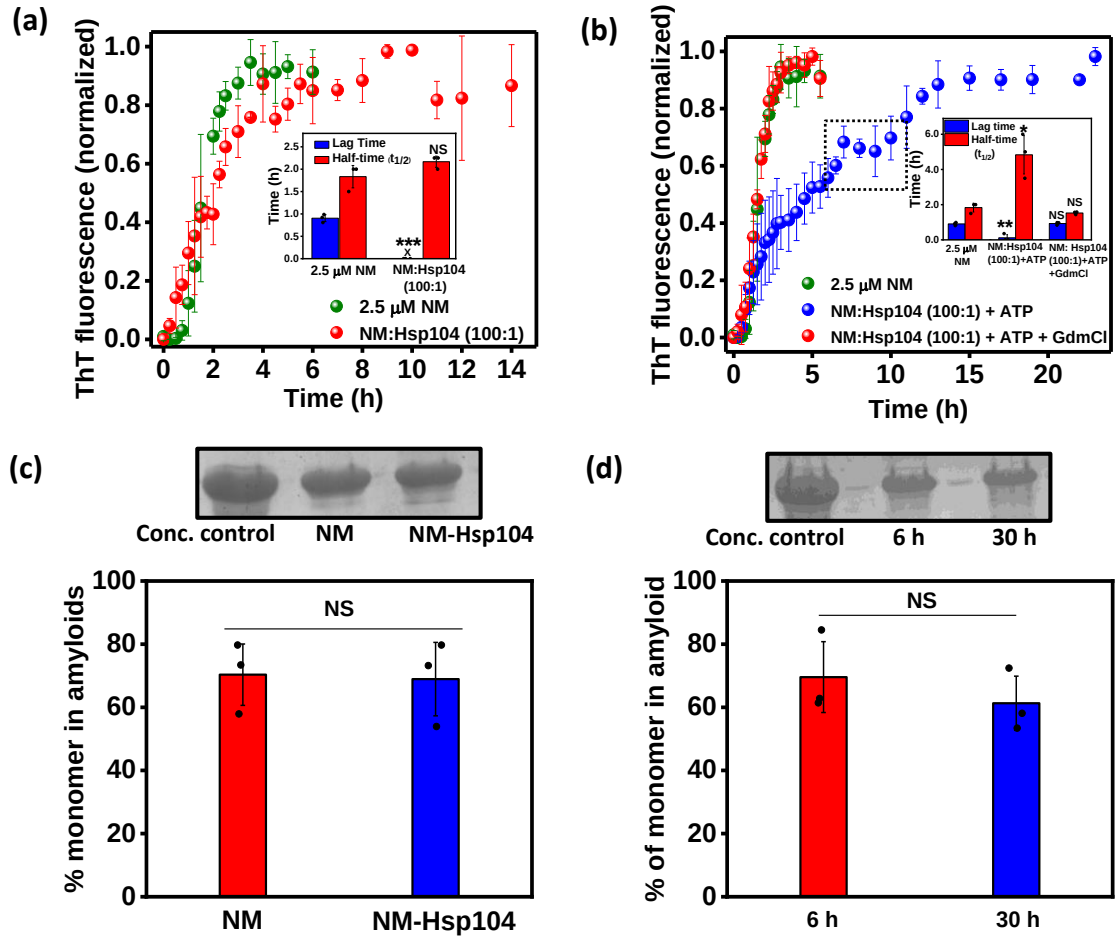

Figure 2.3. (a) Normalized ThT fluorescence kinetics of rotated (80 rpm) NM (2.5 μM) aggregation without or with Hsp104 (0.025 μM). The lag time and $t_{1/2}$ are retrieved from three independent experimental replicates (n = 3), ∗∗∗p < 0.001, NS for lag time and $t_{1/2}$, respectively, compared to the NM-only aggregation. (One-way ANOVA) (inset). (b) Normalized ThT fluorescence kinetics of rotated (80 rpm) NM (2.5 μM) aggregation without or with Hsp104 (0.025 μM), plus ATP and with Hsp104 (0.025 μM) and ATP, in the presence of GdmCl (3 mM) in the assembly buffer that alone does not alter the NM aggregation. Representative 'halt' in the NM-Hsp104 aggregation is marked. The lag time and $t_{1/2}$ are retrieved from three independent experimental replicates (n = 3). NS, NS for lag time and $t_{1/2}$ of NM-Hsp104-GdmCl aggregation and ∗∗p < 0.01, ∗p < 0.05 for lag time and $t_{1/2}$, respectively, for NM-Hsp104 aggregation compared to NM-only aggregation (One-way ANOVA) (inset). (c) The relative quantification by ImageJ software of NM monomers retrieved from the amyloids formed from the rotated (80 rpm) polymerization of NM (2.5 μM) without or with Hsp104 (0.025 μM) and ATP for 6 h or 30 h, respectively, with respect to the concentration control in SDS-PAGE. SDs were estimated from three independent replicates (n = 3), NS compared to NM samples (One-way ANOVA). (d) The relative quantification by ImageJ software of NM monomers retrieved from the amyloids in the aliquots of rotated (80 rpm) polymerization of NM (2.5 μM) with Hsp104 (0.025 μM) and ATP, aliquoted before the 'halt' marked in Figure 2.3b (6 h from the commencement of the aggregation) and at the end of the polymerization (30 h from the commencement of the aggregation). SDs were estimated from three independent replicates (n = 3), NS compared to NM samples (One-way ANOVA).

aggregates in both types of reactions (Figure 2.3c). By the scrutiny of the aggregation profiles, we noticed some temporary halts resulting in separable biphasic kinetics (marked in Figure 3b)

in the amyloid formation in NM-Hsp104 aggregation reactions, more pronounced in the relatively higher ratios of Hsp104, and often these halts in the aggregation are reported to be associated with the fresh recruitment of monomers on preformed amyloid surfaces via the secondary nucleation mechanism[43]. To assess the possibility of secondary nucleation here, we aliquoted the NM-Hsp104 reaction mixture just before the halt and after the completion of the aggregation and then the retrieved amyloids were monomerized using the denaturant. The nearly identical monomeric NM band intensities in the SDS-PAGE in both pre-halt and post-halt samples ensured no additional recruitment of monomers (Figure 2.3d). Also, such Hsp104 dose-dependent halts were absent both in the absence of ATP that drives the Hsp104 disaggregase machinery and in the presence of 3 mM concentration of GdmCl that acts as a small-molecule inhibitor of Hsp104 (Figure 2.3a,b). Together, this set of data suggested the specific ATP-dependent, GdmCl-sensitive, enzymatic activity of Hsp104 in the modulation of the NM assembly kinetics resulted from an intricate balance between the intrinsic propensity of the amyloidogenic intermediates to mature into higher-order amyloid species and Hsp104-mediated amyloid disaggregation. We, however, would like to point out that we cannot completely rule out the possibility of secondary nucleation that might partially contribute to the observed multiphasic kinetics.

2.3.3 The role of Hsp104 in amyloid maturation

During the budding process of yeasts, the daughter cells receive a fraction of the cytoplasm from their mothers containing the preformed amyloid species of various molecular weights. Inefficient conversion of these low molecular weight aggregates into matured fibers is critical to maintain and propagate the amyloid-linked [*PSI*$^{+}$] phenotype because of the limited infectivity of the mature fibers. Therefore, in order to delineate the putative role of Hsp104 in the persistence of low molecular weight amyloid species, we introduced a low concentration of Hsp104 with ATP at the late lag phase (0.5 h after commencement of the reaction) and at the early log phase (1 h after commencement of the reaction) of NM aggregation reactions. The kinetics revealed that Hsp104 delayed the maturation of these already formed particles to the higher-order amyloids resulting in the persistence of shorter protofibrils that eventually converted into matured fibrils at a much later time as observed by AFM (Figure 2.4a-c). In contrast, when Hsp104 and ATP were introduced at the end of the elongation phase (3 h after commencement of the reaction) of the NM aggregation, no significant modulation in the

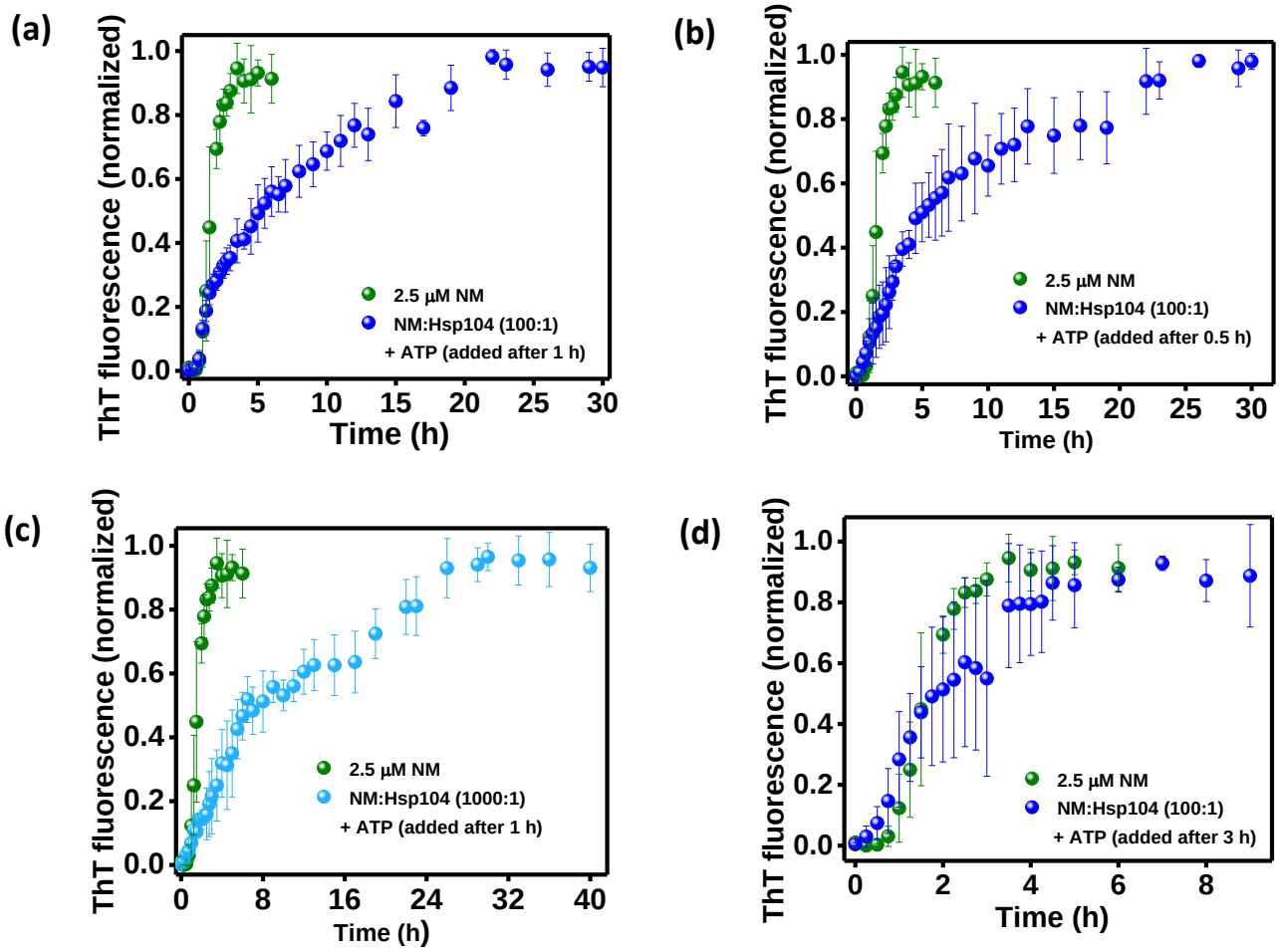

Figure 2.4. (a,b) Normalized ThT fluorescence kinetics of rotated (80 rpm) NM (2.5 μM) aggregation without or with Hsp104 (0.025 μM), plus ATP, introduced after (a) 1 h (b) 0.5 h from the commencement of the reaction. SDs were calculated from three independent experiments (n = 3). (c) Normalized ThT fluorescence kinetics of rotated (80 rpm) NM (2.5 μM) aggregation without or with Hsp104 (0.0025 μM), plus ATP, introduced after 1 h from the commencement of the reaction. Standard deviations were calculated from three independent experiments (n = 3). (d) Normalized ThT fluorescence kinetics of rotated (80 rpm) NM (2.5 μM) aggregation without or with Hsp104 (0.025 μM), plus ATP, introduced after 3 h from the commencement of the reaction. Standard deviations were calculated from three independent experiments (n = 3).

aggregation kinetics was observed. This observation revealed the inability of the low concentration of Hsp104 to manipulate the higher molecular weight aggregates (Figure 2.4d). Together, these results tell us to surmise that the low concentration of Hsp104 enhanced the abundance of low molecular weight species as opposed to mature fibrils not only by amending the de novo aggregation but also decelerating the conversion of the preformed amyloid species to higher molecular weight fibres.

2.4 Discussion

Irrespective of the precise mechanistic differences between the prion-like propagation of neurotoxic species by the transmission of seeds across the cellular membrane and the cross-generational cytoplasmic inheritance of amyloid-associated phenotypic traits by fungal prion particles in the continuous stream of cytoplasm from mother to daughter yeast cells, the successful expedition of infectious amyloid particles into the uninfected cells revolves around the autocatalytic behavior of prefibrillar amyloids[44,31,45]. In this study, by *in vitro* reconstruction, we were able to recapitulate a critical pro-prion aspect of sub-stoichiometric Hsp104.

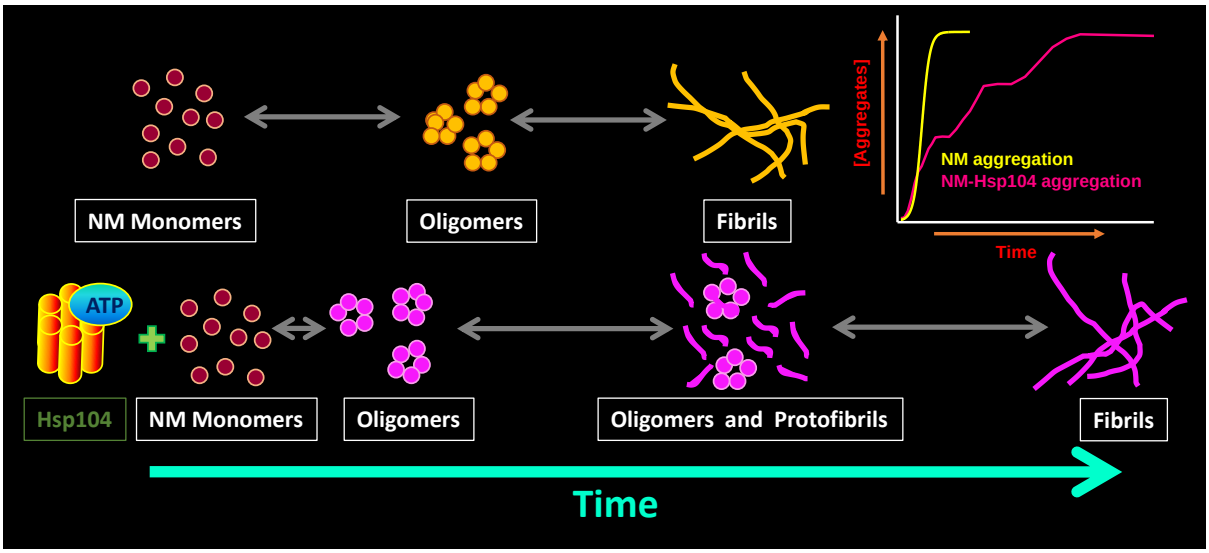

Figure 2.5. Sub-stoichiometric Hsp104 accelerates the formation of amyloids but delays their maturation into fibrils by creating kinetic halts.

low concentrations of the Hsp104 facilitated the production of seeding-competent amyloid entities and decelerated the conversion of these prefibrillar species into matured fibrils. Contrary to the view of irreversible hindrance in the fibrillation of various intermediate amyloid species of different amyloidogenic proteins, including full-length *S. cerevisiae* Sup35 by Hsp104, here we observed a trade-off between the two opposing factors, namely, the intrinsic nature of NM amyloids to polymerize into higher molecular weight aggregates and the ATP-dependent GdmCl-sensitive disaggregation by Hsp104 that delayed but not inhibited the fibrillation as showed in Figure 2.5[46,47]. Furthermore, the critical balance between these two mutually opposing factors resulted in the observed halts resulting in apparent biphasic kinetics as GdmCl, the Hsp104- inhibitor, eliminated the halts. In contrast, the higher concentrations of Hsp104 increased the duration of kinetic halts. These halts allowed a prolonged persistence of the prefibrillar particles, pivotal for the propagation of the prion phenotype.

In summary, our findings indicate the pro-[*PSI*$^{+}$] nature of the sub-stoichiometric concentrations of Hsp104, which aid the generation and persistence of the highly transmissible prefibrillar seeding-proficient amyloid species that do not readily transform into matured fibres. The Hsp104-mediated hindrance in the conversion of low molecular weight aggregates into matured fibres is crucial in maintaining and propagating the amyloid-linked [*PSI*$^{+}$] phenotype in yeast. The disaggregase activity and kinetic modulation of HSPs on a wide range of proteins leading to the generation and persistence of highly transmissible self-replicating amyloid species can potentially underlie a consensus mechanism for the generation and colonization of the toxic, transmissible, neuropathological prefibrillar amyloids.

2.5 References

(1) Chiti, F., and Dobson, C. M. (2006) Protein Misfolding, Functional Amyloid, and Human Disease. *Annu. Rev. Biochem. 75*, 333–366.

(2) Ke, P. C., Zhou, R., Serpell, L. C., Riek, R., Knowles, T. P. J., Lashuel, H. A., Gazit, E., Hamley, I. W., Davis, T. P., Fändrich, M., Otzen, D. E., Chapman, M. R., Dobson, C. M., Eisenberg, D. S., and Mezzenga, R. (2020) Half a century of amyloids: Past, present and future. *Chem. Soc. Rev. 49*, 5473–5509.

(3) Si, K. (2015) Prions: What Are They Good For? *Annu. Rev. Cell Dev. Biol. 31*, 149–169.

(4) Brundin, P., and Melki, R. (2017) Prying into the prion hypothesis for parkinson's disease. *J. Neurosci. 37*, 9808–9818.

(5) Goedert, M., Masuda-Suzukake, M., and Falcon, B. (2017) Like prions: The propagation of aggregated tau and α-synuclein in neurodegeneration. *Brain 140*, 266–278.

(6) Walker, L. C., Schelle, J., and Jucker, M. (2016) The Prion-Like Properties of Amyloid- b Assemblies : Implications for Alzheimer ' s Disease 1–14.

(7) Masnata, M., Sciacca, G., Maxan, A., Bousset, L., Denis, H. L., Lauruol, F., David, L., Saint-Pierre, M., Kordower, J. H., Melki, R., Alpaugh, M., and Cicchetti, F. (2019) Demonstration of prion-like properties of mutant huntingtin fibrils in both in vitro and in vivo paradigms. *Acta Neuropathol. 137*, 981–1001.

(8) Costa, D. C. F., de Oliveira, G. A. P., Cino, E. A., Soares, I. N., Rangel, L. P., and Silva, J. L. (2016) Aggregation and prion-like properties of misfolded tumor suppressors: Is cancer a prion disease? *Cold Spring Harb. Perspect. Biol. 8*, 1–22.

(9) Hou, Y., Dan, X., Babbar, M., Wei, Y., Hasselbalch, S. G., Croteau, D. L., and Bohr, V. A. (2019) Ageing as a risk factor for neurodegenerative disease. *Nat. Rev. Neurol. 15*, 565–581.

(10) Wolff, S., Weissman, J. S., and Dillin, A. (2014) Differential scales of protein quality control. *Cell 157*, 52–64.

(11) Hartl, F. U., Bracher, A., and Hayer-Hartl, M. (2011) Molecular chaperones in protein folding and proteostasis. *Nature 475*, 324–332.

(12) Hipp, M. S. (2019) The proteostasis network and its decline in ageing. *Nat. Rev. Mol. Cell Biol.*

(13) Glover, J. R., and Lindquist, S. (1998) Hsp104, Hsp70, and Hsp40: A novel chaperone system that rescues previously aggregated proteins. *Cell 94*, 73–82.

(14) Yuan, A. H., Garrity, S. J., Nako, E., and Hochschild, A. (2014) Prion propagation can occur in a prokaryote and requires the ClpB chaperone. *Elife 3*, 1–19.

(15) Mogk, A., Bukau, B., and Kampinga, H. H. (2018) Cellular Handling of Protein Aggregates by Disaggregation Machines. *Mol. Cell 69*, 214–226.

(16) Tittelmeier, J., Sandhof, C. A., Ries, H. M., Druffel-Augustin, S., Mogk, A., Bukau, B., and Nussbaum-Krammer, C. (2020) The HSP110/HSP70 disaggregation system generates spreading-competent toxic α-synuclein species. *EMBO J. 39*, 1–16.

(17) Feleciano, D. R., Juenemann, K., Iburg, M., Brás, I. C., Holmberg, C. I., and Kirstein, J. (2019) Crosstalk between chaperone-mediated protein disaggregation and proteolytic pathways in aging and disease. *Front. Aging Neurosci. 11*, 1–16.

(18) Chernova, T. A., Chernoff, Y. O., and Wilkinson, K. D. (2019) Yeast models for amyloids and prions: Environmental modulation and drug discovery. *Molecules 24*, 1–23.

(19) Ter-Avanesyan, M. D., Dagkesamanskaya, A. R., Kushnirov, V. V., and Smirnov, V. N. (1994) The SUP35 omnipotent suppressor gene is involved in the maintenance of the non-Mendelian determinant [psi+] in the yeast Saccharomyces cerevisiae. *Genetics 137*, 671–676.

(20) Parsell, D. A., Kowal, A. S., Singer, M. A., and Lindquist, S. (1994) Protein disaggregation. *Nature 372*, 475–478.

(21) Grimminger-Marquardt, V., and Lashuel, H. A. (2010) Structure and function of the

molecular chaperone Hsp104 from yeast. *Biopolymers 93*, 252–276.

(22) Desantis, M. E., and Shorter, J. (2012) Hsp104 drives "protein-only" positive selection of sup35 prion strains encoding strong [PSI+]. *Chem. Biol. 19*, 1400–1410.

(23) Klaips, C. L., Hochstrasser, M. L., Langlois, C. R., and Serio, T. R. (2014) Spatial quality control bypasses cell-based limitations on proteostasis to promote prion curing. *Elife 3*, 1–24.

(24) Zhao, X., Rodriguez, R., Silberman, R. E., Ahearn, J. M., Saidha, S., Cummins, K. C., Eisenberg, E., and Greene, L. E. (2017) Heat shock protein 104 (Hsp104)-mediated curing of [PSI+] yeast prions depends on both [PSI+] conformation and the properties of the Hsp104 homologs. *J. Biol. Chem. 292*, 8630–8641.

(25) Moriyama, H., Edskes, H. K., and Wickner, R. B. (2000) [URE3] Prion Propagation in Saccharomyces cerevisiae : Requirement for Chaperone Hsp104 and Curing by Overexpressed Chaperone Ydj1p . *Mol. Cell. Biol. 20*, 8916–8922.

(26) Desantis, M. E., and Shorter, J. (2012) Hsp104 drives "protein-only" positive selection of sup35 prion strains encoding strong [PSI+]. *Chem. Biol. 19*, 1400–1410.

(27) Greene, L. E., Zhao, X., and Eisenberg, E. (2018) Curing of [PSI+] by Hsp104 Overexpression: Clues to solving the puzzle. *Prion 12*, 9–15.

(28) Ness, F., Ferreira, P., Cox, B. S., and Tuite, M. F. (2002) Guanidine Hydrochloride Inhibits the Generation of Prion "Seeds" but Not Prion Protein Aggregation in Yeast. *Mol. Cell. Biol. 22*, 5593–5605.

(29) Park, Y. N., Morales, D., Rubinson, E. H., Masison, D., Eisenberg, E., and Greene, L. E. (2012) Differences in the curing of [PSI+] prion by various methods of Hsp104 inactivation. *PLoS One 7*.

(30) Xue, W., Hellewell, A. L., Hewitt, E. W., Radford, S. E., Hellewell, A. L., Hewitt, E. W., Radford, S. E., Xue, W., Hellewell, A. L., Hewitt, E. W., and Radford, S. E. (2010) When size matters *6896*.

(31) Marchante, R., Beal, D. M., Koloteva-Levine, N., Purton, T. J., Tuite, M. F., and Xue, W. F. (2017) The physical dimensions of amyloid aggregates control their infective potential as prion particles. *Elife 6*, 1–20.

(32) Shorter, J., and Lindquist, S. (2004) Hsp104 catalyzes formation and elimination of self-replicating Sup35 prion conformers. *Science 304*, 1793–1797.

(33) Narang, D., Swasthi, H. M., Mahapatra, S., and Mukhopadhyay, S. (2017) Site-Specific Fluorescence Depolarization Kinetics Distinguishes the Amyloid Folds Responsible for Distinct Yeast Prion Strains. *J. Phys. Chem. B 121*, 8447–8453.

(34) Sweeny, E. A., Desantis, M. E., and Shorter, J. (2011) Purification of Hsp104, a protein disaggregase. *J. Vis. Exp.* 2–9.

(35) Schneider, C. A., Rasband, W. S., and Eliceiri, K. W. (2012) HISTORICAL commentary NIH Image to ImageJ : 25 years of image analysis. *Nat. Methods 9*, 671–675.

(36) Horcas, I., Fernández, R., Gómez-Rodríguez, J. M., Colchero, J., Gómez-Herrero, J., and Baro, A. M. (2007) WSXM: A software for scanning probe microscopy and a tool for nanotechnology. *Rev. Sci. Instrum. 78*.

(37) Adamcik, J., and Mezzenga, R. (2018) Amyloid Polymorphism in the Protein Folding and Aggregation Energy Landscape. *Angew. Chemie - Int. Ed. 57*, 8370–8382.

(38) Lakowicz, J. R. (2006) Principles of fluorescence spectroscopy. *Princ. Fluoresc. Spectrosc.*

(39) Kayed, R., Head, E., Sarsoza, F., Saing, T., Cotman, C. W., Necula, M., Margol, L., Wu, J., Breydo, L., Thompson, J. L., Rasool, S., Gurlo, T., Butler, P., and Glabe, C. G. (2007) Fibril specific, conformation dependent antibodies recognize a generic epitope common to amyloid fibrils and fibrillar oligomers that is absent in prefibrillar oligomers. *Mol. Neurodegener. 2*, 1–11.

(40) Madhu, P., and Mukhopadhyay, S. (2020) Preferential Recruitment of Conformationally Distinct Amyloid-β Oligomers by the Intrinsically Disordered Region of the Human Prion Protein. *ACS Chem. Neurosci. 11*, 86–98.

(41) Grimminger, V., Richter, K., Imhof, A., Buchner, J., and Walter, S. (2004) The Prion Curing Agent Guanidinium Chloride Specifically Inhibits ATP Hydrolysis by Hsp104. *J. Biol. Chem. 279*, 7378–7383.

(42) Sweeny, E. A., Jackrel, M. E., Go, M. S., Sochor, M. A., Razzo, B. M., DeSantis, M. E., Gupta, K., and Shorter, J. (2015) The Hsp104 N-Terminal Domain Enables Disaggregase Plasticity and Potentiation. *Mol. Cell 57*, 836–849.

(43) Linse, S. (2017) Monomer-dependent secondary nucleation in amyloid formation. *Biophys. Rev. 9*, 329–338.

(44) Taguchi, H., and Kawai-Noma, S. (2010) Amyloid oligomers: Diffuse oligomer-based transmission of yeast prions. *FEBS J. 277*, 1359–1368.

(45) Jucker, M., and Walker, L. C. (2018) Propagation and spread of pathogenic protein assemblies in neurodegenerative diseases. *Nat. Neurosci. 21*, 1341–1349.

(46) Krzewska, J., and Melki, R. (2006) Molecular chaperones and the assembly of the prion Sup35p, an in vitro study *25*, 822–833.

(47) Arimon, M., Grimminger, V., Sanz, F., and Lashuel, H. A. (2008) Hsp104 Targets Multiple Intermediates on the Amyloid Pathway and Suppresses the Seeding Capacity of A β Fibrils and Protofibrils. *J. Mol. Biol. 384*, 1157–1173.

Conformation alterations in yeast prion amyloids by sub-stoichiometric Hsp104 to facilitate seeded aggregations

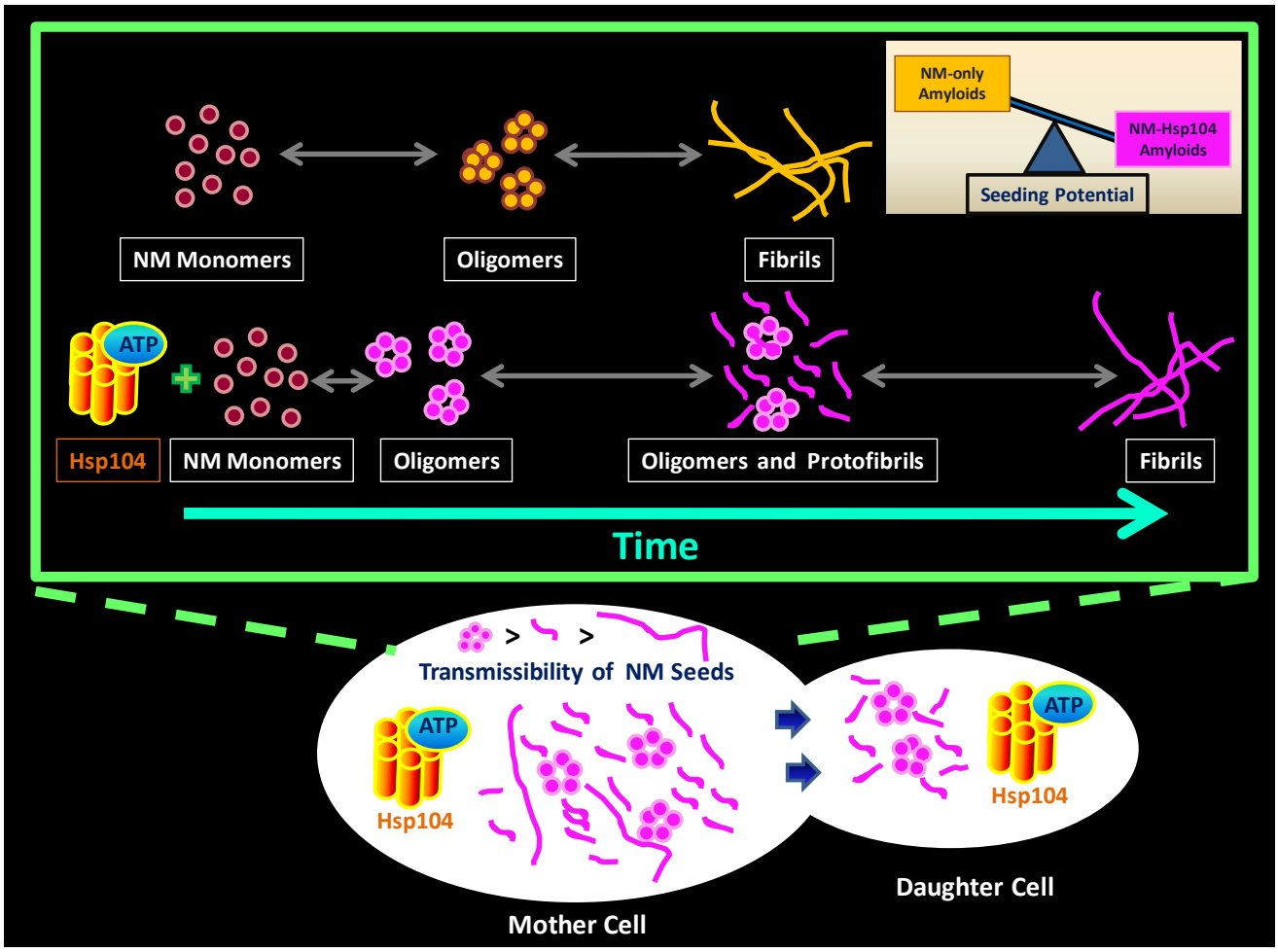

Reference: **Mahapatra, S.,** Sarbahi A., Madhu, P., Swasthi, H. M., Sharma, A., Singh, P., and Mukhopadhyay, S. (2022) Sub-stoichiometric Hsp104 regulates the genesis and persistence of self-replicable amyloid seeds of Sup35 prion domain. *J. Biol. Chem.* 298 ,102143.

3.1 Introduction

All amyloids possess a generic cross-β sheet structure[1,2]. However, the nanoscopic differences in the amyloid architecture lead to varied amyloid-associated physiological or pathological consequences[3]. Conformational heterogeneity in amyloids has perhaps been most evident in prions. It was discovered that two prion conformers from the same protein exhibited different sensitivity against proteases and caused the drowsy and hyper strains in transmissible mink encephalopathy[4,5]. However, such structural diversity is not limited to prions. Recent reports suggest that non-prion amyloids associated with neurodegeneration, such as α-synuclein, tau, and Aβ, constitute a spectrum of neurotoxic structures, challenging the therapeutics against these aggregates. Nevertheless, with the advent of high-resolution imaging tools such as atomic force microscopy (AFM) and cryo-electron microscopy, the varied morphological appearances, which often resulted from conformational differences, were also observed in aggregates[6,7,8]. This structural polymorphism in curvature, persistence length, surface characteristics, and the periodic twist was found regardless of the case of *in vitro* polymerized amyloids or the amyloid deposits isolated from the lesions of the victims of neurological disorders. Not only in the pathological amyloids, but the conformational difference in amyloids also controls the benign non-Mendelian epigenetic traits in yeasts or several beneficial functions in higher eukaryotes[9,10]. Differences in pH, temperature, aggregation buffers, agitations, or several binding partners, such as co-aggregating proteins and other non-protein molecules, are some factors reported to generate structural heterogeneity during aggregation.

Despite the detailed structural characterization of amyloids derived from identical polypeptides using cutting-edge techniques, the underlying molecular mechanism of how the conformers exert different cellular pathology or functionality remains elusive. As discussed in the last chapter, the yeast prion Sup35p that gives rise to the non-Mendelian inheritance of [*PSI*$^+$] phenotype (white colonies) in its aggregated state and [*psi*$^-$] phenotype (red colonies) in its soluble form is a well-celebrated model to study the outcomes of conformational diversity[11]. This is mainly because of the simple conformation-phenotype relationship in yeasts gives rise to easily observable phenotypic traits. The first conformational strain reported for Sup35 was the polymerization temperature-dependent conformational remodeling leading to the formation of unique amyloid structures associated with observable differences in colony colour[12,13]. Seminal *in vitro* and *in vivo* studies on these Sup35 amyloids revealed that the dissimilar interaction with the molecular chaperones, such as the disaggregase Hsp104, plays the most prominent role in controlling the phenotypic traits via regulating the number and self-

templating efficiency of seeds during cytoplasmic inheritance[14,15,16]. Interestingly, in the case of yeast prion Ure2p, the chaperone Sis1, an Hsp40, not only kinetically modulated the amyloidogenesis but also led to structurally distinct amyloids that exhibited reduced proteotoxicity[17]. Along this line, we also postulated that the presence of sub-stoichiometric amounts of Hsp104 during the polymerization of Sup35NM might influence the nanoscale structural organization of NM amyloids, which could alter its properties, such as seeding potential during prion-like transmission.

3.2 Experimental procedures

3.2.1 Materials

HEPES, magnesium chloride hexahydrate, sodium phosphate dibasic dihydrate, tris (hydroxymethyl) aminomethane (Tris), β-mercaptoethanol, ATP disodium salt hydrate, DTT, and ThT were bought from Sigma. GdmCl, proteinase K, and urea were procured from Amresco. Ammonium sulfate, imidazole, lysozyme, SDS, EDTA, and potassium chloride was bought from HIMEDIA. Potassium hydroxide, sodium chloride, sodium hydroxide, glycerol, A-11 antiamyloid oligomer antibody, methanol, horseradish peroxide (HRP)–conjugated goat anti-rabbit antibody was procured from Merck. IPTG and antibiotics (chloramphenicol and ampicillin) were purchased from Gold Biocom. Enhanced chemiluminescence kit, HRP-conjugated rabbit antimouse antibody, was obtained from Thermo Fisher Scientific. Nickel-nitriloacetic acid (Ni-NTA) column and Q-Sepharose were from GE Healthcare Lifesciences. Phosphoenolpyruvate (PEP) and pyruvate kinase (PK) were procured from Roche Diagnostics.

3.2.2 Expression and purification of Sup35NM

The detailed protocol is described in chapter 2 of this thesis (Page 32).

3.2.3 Expression and purification of Hsp104

The detailed protocol is described in chapter 2 of this thesis (Page 32).

3.2.4 Seeded aggregation reactions

Seeds of NM were generated by incubation of monomerized NM (2.5 μM) protein in assembly buffer (40 mM HEPES–KOH pH 7.4, 150 mM KCl, 20 mM $MgCl_2$, 1 mM DTT) without or with Hsp104 (0.025 μM), ATP (5 mM), and ATP-regeneration system (20 mM PEP and 15 μg/ml PK) at RT under stirring at 80 rpm using magnetic beads. The resulting amyloid seeds from NM or Hsp104-controlled NM aggregation reactions were aliquoted after certain time

points from the commencement of the aggregation reactions and added to a 10% (w/w) ratio to the fresh aggregation reaction of NM monomers (2.5 μM) in seeded assembly buffer (40 mM HEPES–KOH PH 7.4, 150 mM KCl, 20 mM $MgCl_2$, 1 mM DTT, 10 μM ThT, 3 mM GdmCl). The seeded aggregation reactions were kept at RT under stirring at 80 rpm using magnetic beads, and the ThT fluorescence was recorded with time.

3.2.5 Thermal melting of fibrils

Monomeric NM (2.5 μM) was aggregated for 6 h or 30 h in assembly buffer (40 mM HEPES–KOH pH 7.4, 150 mM KCl, 20 mM $MgCl_2$, 1 mM DTT) in the absence or presence of (0.025 μM) Hsp104 with ATP (5 mM) and the ATP-regeneration system (20 mM PEP and 15 μg/ml PK), respectively, at RT under stirring at 80 rpm using a magnetic bead for the fibril formation. Then, fibrils were passed through a 50 kDa filter to concentrate ∼20 times and eliminate the unrecruited monomers. The concentrated fibrils, with SDS-PAGE loading dye (2% SDS), were incubated at different temperatures for 5 min, and then SDS-PAGE was performed. Coomassie-stained bands were quantified using ImageJ software[18]. The band intensities were plotted against the incubation temperatures and fitted to the sigmoidal function. NM (2.5 μM) was also aggregated in the same assembly buffer, additionally having GdmCl (3 mM) in the presence of the same amount of Hsp104, ATP, and ATP-regeneration system for 6 h for the fibrillization, and the thermal melting experiment was performed on these fibrils as well.

3.2.6 The proteinase K digestion of fibrils

Monomeric NM (2.5 μM) was aggregated in the assembly buffer (40 mM HEPES–KOH pH 7.4, 150 mM KCl, 20 mM $MgCl_2$, 1 mM DTT) in the absence or presence of Hsp104 (0.025 μM), ATP (5 mM), and ATP-regeneration system (20 mM PEP and 15 μg/ml PK) for 6 h or 30 h, respectively, to generate the fibrils, and after that, the fibrils were concentrated and freed from unrecruited monomers using a 50 kDa filter. The concentrated fibrils (in the supernatant) from both the aggregation reactions were incubated with proteinase K in multiple ratios at 37 °C for 30 min, and digestion reactions were terminated by adding SDS-PAGE loading dye, and then SDS-PAGE was performed. The undigested NM monomers were also probed with (anti-His; 1:10,000) antibodies in Western blot analysis. PK (15 μg/ml) was added after fibrillation in the case of NM-only aggregation to make the reaction mixture comparable to the NM-Hsp104 aggregation reaction.

3.2.7 Disaggregation of fibrils

Monomeric NM (2.5 μ M) were aggregated in the assembly buffer (40 mM HEPES–KOH pH 7.4, 150 mM KCl, 20 mM $MgCl_2$, 1 mM DTT, 10 μM ThT) without or with Hsp104 (0.025 μM) , ATP (5 mM), and the ATP-regeneration system (20 mM PEP and 15 μg/ml PK) for 6 h or 30 h, respectively, at RT under stirring at 80 rpm to generate the fibrils, and after that, Hsp104 was added in both the reactions to a final concentration of 0.5 μM along with ATP (5 mM) and the ATP-regeneration system (20 mM PEP, and 15 μg/ml PK); all the components were mixed thoroughly and kept at RT under stirring at 80 rpm in the dark to avoid photobleaching. ATP was added last to avoid the disaggregation by ATP itself due to its hydrotropic property. A drop in the ThT fluorescence at 480 nm was recorded as a function of time that signified fibril disaggregation. Alternatively, the fibrils were also disaggregated by the ultrasonic sound (Qsonica probe sonicator) of amplitude 5 for 30 s for several pulses, and the ThT fluorescence was recorded after each 30 s pulse. Also, the fibrils were kept at RT for 24 h in the dark, static condition to record the decrease in the ThT fluorescence due to the autodisaggregation. The percentage of disaggregation was estimated using ([Initial ThT fluorescence intensity - final ThT fluorescence intensity]/Initial ThT fluorescence intensity) × 100%. Normalization was performed with respect to the initial ThT fluorescence intensity for the disaggregation kinetics.

3.2.8 Steady-state fluorescence measurements

Steady-state fluorescence measurements for Trp mutants of Sup35NM were performed in NM and NM-Hsp104 amyloid states using the FluoroMax-4 spectrofluorometer (Horiba Jobin Yvon). For recording the fluorescence spectra, the mutants were excited at 295 nm, where the excitation and emission slit widths were 1.75 and 6 nm, respectively. Concomitantly, steady-state anisotropy measurements were performed by setting the excitation wavelength at 295 nm and emission wavelength at 330 nm with an integration time of 2 s and a bandpass of 2.5 nm and 10 nm, respectively. All of the aforementioned measurements were done at 24 ± 1 °C, and steady-state fluorescence measurements were estimated by using the parallel and perpendicular intensities taking into consideration the G-factor.

3.2.9 Statistical analysis

All the experiments were repeated at least three times, and the data are represented as mean ± SD showing the scattered data points from independent experimental replicates. The statistical significance analysis was performed by carrying out one-way ANOVA tests, and the *p*-values

were reported in the figure legends. All the data analysis, data fitting (adjusted $R^2 > 0.95$), and data plotting was performed using Origin 9.6.

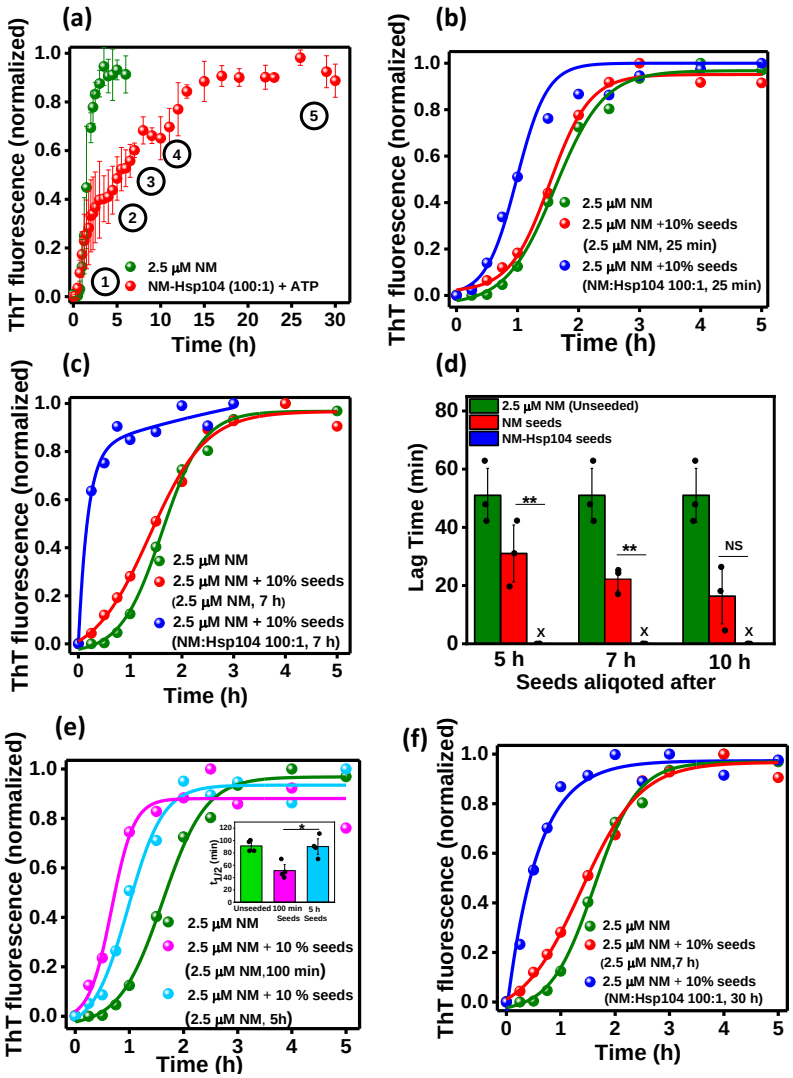

Figure 3.1. (a) ThT fluorescence kinetics of rotated (80 rpm) NM (2.5 μM) aggregation without or with Hsp104 (0.025 μM), plus ATP, and aliquots were withdrawn from these reactions as seeds at the indicated time points (*circled numbers*) and introduced to the fresh aggregation of NM (2.5 μM) in assembly buffer containing GdmCl (3 mM). (b) Representative normalized ThT fluorescence kinetics of rotated (80 rpm) NM (2.5 μM) aggregation without or with 10% (w/w) seeds of NM-Hsp104 or NM aggregation which were aliquoted after 25 min from the commencement of the aggregation reaction. (c) Representative normalized ThT fluorescence kinetics of rotated (80 rpm) NM (2.5 μM) aggregation without or with 10% (w/w) seeds of NM-Hsp104 or NM aggregation which were aliquoted after 7 h. (d) Lag times of rotated (80 rpm) NM (2.5 μM) aggregation without or with 10% (w/w) seeds of NM-Hsp104 or NM aggregation which were aliquoted after 5 h, 7 h, and 10 h. The standard deviations were estimated from three independent experiments (n = 3) and **P < 0.01, **P < 0.01, NS, respectively, for 5 h, 7 h, and 10 h NM-Hsp104 seeds compared to NM seeds. (e) Representative normalized ThT fluorescence kinetics of rotated (80 rpm) NM (2.5 μM) without or with 10% (w/w) seeds from NM aggregation that were aliquoted after 100 min and 5 h showing the $t_{1/2}$ of the unseeded and seeded aggregations. SDs were calculated from four individual experiments (n = 4), ∗p < 0.05 with respect to 100 min seeds and 5 h seeds (inset). (f) Representative normalized ThT fluorescence kinetics of rotated (80 rpm) NM (2.5 μM) aggregation without or with 10% (w/w) seeds from NM or NM-Hsp104

aggregation that were aliquoted after 7 h or 30 h, respectively. Statistical significance is estimated using one-way ANOVA.

3.3 Results

3.3.1 The seeding capability of the Hsp104-remodelled amyloid

To continue the cycle of typical prion-like amplification for the inheritance of the [*PSI*$^{+}$] phenotype, both the abundance and the effective seeding ability of prefibrillar particles are vital. To shed light on this critical aspect of prion inheritance, we studied the seeding capability of the amyloid species of Hsp104-mediated NM aggregation by aliquoting preformed amyloids from the reaction mixture at different time points (Figure 3.1a). The NM-Hsp104 aggregation mixture was introduced into the fresh NM-only polymerization reactions in the buffer containing 3 mM GdmCl to suppress the effect of Hsp104 as a small molecule inhibitor[19,20]. This allowed us to study the impact of Hsp104-remodeled aggregates in seeding the NM-only aggregation kinetics without the influence of Hsp104 in seeded reactions. This set of studies showed that the amyloid prefibrillar entities of Hsp104-induced NM aggregation had a greater potential to accelerate the fresh NM fibrillization compared to the amyloids of NM-only aggregation reactions as reflected in the lag time of the seeded kinetics. Moreover, the seeding ability of the particles of NM-Hsp104 aggregation reactions that aliquoted after 25 min demonstrated the early appearance of the seeding-competent amyloid species in Hsp104-mediated NM aggregation compared to the NM-only aggregation reaction (Figure 3.1b-d). This observation indicated that the seeding ability was associated with the composition of the amyloid particles of the NM-Hsp104 aggregation, which was enriched in the precursor of fibrillar amyloids of NM having a better seeding potential as opposed to matured fibrils (Figure 3.1e). We also surmise that the intermediate NM particles demonstrated higher seeding potential than matured fibers. However, intriguingly, even the NM-Hsp104 fibrils displayed better seeding potential than the NM fibrils (Figure 3.1f). Taken together, the greater capability of Hsp104-designed NM fibrils to catalyze the NM assembly than the typical NM fibrils established the fact that the reason behind their better seeding ability was not only related to the polymerization hierarchies and sizes of the amyloids present in the seed aliquots but also the conformational attribute of Hsp104-remodeled fibrils. Therefore, we postulated that Hsp104, at sub-stoichiometric concentrations, can create structurally altered amyloids that can autocatalytically accelerate a fresh aggregation reaction more efficiently owing to their distinct

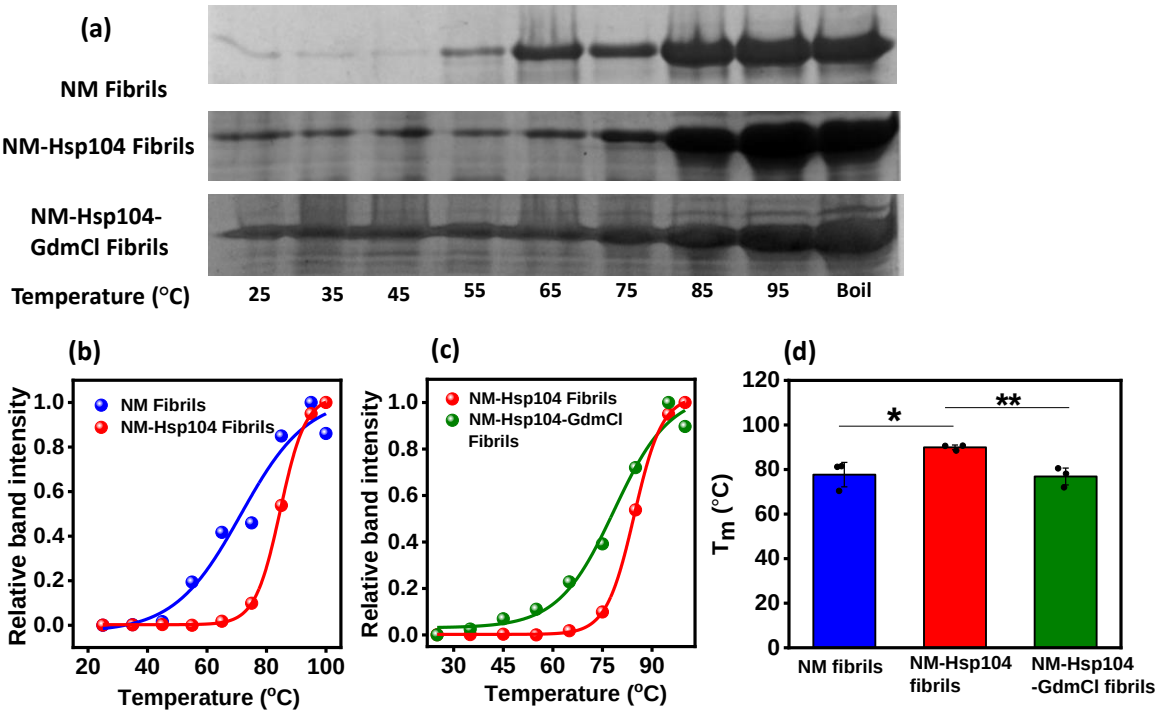

Figure 3.2. (a) SDS-PAGE gel image of concentrated fibrils formed from the NM monomers (2.5 μM) that fibrillized in the absence or presence of Hsp104 (0.025 μM) and ATP and also in the presence of Hsp104 (0.025 μM), ATP, and GdmCl (3 mM), which were then heated with SDS-PAGE loading dye (2% SDS) for 5 min at indicated temperatures. (b,c) the fitted band intensity of the monomers melted from (b) NM and NM-Hsp104 fibrils, (c) NM-Hsp104, and NM-Hsp104-GdmCl fibrils with temperature to sigmoidal functions after relatively quantified using ImageJ software. (d) Melting temperature (T_m) of NM, NM-Hsp104, and NM-Hsp104-GdmCl fibrils retrieved from the midpoint of the sigmoidal melting curve. SDs were calculated from three individual experimental replicates (n = 3), $*p < 0.05$ (NM and NM-Hsp104 fibrils), $**p < 0.01$ (NM-Hsp104 and NM-Hsp104-GdmCl fibrils) (One-way ANOVA).

amyloid packing. Next, we aimed to distinguish the conformational characteristics of NM-only and NM-Hsp104 amyloids by following an array of distinct biochemical and biophysical readouts using matured NM-only or NM-Hsp104 fibrils from the saturation phase of aggregation reactions that were devoid of any detectable oligomers.

3.3.2 Hsp104 induces amyloid structural diversity

To monitor the amyloid structural diversity, we first studied the SDS solubility of NM-only and NM-Hsp104 aggregates. The SDS-induced thermal denaturation was earlier used to identify the structural diversity by monitoring the dissimilar thermal stability of two different yeast prion strains generated in vitro. We fibrillized NM without or with Hsp104 at the sub-stoichiometric ratio and then treated these fibrils with 2% SDS and heated them from 25 °C to 100 °C. Then, we quantified the monomeric fraction derived from this treatment on SDS-PAGE. The temperature dependence of the monomeric fraction exhibited a sigmoidal profile

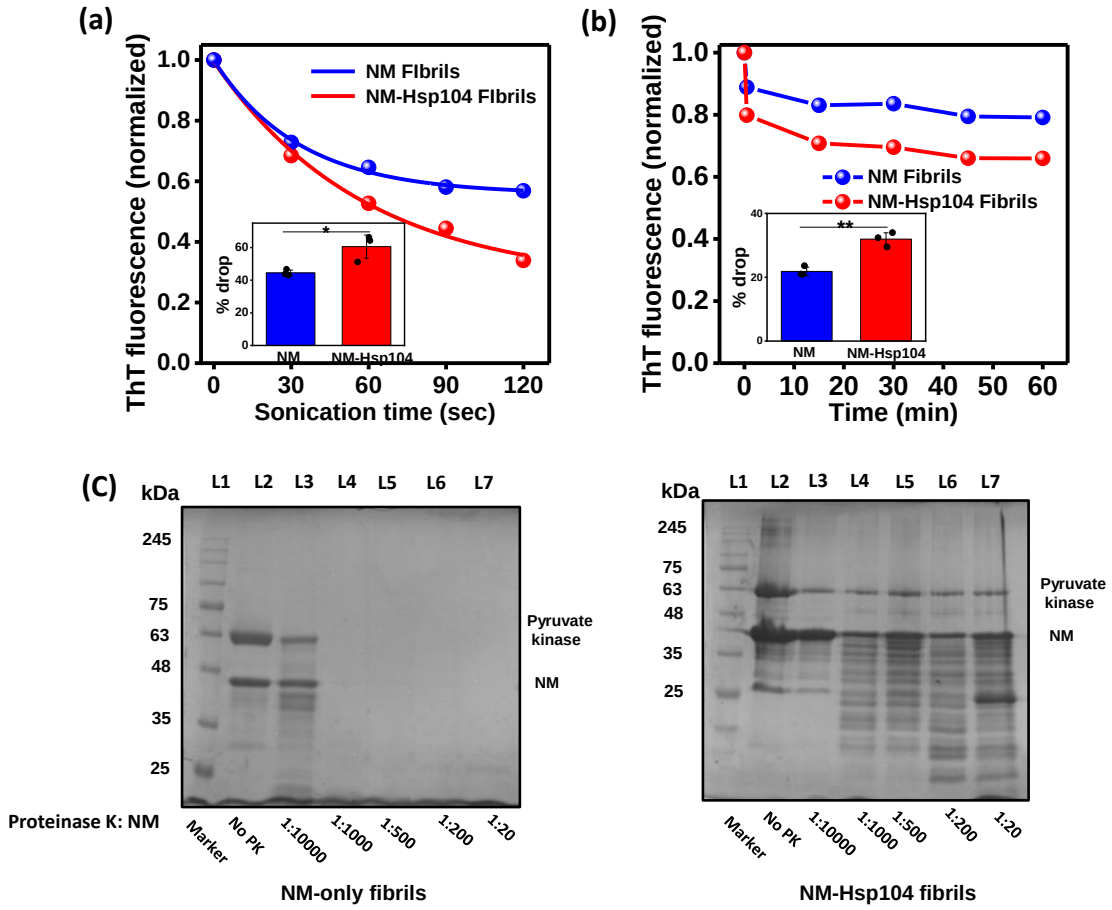

Figure 3.3. (a,b) Monomeric NM (2.5 μM) was fibrillized without or with Hsp104 (0.025 μM) plus ATP and then disaggregated by two methods. (a) Representative disaggregation kinetics using the ultrasonic sound pulse of amplitude 5 for several pulses of 30 s and the drop in the ThT fluorescence was recorded after each pulse. The ThT fluorescence intensities were normalized with respect to the initial ThT fluorescence intensity. The extent of disaggregation at 80 rpm was estimated from three experimental replicates to calculate the SD (n = 3), ∗p < 0.05 compared to NM fibrils (One-way ANOVA) (inset). (b) Representative disaggregation kinetics by Hsp104 (0.5 μM), ATP (5 mM), and drop in ThT fluorescence with time at 80 rpm were recorded. The ThT fluorescence intensities were normalized, and the extent of disaggregation was estimated from three independent replicates (n = 3), ∗∗p < 0.01, compared to NM fibrils (One-way ANOVA) (inset). (c) The concentrated fibrils formed from monomeric NM (2.5 μM) without or with Hsp104 (0.025 μM), plus ATP were incubated at 37 °C for 30 min with multiple concentrations of proteinase K followed by the SDS-PAGE analysis and stained with Coomassie dye. Pyruvate kinase was added after the fibrillation in the case of NM-only aggregation to make the reaction mixtures comparable to the NM-Hsp104 aggregation reaction.

showing an increase in the monomeric population with increasing temperature in the two types of fibrils. The different melting temperatures (T_m) of NM-only and NM-Hsp104 fibrils revealed altered thermal stability due to their distinct supramolecular structural differences despite having similar nanoscale morphologies. However, NM-Hsp104 fibrils prepared in the presence of 3 mM GdmCl that acts as a small-molecule inhibitor of Hsp104 by binding with the nucleotide-binding domains exhibited thermal stability similar to NM-only fibrils. These

results together indicated that the disaggregation-competent Hsp104 induces an altered amyloid packing of NM compared to pure NM fibrils (Figure 3.2).

3.3.3 Hsp104 alters fibril fragility and protease digestion profiles

To further support our assertion that Hsp104 induces conformationally altered fibrillar architecture, we intended to distinguish NM-only and Hsp104-mediated fibrils by their fragility. We fragmented the NM-only and Hsp104-designed NM fibrils using two ways: fragmenting fibrils by ultrasonic sound and incubating fibrils at a high concentration of Hsp104. Irrespective of the fragmentation method, the ThT fluorescence exhibited different kinetics for NM-only and NM-Hsp104 fibrils, indicating their altered structural packing in these two fibril variants (Figure 3.3a,b). This is because the different supramolecular arrangements within the fibrils can give rise to the observed kinetic difference in the fragmentation propensity. Next, we performed protease digestion assays to further probe into the kinetic stability of these two types of NM fibrils. Despite having a generic cross β-sheet secondary structure in different amyloid variants of a given protein, the monomeric polypeptide units' varied supramolecular packing and nanoscale organization of the polymeric architecture lead to altered sensitivity to proteolytic digestion[21]. We incubated NM-only and NM-Hsp104 fibrils with an increasing concentration of proteinase K and observed a different digestion pattern on SDS-PAGE. The binding of Hsp104 to the fibrils may only minimally control the digestion of NM-Hsp104 fibrils, as we used a sub-stoichiometric concentration of Hsp104 for these experiments. We want to mention that even in the absence of proteinase K for both NM-only and NM-Hsp104 samples, we observed a few lower molecular weight bands on the gel, possibly due to an esterase-like activity of amyloids. In the case of NM-only fibrils, an intact monomeric NM band was visible only in the presence of the lowest amount of protease, as the higher ratios of proteinase K completely digested NM into low molecular weight peptides. In contrast, the NM fibrils designed by Hsp104 showed much more resistance toward protease digestion, and the appearance of the undigested monomeric NM bands and partially digested NM peptides at relatively higher concentrations of proteinase K suggested the existence of a more resistant amyloid core in NM-Hsp104 fibrils compared to NM-only fibrils (Figure 3.3c).

3.3.4 Site-specific conformational mobility distinguishes the types of amyloids

Next, to directly capture the site-specific structural information within the amyloid conformers, we performed site-specific fluorescence polarization anisotropy measurements to monitor the conformational dynamics in two types of NM fibrils. NM and Hsp104 sequences are devoid of

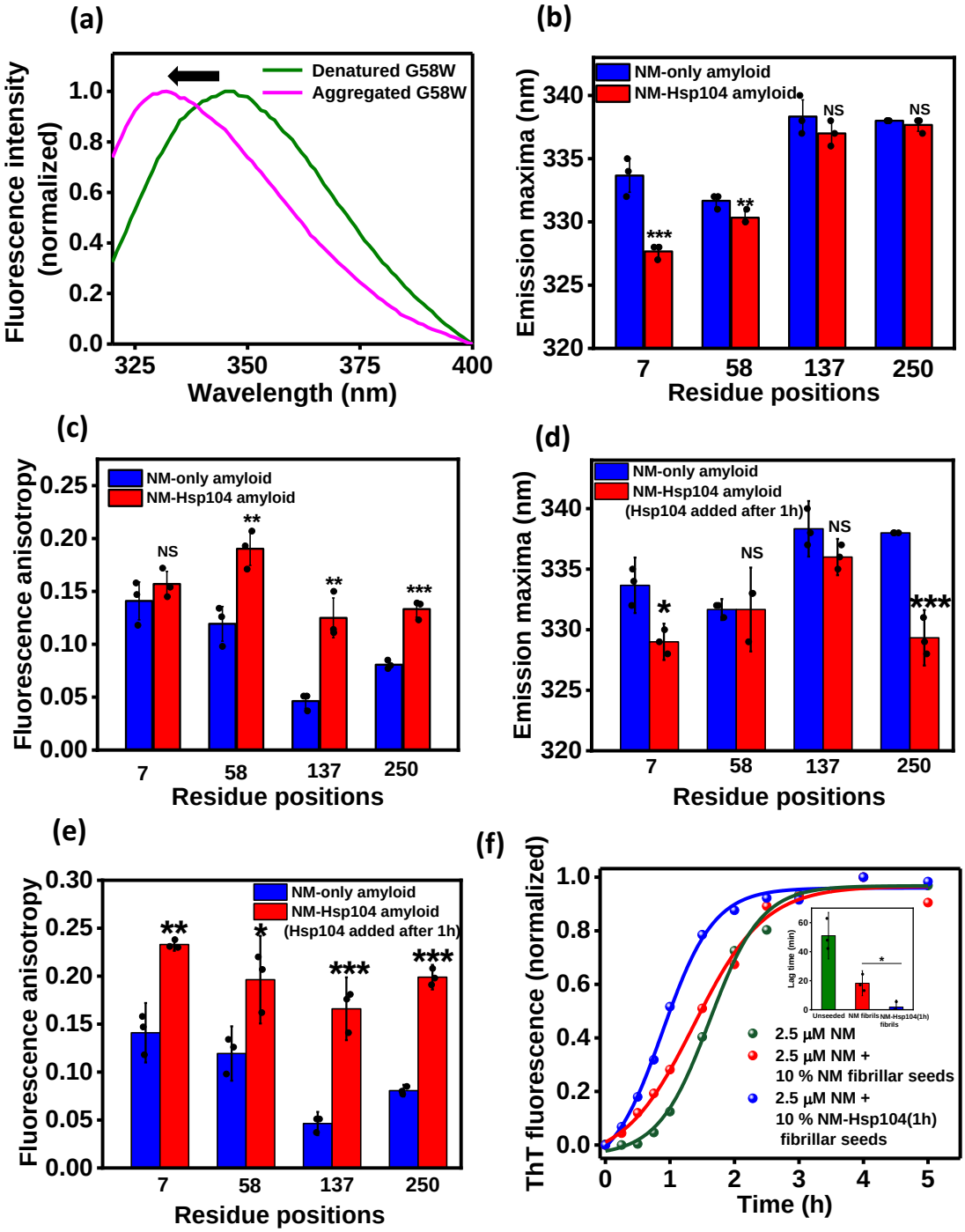

Figure 3.4. (a) Normalized Trp fluorescence spectra of residue position 58 depicting the blueshift (black arrow) upon conversion into the amyloids. (b) Trp emission maxima of different residue positions in two different amyloid forms, NM and NM-Hsp104 (NM: Hsp104 100:1). The excitation and emission slit widths were 1.75 and 6 nm, respectively. SDs were estimated from three different experimental replicates (n = 3), ***p < 0.001, **p < 0.01, NS, NS (One-way ANOVA) for locations 7, 58, 137, and 250, respectively, with respect to the NM-only amyloids. (c) Steady-state fluorescence anisotropies of different residue positions in two amyloid states (NM and NM-Hsp104, NM: Hsp104 100:1). SDs were estimated from three independent replicates (n = 3), NS, **p < 0.01, **p < 0.01, ***p < 0.001 (One-way ANOVA) for locations 7, 58, 137, 250, respectively, with respect to the NM-only amyloids. (d) Trp emission maxima of different residue positions in two different amyloid forms, NM and NM-Hsp104 (NM: Hsp104 100:1, Hsp104 and ATP were introduced after 1 h). The excitation and emission

slit widths were 1.75 and 6 nm, respectively. Standard deviations were estimated from three different experimental replicates (n = 3), ∗p < 0.05, NS, NS, ∗∗∗p < 0.001 (One-way ANOVA) for locations 7,58,137,250, respectively, with respect to the NM-only amyloids. (e) Steady-state fluorescence anisotropies of different residue reactions (n = 3), *P < 0.05 compared to the NM fibrils. positions in two amyloid states NM and NM-Hsp104 (NM:Hsp104 100:1, Hsp104 and ATP were introduced after 1 h). Standard deviations were estimated from three different experimental replicates (n = 3), **P < 0.01, *P < 0.05, ***P < 0.001, ***P < 0.001 (One-way ANOVA) for locations 7,58,137,250, respectively, with respect to the NM-only amyloids. (f) Representative normalized ThT fluorescence kinetics of rotated (80 rpm) NM (2.5 μM) aggregation without seeds or with 10% (w/w) NM fibrillar seeds and NM-Hsp104 (Hsp104 and ATP were introduced after 1 h) fibrillar seeds in assembly buffer containing GdmCl (3 mM). The lag times of all the aggregation reactions were retrieved. Standard deviations were estimated from three independent unseeded or seeded aggregations (inset).

any tryptophan (Trp) residue, and therefore, we used single-Trp variants spanning the NM polypeptide sequence. We then compared the Trp emission spectra in the monomeric and amyloid states. We observed a blueshift for all residue positions in the aggregated form with respect to the denatured monomeric form, which is in line with our earlier studies (Figure 3.4a). In both types of fibrils, NM-only and NM-Hsp104, the extent of the blueshift was more for N-domain residues than for M-domain residues, indicating a solvent-excluded environment in the N-domain. Moreover, comparing the two different fibrils, we observed a greater extent of blueshift for NM-Hsp104 fibrils. This blueshift is more pronounced in the N- terminal segment containing residue 7 (Figure 3.4b). This finding indicated that the NM sequence, especially the N-terminal part, experiences more solvent protection in NM-Hsp104 fibrils compared to NM-only fibrils. Next, we performed the steady-state fluorescence anisotropy measurements that report the site-specific rotational flexibility of Trp in the NM sequence. Upon conversion to amyloids, N-domain residues exhibited higher anisotropies indicating the more restricted rotation due to the preferential recruitment of the N-domain into the amyloid core. In contrast, the M-segment (residue 137) exhibited a much lower fluorescence anisotropy in both types of amyloids, an observation consistent with previous structural studies on NM amyloid, indicating the higher flexibility of the M-segment that is not sequestered into the amyloid core. The significantly high anisotropy for NM-Hsp104 fibrils at this residue location possibly indicated the Hsp104-binding induced restricted rotation. Additionally, higher fluorescence anisotropy in all residue locations for NM-Hsp104 fibrils than NM-only fibrils suggested more closely packed ordered organization in NM-Hsp104 fibrils corroborating our protease digestion results (Figure 3.4c). Next, in order to further test the hypothesis of Hsp104-mediated remodeling of amyloid conformers for preformed low molecular weight NM species, we introduced sub-stoichiometric Hsp104 at the early log phase of the NM fibrillation reaction, that is, one hour after the commencement. Our site-specific fluorescence studies on such amyloids exhibited

dynamical characteristics that are similar to NM-Hsp104 amyloids, in which Hsp104 was introduced at the beginning of the reaction (Figure 3.4d,e). These NM-Hsp104 particles formed by introducing Hsp104 at the early log phase also displayed an enhanced seeding capability compared to NM-only fibrils (Figure 3.4f). These results suggested that the Hsp104-induced remodeling is similar when added either in the beginning or at the early log phase of the aggregation reaction. Taken together, a series of biochemical and biophysical studies supported our hypothesis that apart from the composition of the seeds enriched in prefibrillar aggregates, NM-Hsp104 aggregates, in contrast to NM-only aggregates, comprise an altered and more ordered amyloid packing that allows them to display their enhanced autocatalytic self-templating ability.

3.4 Discussion

In this study, by *in vitro* reconstruction, we identified a conformational remodeling in the amyloids generated by Hsp104, contributing to a greater seeding potential of these amyloid entities. Besides ensuring the abundance of highly transmissible, seeding-proficient fibrillar precursors over fewer, less transmissible matured fibrils, low concentrations of Hsp104 created conformationally distinct seeds with greater seeding potential. The remodeling of the NM monomers or early soluble species by sub-stoichiometric Hsp104 aided the early oligomerization of NM, leading to the bypass of the lag phase. This remodeled NM species probably also created the altered building blocks for conformationally unique NM-Hsp104 fibrils as shown in Figure 3.5. In this work, we probed the conformational characters using a host of biochemical tools that revealed Hsp104-mediated NM fibrils are more stable and contain a more ordered amyloid core compared to NM-only aggregates. In accordance with our biochemical findings, location-specific spectral shifts and dynamics revealed via fluorescence anisotropy measurements indicated more buried locations and higher polypeptide ordering in Hsp104-mediated fibrils. Nevertheless, the amyloidogenic N-segment is known to constitute the amyloid core, whereas the charged M-region possesses some conformational flexibility, as detected by fluorescence anisotropy measurements also[10,22]. Hsp104 is known to interact with the M-region of NM and, therefore, can result in the binding-induced restriction in the conformational dynamics of the M-region[23]. However, higher anisotropy in the N-domain in the presence of Hsp104 is likely to be caused by the higher structural ordering of the amyloid core in Hsp104-mediated NM fibrils. We want to note that in contrast to previously reported yeast prion strains, in our case, more stable and ordered NM-Hsp104 fibrils were found to be

more fragile to fragmentation by Hsp104, which indicates an intriguing interplay of stability and fragility that can have a diverse phenotypic outcome[12,24,25,26,27].

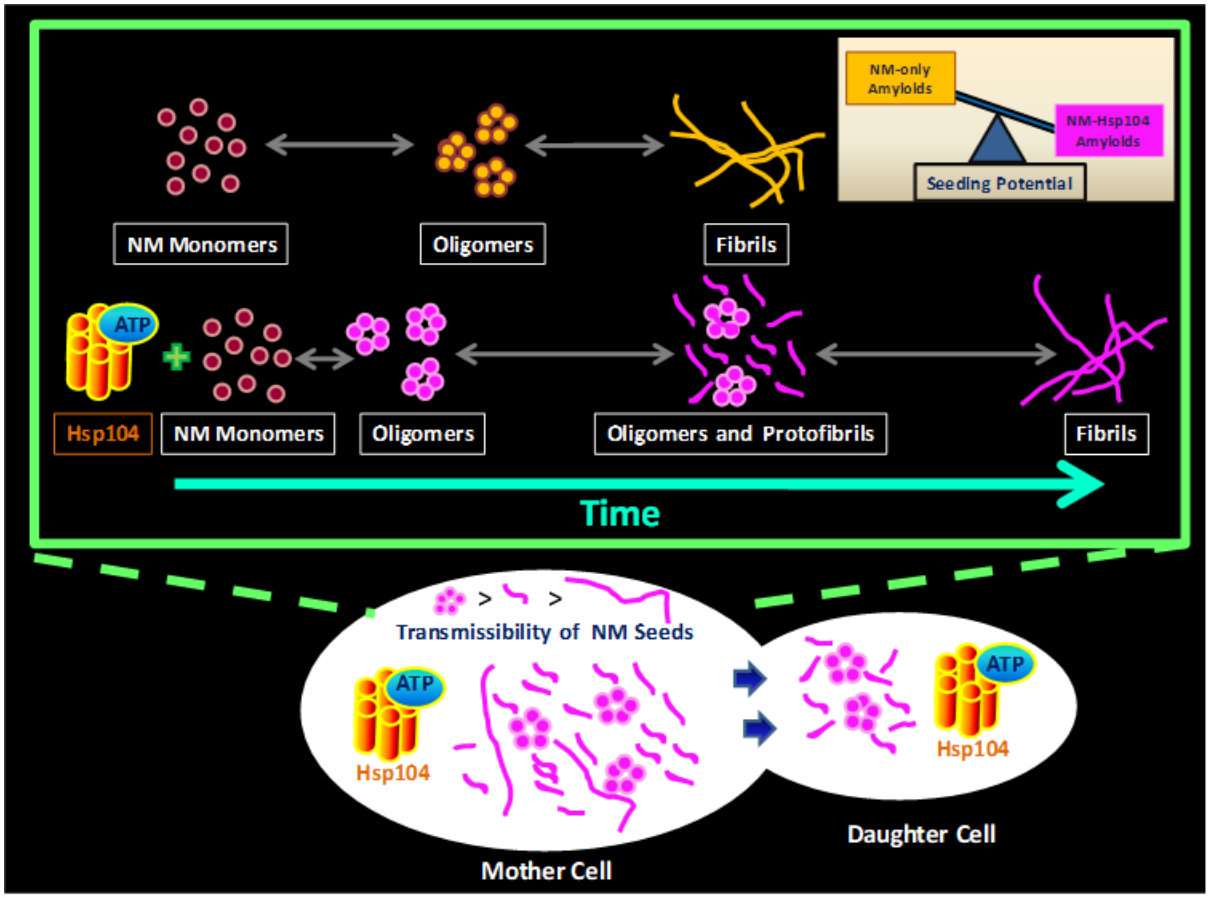

Figure 3.5. The proposed model for the NM aggregation in the presence of sub-stoichiometric Hsp104. Hsp104 with ATP ensures the abundance of highly transmissible prefibrillar amyloids (oligomers and protofibrils but not long and matured fibrils) that show greater seeding potential than amyloid fibrils generated in the absence of Hsp104.

In summary, our results unmasked another striking example of binding-partner-induced structural changes in amyloids generating amyloids with higher seeding potential. This increased seeding potential may facilitate the formation of more amyloids during autocatalytic amplification cycles. Therefore, apart from the kinetic alteration favoring the persistence of transmissible prefibrillar amyloids, low concentrations of Hsp104 also generated conformationally modulated amyloids that exhibited more seeding to function as a pro-propagation factor for [*PSI*$^{+}$]. The chaperone under-expression in aged cells, including disaggregases, can be helpful for the genesis and transmission of amyloids related to neurodegenerative diseases. Our results point to the potential molecular connections between aging and amyloid-associated neurodegeneration.

3.5 References

(1) Ke, P. C., Zhou, R., Serpell, L. C., Riek, R., Knowles, T. P. J., Lashuel, H. A., Gazit, E., Hamley, I. W., Davis, T. P., Fändrich, M., Otzen, D. E., Chapman, M. R., Dobson, C. M., Eisenberg, D. S., and Mezzenga, R. (2020) Half a century of amyloids: Past, present and future. *Chem. Soc. Rev. 49*, 5473–5509.

(2) Chiti, F., and Dobson, C. M. (2017) Protein misfolding, amyloid formation, and human disease: A summary of progress over the last decade. *Annu. Rev. Biochem. 86*, 27–68.

(3) Xu, Y., Maya-Martinez, R., and Radford, S. E. (2022) Controlling amyloid formation of intrinsically disordered proteins and peptides: slowing down or speeding up? *Essays Biochem.* 1–17.

(4) Aguzzi, A., Heikenwalder, M., and Polymenidou, M. (2007) Insights into prion strains and neurotoxicity. *Nat. Rev. Mol. Cell Biol. 8*, 552–561.

(5) Collinge, J., and Clarke, A. R. (2007) A general model of prion strains and their pathogenicity. *Science 318*, 930–936.

(6) Close, W., Neumann, M., Schmidt, A., Hora, M., Annamalai, K., Schmidt, M., Reif, B., Schmidt, V., Grigorieff, N., and Fändrich, M. (2018) Physical basis of amyloid fibril polymorphism. *Nat. Commun. 9*, 1–7.

(7) Kodali, R., Williams, A. D., Chemuru, S., and Wetzel, R. (2010) Aβ(1-40) forms five distinct amyloid structures whose β-sheet contents and fibril stabilities are correlated. *J. Mol. Biol. 401*, 503–517.

(8) Strohäker, T., Jung, B. C., Liou, S. H., Fernandez, C. O., Riedel, D., Becker, S., Halliday, G. M., Bennati, M., Kim, W. S., Lee, S. J., and Zweckstetter, M. (2019) Structural heterogeneity of α-synuclein fibrils amplified from patient brain extracts. *Nat. Commun. 10*, 1–12.

(9) Wickner, R. B., Edskes, H. K., Son, M., Bezsonov, E. E., Dewilde, M., and Ducatez, M. (2018) Yeast Prions Compared to Functional Prions and Amyloids. *J. Mol. Biol. 430*, 3707–3719.

(10) Krishnan, R., and Lindquist, S. L. (2005) Structural insights into a yeast prion illuminate nucleation and strain diversity. *Nature 435*, 765–772.

(11) Wickner, R. B. (2016) Yeast and fungal prions. *Cold Spring Harb. Perspect. Biol. 8*, 1–16.

(12) Tanaka, M., Chien, P., Naber, N., Cooke, R., and Weissman, J. S. (2004) Conformational variations in an infectious protein determine prion strain differences. *Nature 428*, 323–328.

(13) Narang, D., Swasthi, H. M., Mahapatra, S., and Mukhopadhyay, S. (2017) Site-Specific Fluorescence Depolarization Kinetics Distinguishes the Amyloid Folds Responsible for Distinct Yeast Prion Strains. *J. Phys. Chem. B 121*, 8447–8453.

(14) Desantis, M. E., and Shorter, J. (2012) Hsp104 drives "protein-only" positive selection of sup35 prion strains encoding strong [PSI+]. *Chem. Biol. 19*, 1400–1410.

(15) Nakagawa, Y., Shen, H. C. H., Komi, Y., Sugiyama, S., Kurinomaru, T., Tomabechi, Y., Krayukhina, E., Okamoto, K., Yokoyama, T., Shirouzu, M., Uchiyama, S., Inaba, M., Niwa, T., Sako, Y., Taguchi, H., and Tanaka, M. (2022) Amyloid conformation-dependent disaggregation in a reconstituted yeast prion system. *Nat. Chem. Biol. 18*, 321–331.

(16) Tanaka, M., Collins, S. R., Toyama, B. H., and Weissman, J. S. (2006) The physical basis of how prion conformations determine strain phenotypes. *Nature 442*, 585–589.

(17) Douglas, P. M., Treusch, S., Ren, H. Y., Halfmann, R., Duennwald, M. L., Lindquist, S., and Cyr, D. M. (2008) Chaperone-dependent amyloid assembly protects cells from prion toxicity. *Proc. Natl. Acad. Sci. U. S. A. 105*, 7206–7211.

(18) Schneider, C. A., Rasband, W. S., and Eliceiri, K. W. (2012) HISTORICAL commentary NIH Image to ImageJ : 25 years of image analysis. *Nat. Methods 9*, 671–675.

(19) Möglich, A., Krieger, F., and Kiefhaber, T. (2005) Molecular basis for the effect of urea and guanidinium chloride on the dynamics of unfolded polypeptide chains. *J. Mol. Biol. 345*, 153–162.

(20) Grimminger, V., Richter, K., Imhof, A., Buchner, J., and Walter, S. (2004) The Prion Curing Agent Guanidinium Chloride Specifically Inhibits ATP Hydrolysis by Hsp104. *J. Biol. Chem. 279*, 7378–7383.

(21) Kushnirov, V. V., Dergalev, A. A., and Alexandrov, A. I. (2020) Proteinase K resistant cores of prions and amyloids. *Prion 14*, 11–19.

(22) Narang, D., Swasthi, H. M., Mahapatra, S., and Mukhopadhyay, S. (2017) Site-Speci fi c

Fluorescence Depolarization Kinetics Distinguishes the Amyloid Folds Responsible for Distinct Yeast Prion Strains.

(23) Helsen, C. W., and Glover, J. R. (2012) Insight into molecular basis of curing of [PSI +] prion by overexpression of 104-kDa heat shock protein (Hsp104). *J. Biol. Chem. 287*, 542–556.

(24) Stein, K. C., and True, H. L. (2014) Extensive Diversity of Prion Strains Is Defined by Differential Chaperone Interactions and Distinct Amyloidogenic Regions. *PLoS Genet. 10*.

(25) Huang, V. J., Stein, K. C., and True, H. L. (2013) Spontaneous Variants of the [RNQ+] Prion in Yeast Demonstrate the Extensive Conformational Diversity Possible with Prion Proteins. *PLoS One 8*, 1–14.

(26) Cobb, N. J., Apostol, M. I., Chen, S., Smirnovas, V., and Surewicz, W. K. (2014) Conformational stability of mammalian prion protein amyloid fibrils is dictated by a packing polymorphism within the core region. *J. Biol. Chem. 289*, 2643–2650.

(27) Ayers, J. I., Schutt, C. R., Shikiya, R. A., Aguzzi, A., Kincaid, A. E., and Bartz, J. C. (2011) The strain-encoded relationship between PrPSc replication, stability and processing in neurons is predictive of the incubation period of disease. *PLoS Pathog. 7*.

ATP modulates self-perpetuating conformational conversion generating structurally distinct yeast prion amyloids that limit autocatalytic amplification

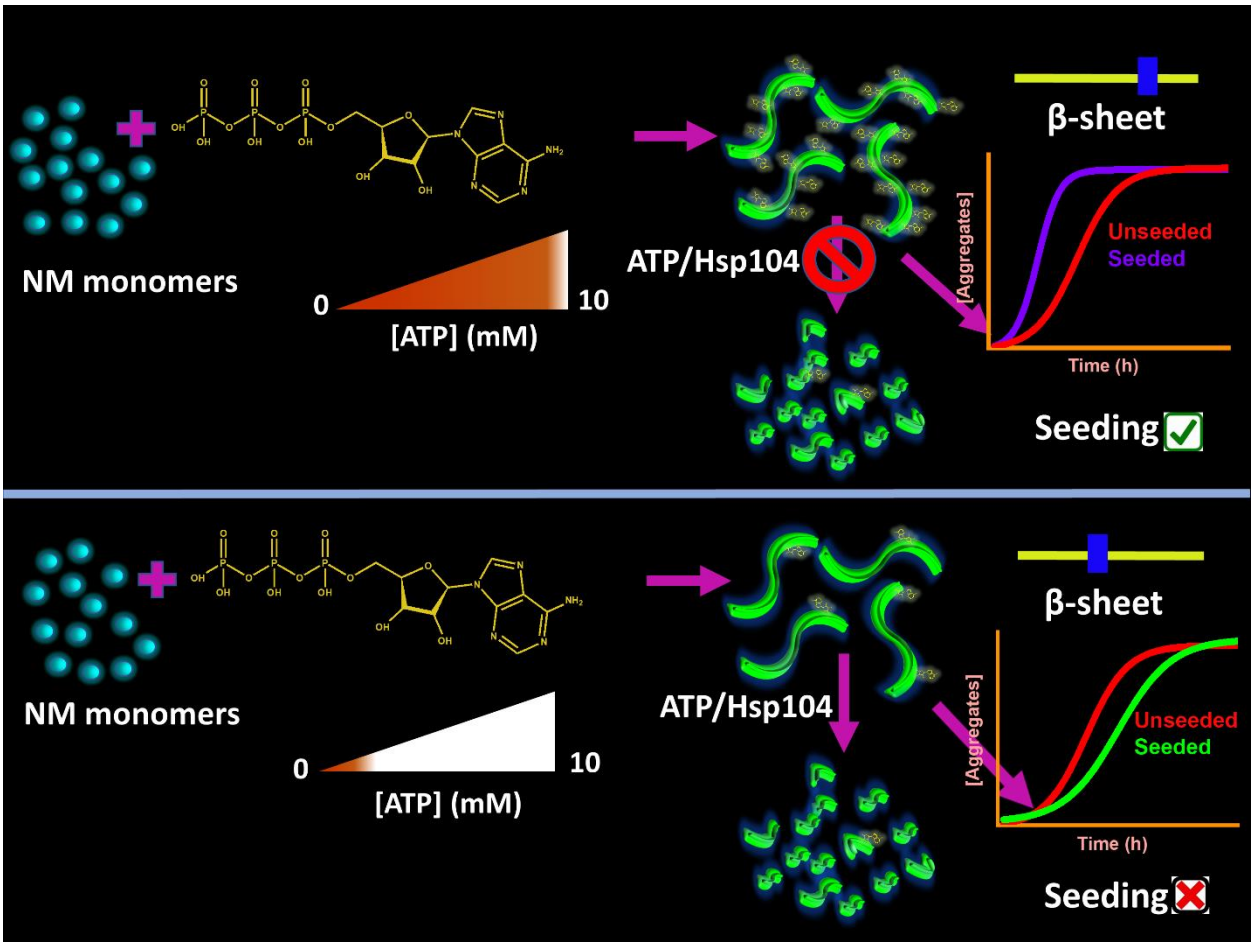

Reference: **Mahapatra, S.*,** Sarbahi, A., Punia, N., Joshi, A., Avni, A., Walimbe, A., and Mukhopadhyay, S*. (2023) ATP molecules generate structurally-distinct amyloids to restrict seeded amplification of a yeast prion determinant. *J. Biol. Chem.* 299, 104654.***Co-corresponding authors.**

4.1 Introduction

Amyloids are proteinaceous, β-sheet-rich ordered assemblies of misfolded proteins that bypass all the surveillance of the protein quality control (PQC) machinery and are often linked with some of the deadly neurodegenerative diseases such as Alzheimer's, Parkinson's, prion diseases, amyotrophic lateral sclerosis (ALS), and so on[1,2,3]. The PQC system is a network of proteins devoted to countering protein misfolding and aggregation, where adenosine triphosphate (ATP) plays an indirect, yet important, role by providing energy to the chaperones involved in protein homeostasis[4]. Although only micromolar concentrations of ATP are required for the function of enzymes that include this PQC machinery, the question as to why cells maintain a multifold higher concentration of ATP fascinated researchers to investigate the molecular role of ATP in cells apart from just being the cellular energy currency[5,6]. Intriguingly, in the amyloid deposits isolated from the brain tissues of patients with neurodegenerative diseases, biologically relevant polyanions such as nucleic acids, heparin, and glycosaminoglycans were detected. These reports hinted at a direct interaction between amyloidogenic proteins and the polyanions such as ATP and unveiled a less explored aspect of molecular ATP in protein solubility and aggregation[7,8,9].

The amphiphilic ATP molecule consists of the relatively hydrophobic aromatic pyrimidine base connected via a moderately polar ribose sugar unit to a strongly hydrophilic negatively charged triphosphate moiety (Figure 4.1a). Previous studies showed that ATP alters the aggregation kinetics of various amyloidogenic proteins. For example, it promotes the assembly of acyl phosphatase (AcP), TauK18, amylin, and so on. Whereas, it inhibits the aggregation of eye lens protein γS-Crystallin, synthetic Aβ42 peptide, the prion domain of Mot3, and FUS (Fused in Sarcoma)[5,10,11,12]. ATP also disassembles preformed amyloids of FUS at physiologically relevant concentrations[5,13]. Despite several attempts, the chemical nature of interactions of ATP with amyloidogenic proteins or preassembled amyloid aggregates remains poorly understood. In the case of AcP, the electrostatic charge screening by the triphosphate part of ATP was proposed to be responsible for the accelerated aggregation[10]. Whereas, for the TauK18 fragment enriched in positively charged residues, the negatively charged triphosphate moiety of ATP promoted fibrillation due to the rapid dimerization via electrostatic crosslinking between lysine residues[11]. On the contrary, the solubilization of proteins to inhibit the amyloid formation or the disassembly of existing aggregates is believed to happen due to the hydrotropic properties of ATP by its aromatic moiety, like the typical hydrotropes that are generally used to solubilize hydrophobic compounds[5]. However, in another report, this

perspective was challenged as ATP was classified as a chaotropic salt in protein solubilization[14]. ATP also has shown its ability to alter phase separation, which may control the aggregation of different proteins[15].

The unique potential of molecular ATP to control both the formation and dissolution of amyloids might play a pivotal role in regulating prion-like colonization of amyloids, which remains largely uncharacterized. A body of recent evidence suggests that pathological amyloids such as Aβ, tau, α-synuclein, FUS, Huntingtin, p53, and so on follow the prion-like mechanism to invade the uninfected tissues[16,17,18,19,20]. According to this mechanism, preformed amyloid entities known as seeds can be transmitted to the neighboring healthy cells, where they can template amyloid formation[21]. Apart from the formation, the fragmentation of high molecular weight fibrils by cellular disaggregases is critical to generate growth-competent amyloids that facilitate prion-like propagation[22,23,24,25]. Such fragmented fibrils and oligomers exhibit higher permeability through lipid bilayers of both donor and acceptor cells and are considered as the predominant species for infection and toxicity across amyloid-associated diseases[26,27,28]. The yeast functional prion protein, Sup35, serves as an excellent model to study the prion-like behavior of transmissible amyloids. The intrinsically disordered prion domain of Sup35 (NM domain) governs the ability of the protein to exist either in soluble or in the amyloid form giving rise to two distinct phenotypes, [*psi*$^-$] and [*PSI*$^+$], respectively (Figure 4.1b). Furthermore, the cross-generational, non-Mendelian inheritance of [*PSI*$^+$] phenotype in budding yeasts can be utilized as the indicator of a prion-like mechanism[29,30]. Additionally, regions comprising positively charged amino acids often linked to prion-like low-complexity domains are associated with physiological functions and diseases. These regions can electrostatically interact with ATP and can be used as archetypes to elucidate its influence in the cascade of seeded amyloid amplification. In this work, we show the ATP-dependent modulation of amyloid aggregation of prion determinant (NM) of a yeast prion protein, Sup35. We further demonstrate that the ATP controls the prion-like propagation in a concentration-dependent manner by altering the amount and ability of fragmentable and self-templating amyloid seeds.

4.2 Experimental procedures

4.2.1 Materials

Sodium phosphate dibasic dihydrate, magnesium chloride hexahydrate, Thioflavin-T (ThT), adenosine-5’-triphosphate disodium salt hydrate (ATP), dimethyl sulfoxide (DMSO),

guanidinium hydrochloride (GdmCl), β-mercaptoethanol and HEPES [4-(2-hydroxyethyl)-1-piperazineethanesulfonic acid] were procured from Sigma (St. Louis, MO, USA). Urea and proteinase-K were bought from Amresco. Sodium dodecyl sulfate (SDS), imidazole, ammonium sulfate, lysozyme, potassium chloride, and ethylenediaminetetraacetic acid (EDTA) were purchased from HIMEDIA. Sodium hydroxide, potassium hydroxide, glycerol, methanol, nitrocellulose membrane, A11 (anti-amyloid oligomer antibody), OC (anti-amyloid fibril antibody), HRP-conjugated goat anti-rabbit antibody, and sodium chloride were bought from Merck. Antibiotics (ampicillin and chloramphenicol) and Isopropyl-β-thiogalactopyranoside (IPTG) were procured from Gold Biocom (USA). Q-sepharose and Ni-NTA columns were bought from GE Healthcare Lifesciences, USA. Fluorescein-5-maleimide was procured from Invitrogen. 96-well NUNC optical bottom plates were purchased from ThermoFisher Scientific (Waltham, Massachusetts, USA).

4.2.2 Expression and Purification of NM

C-terminal hexa-histidine tagged recombinant Sup35NM protein was overexpressed in BL21 (DE3)/pLysS cells using IPTG, and then from harvested cells, proteins were extracted; the extracted proteins were subjected to first Ni-NTA purification by applying a gradient of imidazole and further from a Q-sepharose column using the gradient of sodium chloride. Also, for the single cysteine mutant of NM, the purification remains the same as mentioned above with the addition of β-mercaptoethanol.

4.2.3 Site-directed mutagenesis for NM

Recombinant NM was cloned into the pET23a vector using appropriate primers. A single cysteine mutant was created using the site-directed mutagenesis kit, Quikchange (Stratagene). The following primers were used to create the mutation;

S150C Forward: GAAGCTTGTCTCCAGTTGCGGTATCAAGTTGG

S150C Reverse: GGCCAACTTGATACCGCAACTGGAGACAAGCTTC

DNA sequencing was performed to confirm the mutation.

4.2.4 Expression and Purification of Hsp104

The detailed protocol is mentioned in chapter 2 (page 32).

4.2.5 Amyloid aggregation reaction

Methanol-precipitated protein was dissolved and kept in a denaturation buffer (8 M Urea, 20 mM Tris-HCl, pH 7.4) at room temperature for at least 3 h. Denatured protein was passed through a 100-kDa filter first to remove any aggregates if present and then concentrated further using a 3-kDa filter for the amyloid aggregation reactions. The aggregation reactions were set up by incubating monomeric NM in assembly buffer (40 mM HEPES-KOH pH 7.4, 150 mM KCl, 1 mM DTT, 20 mM $MgCl_2$, and 20 μM ThT) at room temperature and stirred at 80 rpm with the final protein concentration of 2.5 μM without or with different concentrations of ATP and 1o mM ADP. ThT fluorescence was monitored at 450 nm excitation at room temperature, and emission was recorded at 480 nm. Also, NM aggregation reactions of 2.5 μM monomeric NM were set up in the presence of 10 mM ATP without $MgCl_2$ in the assembly buffer under the same aggregation conditions. Alternatively, amyloid aggregation reactions of monomeric NM (2.5 μM) were carried out in 100 mM, 150 mM, and 250 mM $MgCl_2$ (40 mM HEPES-KOH pH 7.4, 150 mM KCl, 1 mM DTT, and 20 μM ThT) buffer under the conditions as mentioned above.

4.2.6 Seeded aggregation reaction

Amyloid seeds were generated by incubating monomeric NM (2.5 μM) in assembly buffer (40 mM HEPES-KOH pH 7.4, 150 mM KCl, 1 mM DTT, and 20 mM $MgCl_2$) in the absence or presence of different concentrations of ATP at room temperature and stirring at 80 rpm. The resultant NM or NM-ATP amyloid seeds, after 6 h of aggregation reactions, were introduced to fresh aggregation reactions in assembly buffer (40 mM HEPES-KOH pH 7.4, 150 mM KCl, 1 mM DTT, 20 mM $MgCl_2$, and 20 μM ThT) such that the seeds constitute 10% (w/w) of the total protein concentration (2.5 μM). The reactions were kept at room temperature and stirred at 80 rpm, and ThT fluorescence was recorded at specified time intervals. Alternatively, the NM-ATP amyloids generated in the presence of 2.5 μM ATP, as mentioned above, were buffer exchanged with buffer B (40 mM HEPES-KOH pH 7.4, 150 mM KCl, 1 mM DTT, and 250 mM $MgCl_2$) and buffer A (40 mM HEPES-KOH pH 7.4, 150 mM KCl, 1 mM DTT, and 20 mM $MgCl_2$), sequentially. These amyloids were introduced as seeds to fresh aggregation reactions in assembly buffer (40 mM HEPES-KOH pH 7.4, 150 mM KCl, 1 mM DTT, 20 mM $MgCl_2$, and 20 μM ThT) as mentioned above, and ThT fluorescence was recorded with time. Also, amyloid seeds were generated by aggregating monomeric NM (2.5 μM) in assembly buffer (40 mM HEPES-KOH pH 7.4, 150 mM KCl, 1 mM DTT, and 20 mM $MgCl_2$) at room

temperature and stirring at 80 rpm, followed by sonication (Qsonica probe sonicator) at amplitude 5 for 2 pulses of 30 sec. These amyloid seeds were used in the seeded aggregation reaction, as mentioned above, by forming 10% (w/w) of the total protein concentration.

4.2.7 Disaggregation of NM-only and NM-ATP fibrils

NM monomers (2.5 μM) were aggregated in assembly buffer (40 mM HEPES-KOH pH 7.4, 150 mM KCl, 1 mM DTT, 20 mM $MgCl_2$, and 20 μM ThT) at room temperature and stirred at 80 rpm in the presence or absence of different concentrations of ATP and ADP. Different concentrations of ATP or ADP were introduced to the saturated aggregation reactions after 6 h of NM-only or NM-ATP aggregation, and a drop in ThT fluorescence was recorded at specific intervals. The ThT fluorescence intensities were normalized to the initial ThT fluorescence intensity before adding ATP or ADP. The percentage of disaggregation was calculated using [(Initial ThT fluorescence intensity - final ThT fluorescence intensity) / ThT fluorescence intensity] × 100% after 2 h. Alternatively, NM (2.5 μM) aggregation reaction was set up in the absence of $MgCl_2$ in the buffer (40 mM HEPES-KOH pH 7.4, 150 mM KCl, 1 mM DTT, and 20 μM ThT) at room temperature and stirred at 80 rpm, and a drop in ThT fluorescence intensity with time on the addition of 10 mM ATP was recorded.

4.2.8 Atomic force microscopy

Aggregation reactions of 2.5 μM of monomeric NM were set up in the assembly buffer (40 mM HEPES-KOH pH 7.4, 150 mM KCl, 20 mM $MgCl_2$, 1 mM DTT) in the absence or presence of different concentrations of ATP, and samples were aliquoted after 6 h from the commencement of the reactions. Alternatively, NM-only fibrils (2.5 μM monomers) were disaggregated using different concentrations of ATP and also with 0.5 μM Hsp104 plus 5 mM ATP and ATP regeneration system (20 mM PEP and 15 μg/ml pyruvate kinase). Samples (10 μL) were deposited on a freshly cleaved mica and were then thoroughly washed with filtered water after 2 min of incubation with 200 μl of filtered water and later dried under a gentle stream of nitrogen. The AFM images were acquired on Innova atomic force microscopy (Bruker) using NanoDrive (v8.03) software. The images were processed and analyzed using WSxM 5.0 Develop 8.1 software [43], and height profiles were plotted using Origin.

4.2.9 Sedimentation Assay

2.5 μM monomeric NM was aggregated in the presence of different concentrations of ATP in the assembly buffer (40 mM HEPES-KOH pH 7.4, 150 mM KCl, 1 mM DTT, 20 mM $MgCl_2$) at room temperature with stirring at 80 rpm. Later we pelleted amyloid species at 16,400 rpm

for 30 min. These pellets were resuspended in in 8 M Urea (20 mM Tris-HCl pH 7.4) and incubated overnight to monomerize the amyloids followed by SDS-PAGE analysis. Monomeric NM (2.5 μM) was aggregated in the assembly buffer (40 mM HEPES-KOH pH 7.4, 150 mM KCl, 1 mM DTT, 20 mM $MgCl_2$) at room temperature with stirring at 80 rpm. Multiple concentrations of ATP were added after 6 h from the commencement of the aggregation reaction and mixed thoroughly. Next, we pelleted amyloid species before and after the introduction of ATP at 16,400 rpm for 30 min. These pellets were resuspended in 8 M Urea (20 mM Tris-HCl pH 7.4) and incubated overnight to monomerize the amyloids. SDS-PAGE was performed, and band intensities were estimated using ImageJ software [44].

4.2.10 The proteinase K digestion of fibrils

Monomeric NM (2.5 μM) was aggregated in the assembly buffer (40 mM HEPES-KOH pH 7.4, 150 mM KCl, 1 mM DTT, 20 mM $MgCl_2$) without or with varying concentrations of ATP (2.5 nM, 2.5 μM, 2.5 mM, and 10 mM) for 6 h.The fibrils formed were pelleted by centrifugation at 16,400 rpm, 25 °C for 30 min, resuspended in the same buffer. We assumed 100 % recruitment of monomer to form fibrils. The sedimented fibrils were resuspended in a lower volume of aggregation buffer before PK digestion and according to the volume of that buffer, the fibril concentration is calculated from the monomer concentration of NM. Then these NM fibrils were incubated with proteinase K (PK) ([PK]: [Protein] 1:1000) at 37 °C for 30 min. Digestion reactions were stopped by adding SDS-loading dye and boiling them at 100 °C, followed by SDS-PAGE. Alternatively, the amyloid species retrieved from the pellets were resuspended in buffer B (150 mM KCl, 1mM DTT, 250 mM $MgCl_2$, and 40 mM HEPES-KOH pH 7.4) and were centrifuged at 16,400 rpm, 25 °C for 30 min. The retrieved pellets were resuspended again in the assembly buffer, followed by PK digestion and SDS-PAGE, as mentioned above.

4.2.11 Dot blot assay

Aggregation reactions of monomeric NM (2.5 μM) were set up in the assembly buffer (40 mM HEPES-KOH pH 7.4, 150 mM KCl, 1 mM DTT, 20 mM $MgCl_2$) at room temperature with stirring at 80 rpm. 2.5 nM or 10 mM ATP was introduced to the amyloids formed after 6 h from the commencement of the reaction. Alternatively, monomeric NM (2.5 μM) was aggregated in the assembly buffer (40 mM HEPES-KOH pH 7.4, 150 mM KCl, 1 mM DTT, 20 mM $MgCl_2$) at room temperature with stirring at 80 rpm. Then after 6 h from the commencement of the reaction, Hsp104 (0.5 μM), ATP (5 mM), and ATP regeneration system

(20 mM PEP and 15 µg/ml pyruvate kinase) were added. Two microlitres of samples were spotted on the nitrocellulose membrane before and after adding ATP or Hsp104. Next, for blocking, 3% BSA in PBST (0.05% Tween-20) was added and incubated for 1 h at room temperature, then blots were probed using a primary antibody (A11, 1:500; OC, 1:1000) overnight at 4 ºC. Next, the blots were washed six times with PBST and incubated with HRP-conjugated secondary antibody for 1 h at room temperature. The blots were thoroughly washed three times using PBST and subsequently developed using an ECL kit.

4.2.11 Circular dichroism (CD) measurements

Monomeric NM (2.5 µM) was aggregated in assembly buffer (40 mM HEPES-KOH pH 7.4, 150 mM KCl, 1 mM DTT, 20 mM $MgCl_2$) without or with several concentrations of ATP (2.5 nM, 2.5 µM, 2.5 mM, and 10 mM) at room temperature with stirring at 80 rpm for 6 h. The amyloid species were pelleted after 6 h at 16,400 rpm for 30 min and resuspended in 10 mM Na_2PO_4 (pH 7.4) buffer. The final concentration of NM was ~8 µM, after which far-UV CD spectra were recorded on a Chirascan CD spectrometer (Applied Photophysics, UK) at room temperature. All the spectra were collected and recorded in the scan range 195-260 nm with a 1 nm step size and a quartz cuvette of 1 mm path length. The spectra were averaged over 5-10 scans, and the buffer signal was subtracted. All the spectra were smoothened using the ProData software provided with the Chirascan CD Spectrometer. Finally, the mean residue ellipticity [θ] was calculated, and plots were generated using Origin software.

4.2.12 Fluorescence labeling of NM

Cysteine mutant of NM was labeled in the denaturation buffer 8 M Urea (20 mM Tris-HCl pH 7.4). A 30 mM stock of Fluorescin-5-maleimide was prepared in DMSO and was mixed in a ratio of 1:10 with the NM mutant. The reaction mixtures were kept in the dark for 2-3 h at room temperature on rotor spin. Next, to remove excess dye, the labeled protein was then buffer exchanged in a 3-kDa filter using 8 M Urea (20 mM Tris-HCl pH 7.4). The concentration of labeled protein was estimated using ε_{494} = 68000 $M^{-1}cm^{-1}$, and the labeling efficiency was >90% for the mutant protein.

4.2.13 Steady-state fluorescence measurements

Steady-state fluorescence measurements of a single cysteine mutant of NM (S150C) were carried out using a FluoroMax-4 spectrofluorometer (Horiba Jobin Yvon, NJ) at room temperature quartz cuvette of 1 mm path length. For recording the fluorescence spectra, the

mutants were excited at 485 nm, where the excitation and emission slits were 1.75 and 5 nm, respectively. Concomitantly, steady-state anisotropy measurements were performed by setting the excitation wavelength at 485 nm and emission wavelength at ~518 nm with excitation and emission slits as 2 and 8 nm, respectively.

4.2.14 Statistical analysis

All the experiments were performed three times, and the data are represented as mean ± SD indicated by scattered data points from independent experimental replicates. The statistical significance analysis was performed using one-way ANOVA tests, and the *p*-values were indicated in the figure legends. All the data analysis, data fitting (adjusted $R^2 > 0.95$), and data plotting were performed with the help of Origin.

4.3. Results

4.3.1 ATP accelerates amyloid aggregation of NM

The aggregation of NM displayed typical nucleation-dependent polymerization kinetics with a lag phase of ~55 min[31]. The lag phase was eliminated in the presence of 10 mM ATP ([NM] = 2.5 μM). However, such an acceleration of aggregation was not observed for the lower concentrations of ATP that showed comparable lag times with respect to the NM-only aggregation (Figure 4.1c). Additionally, 10 mM ADP also failed to eliminate the lag time of NM aggregation like ATP (Figure 4.1g). Next, in order to visualize the nanoscale morphology of these fibrils, we performed atomic force microscopy (AFM). We observed that the NM-only fibrils or NM fibrils formed from ATP-controlled aggregation (NM-ATP fibrils) possess morphological similarities despite their distinct kinetic profiles (Figure 4.1d-f). Over the years, magnesium ions have been reported to be indispensable with ATP as a cofactor to interact with several enzymes[32]. Hence, this experimental design permitted us to decipher the role of magnesium ions along with ATP in modulating the aggregation behavior, as we could set up the aggregation in the absence of magnesium ions. Interestingly, without Mg^{2+}, ATP did not alter the aggregation of NM, corroborating the importance of the Mg^{2+}-ATP complex in promoting the assembly of NM (Figure 4.1h,i). We would like to mention that we used the sodium salt of ATP instead of the magnesium salt and a buffer with 20 mM $MgCl_2$ for our studies if not otherwise stated. Next, we hypothesized that this effect of ATP in accelerating the aggregation is because NM harbors a lot of positively charged amino acid residues, such as lysine. Therefore, these positively charged moieties were possibly electrostatically screened by

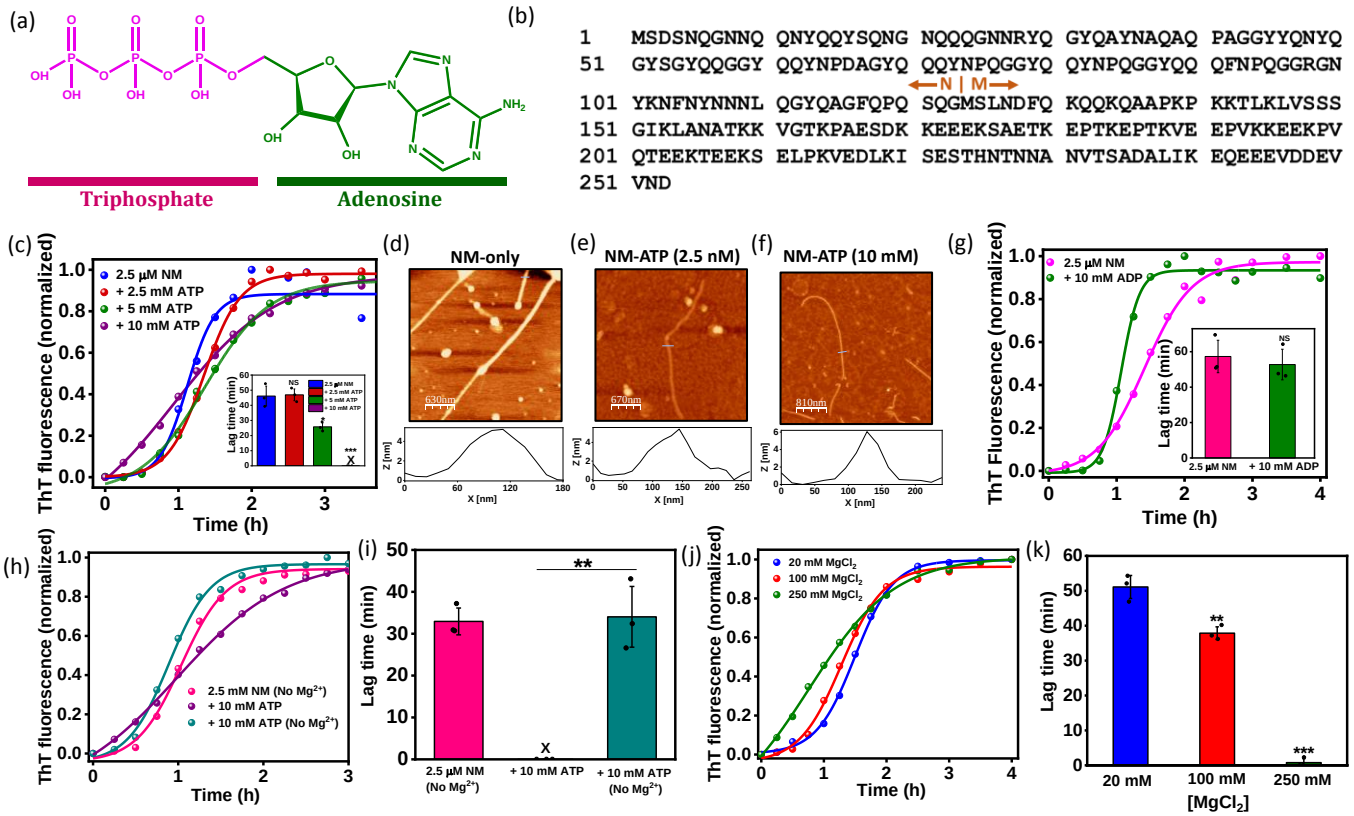

Figure 4.1. (a) The chemical structure of the ATP molecule highlighting the triphosphate (pink) and adenosine (green) moieties. The structure was drawn using ChemDraw. (b) The amino acid sequence of Sup35NM showing the putative boundary between the N and M-domains. (c) Representative normalized ThT fluorescence kinetics of rotated (80 rpm) NM (2.5 µM) aggregation without or with ATP at room temperature. All reaction mixtures contained 20 mM $MgCl_2$ unless otherwise stated. Lag times were retrieved from fitting fluorescence intensities to sigmoidal function. ATP accelerates NM aggregation. (Standard deviations were estimated from three independent replicates (n = 3), NS, $P < 0.05$, $P < 0.001$ for 2.5 mM, 5 mM, and 10 mM, respectively, compared to the NM-only aggregation (inset). (d) AFM image of NM-only fibrils (2.5 µM monomers) formed after 6 h of aggregation reaction with a height of ~ 6 nm. (e,f) AFM images of ATP-mediated NM fibrils (2.5 µM monomers) aggregated in the presence of (e) 2.5 nM ATP and (f) 10 mM ATP, with a height of ~5 nm. The ATP concentration with which the aggregation of 2.5 µM NM was set up is mentioned in the parenthesis in the case of NM-ATP amyloids. (h,i) Representative normalized ThT fluorescence kinetics of rotated (80 rpm) NM (2.5 µM monomers) aggregation in the absence of ATP and $MgCl_2$. Also, NM (2.5 µM monomer) was polymerized in the presence of 10 mM ATP without or with $MgCl_2$ at room temperature and 80 rpm. Lag times were retrieved from three independent replicates (n = 3), $P < 0.01$ for lag time of NM aggregation with ATP and without $MgCl_2$ compared to the NM aggregation with $MgCl_2$ and ATP. (j) Representative normalized ThT fluorescence kinetics of rotated (80 rpm) NM (2.5 µM) aggregation in the presence of 20 mM, 100 mM, and 250 mM $MgCl_2$ at room temperature. (k) Lag times of rotated (80 rpm) aggregation of NM monomers (2.5 µM) in the presence of 20 mM, 100 mM, and 250 mM $MgCl_2$ at room temperature. Standard deviations were calculated from three independent replicates (n = 3), $P < 0.01$, $P < 0.001$ for lag times in presence of 100 mM and 250 mM $MgCl_2$, respectively, compared to the lag time in the presence of 20 mM $MgCl_2$.)

the polyanion ATP at higher concentrations resulting in speeding up aggregation by reducing the repulsion between precursors. However, our aggregation kinetics studies in the presence ofvarious concentrations of $MgCl_2$ revealed that a much higher concentration of $MgCl_2$ was required to eliminate the lag phase of NM aggregation compared to the ATP (Figure 4.1j). This corroborated that the charge compensation might not be the reason that altered the fibrillation kinetics. These results pointed out that a high amount of ATP, with the help of Mg^{2+}, accelerates the NM aggregation that generates fibrils that morphologically resemble the NM-only fibrils.

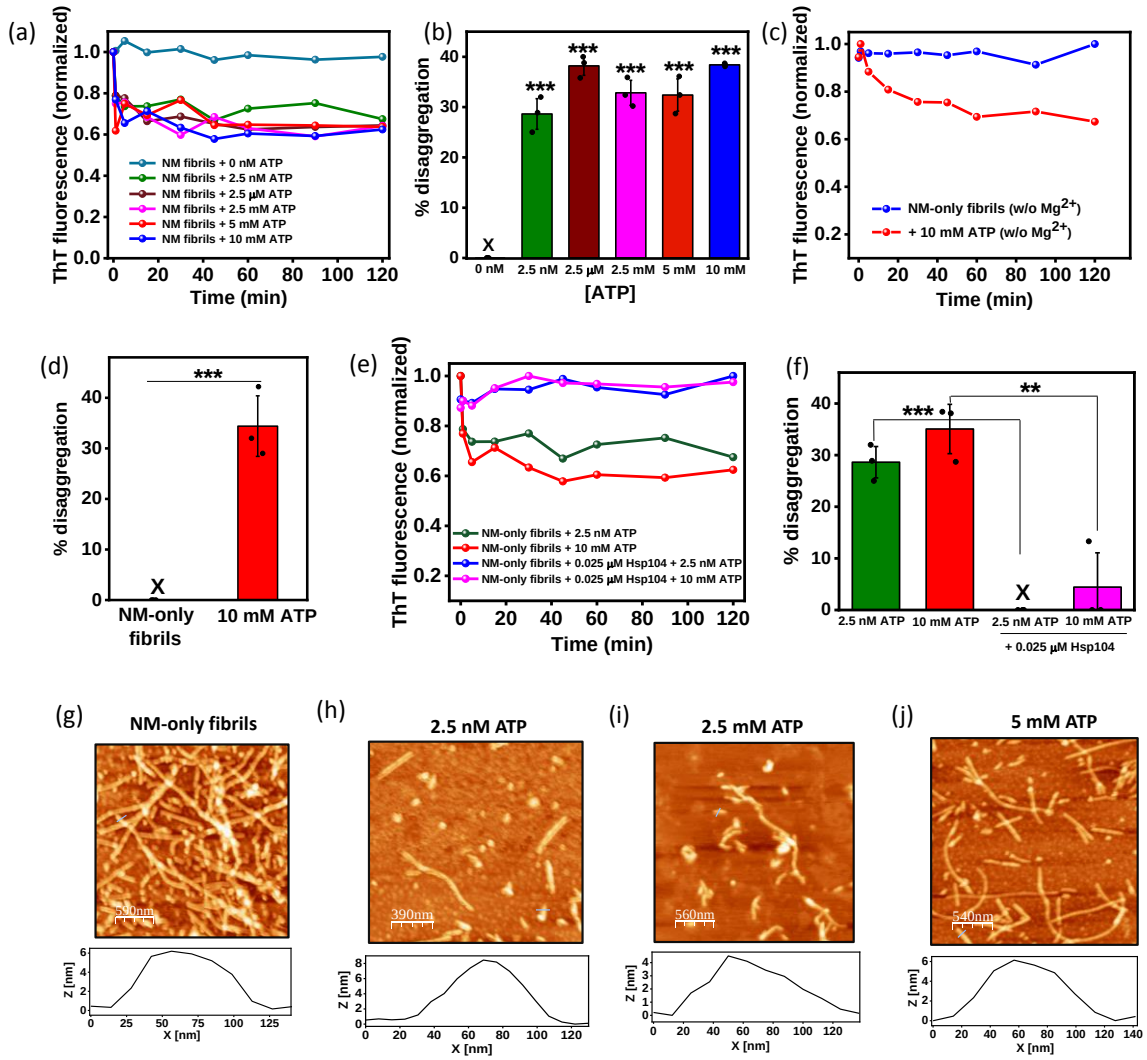

Figure 4.2. ATP disaggregates matured NM-only fibrils. (a) Representative disaggregation kinetics of NM-only fibrils (2.5 µM monomers) without or with ATP at room temperature and 80 rpm and (b) the percentage of disaggregation. Standard deviations were estimated from three independent replicates ($P < 0.001$) for the percentage of disaggregation with respect to no ATP. (c) Representative disaggregation kinetics of NM-only fibrils (2.5 µM monomers) without or with 10 mM ATP in the absence of $MgCl_2$ at room temperature and 80 rpm, showing the percentage of disaggregation in Figure 4.2d. Standard deviations were calculated from three independent replicates (n = 3), $P < 0.001$ for disaggregation by 10 mM ATP compared to NM-only fibrils. (e) Representative disaggregation kinetics of NM-only

fibrils (2.5 μM monomers) by ATP in the absence or presence of Hsp104 (0.025 μM) at room temperature and 80 rpm. (f) Percentage of disaggregation of NM-only fibrils (2.5 μM monomer) formed at room temperature and 80 rpm by ATP in the absence or presence of Hsp104 (0.025 μM). Standard deviations were calculated from three independent replicates (n = 3), $P < 0.001$ for disaggregation by 2.5 nM ATP in the presence of Hsp104 compared to in the absence of Hsp104; $P < 0.01$ for disaggregation by 10 mM ATP in the presence of Hsp104 compared to in the absence of Hsp104. (g) AFM image of intact NM-only fibrils (2.5 μM monomers) formed after 6 h of rotated aggregation (80 rpm) at room temperature with a height of ~5 nm. (h-j) AFM images of ATP-disaggregated NM amyloids by (h) 2.5 nM ATP (i) 2.5 mM ATP (j) 5 mM ATP with a height of ~6 nm after 15 min of the introduction of ATP.

4.3.2 ATP non-stoichiometrically disaggregates preformed amyloids

In order to discern the role of ATP as an amyloid disaggregating agent, we introduced ATP in a wide range of concentrations to the NM-only fibrils in the saturation phase of the aggregation reactions. Interestingly, we observed an immediate drop in ThT fluorescence upon the addition of ATP that indicated the disaggregation of fibrils, which was found to be independent of the presence or absence of $MgCl_2$ (Figure 4.2a-d). A very low concentration of Hsp104, which can disaggregate amyloids only in higher concentrations, inhibited the ATP-mediated disaggregation probably by hydrolyzing ATP due to its ATPase activity when it was introduced prior to ATP to the fibrils (Figure 4.2e,f). This observation further confirmed the role of ATP in amyloid dissolution. We observed fragmented fibrils in AFM after ATP-mediated disaggregation (Figure 4.2g-k). Next, upon careful analysis of the ThT fluorescence before and after disaggregation, we estimated that the extent of disaggregation remained similar, irrespective of the dose of ATP (Figure 4.2b). To further establish the non-stoichiometric nature of ATP-amyloid interaction in aggregate solubilization, we sedimented NM amyloids before and after the introduction of ATP. However, we noticed a minimal yet similar decrease in the fraction of sedimentable amyloids after disaggregation, irrespective of the concentration of ATP used (Figure 4.3a,b). Furthermore, this led us to postulate that there was only a nominal fibril to non-sedimentable amyloid conversion upon the ATP-mediated amyloid disassembly. Therefore, we utilized the AFM imaging in conjunction with immunoreactivity against the A11 and OC antibodies that specifically detects amyloidogenic oligomers and amyloid fibrils, respectively, to precisely characterize the products of the disaggregation caused by ATP. Moreover, we compared these particles with the species generated from the disaggregation of NM fibrils by the canonical disaggregating chaperone of yeasts called Hsp104. The AFM images showed that the matured fibrils fragmented into protofibrillar aggregates with reduced length and no spherical particles reminiscent of oligomers by ATP. In contrast, disassembly by

Hsp104 resulted in a mixture of oligomers and short protofibrils in AFM. Further, we observed an increase in the A11 signal on Hsp104-induced NM disaggregation, confirming fibril to

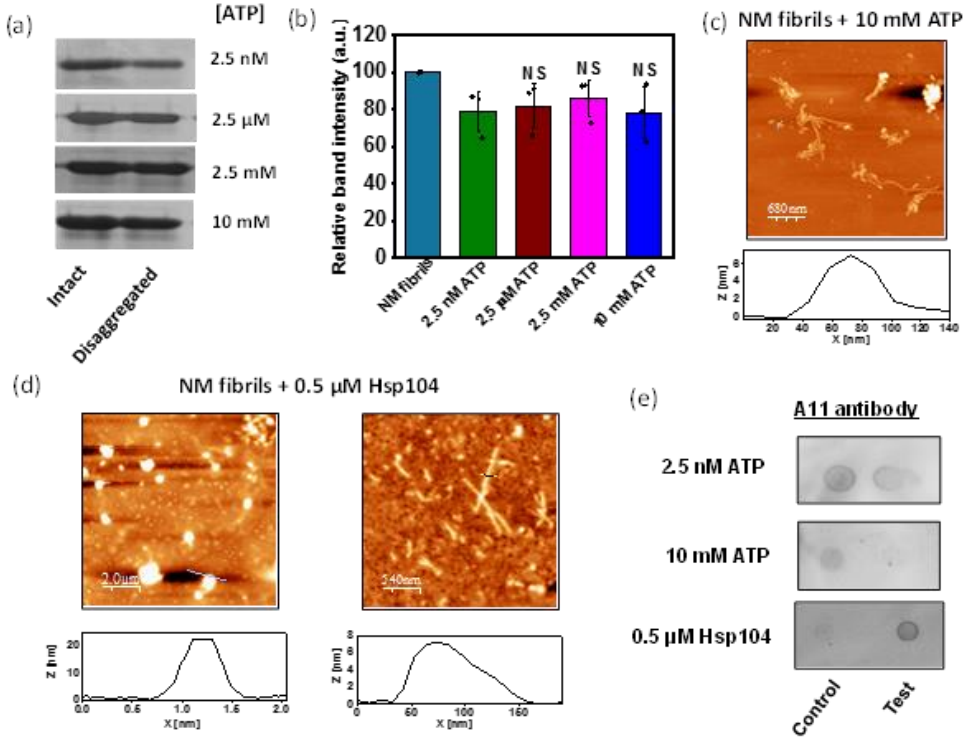

Figure 4.3. (a) SDS-PAGE image showing the monomers retrieved before and after disaggregation by ATP of amyloids formed from the rotated (80 rpm) polymerization of NM (2.5 µM) at room temperature after pelleting down amyloids and incubating the pellet in 8 M Urea (20 mM Tris-HCl pH 7.4) overnight. (b) The relative quantification of NM monomers retrieved before and after disaggregation of amyloids by ATP with respect to the band intensity of intact NM-only fibrils in SDS-PAGE by ImageJ software. Standard deviations were calculated from three independent replicates (n = 3); NS, NS, and NS for relative band intensity after disaggregation by 2.5 µM, 2.5 mM, and 10 mM compared to 2.5 nM ATP, respectively. (c) AFM images of ATP-disaggregated NM amyloids by 10 mM ATP with a height of ~6 nm after 15 min of the introduction of ATP. (d) AFM images showing disaggregation of amyloids formed from rotated (80 rpm) aggregation reaction of NM (2.5 µM) at room temperature by Hsp104 (0.5 µM) with the heights of ~22 nm for oligomers and ~7 nm for protofibrils. (e) Samples from the NM aggregation reactions before and after disaggregation by 2.5 nM ATP, 10 mM ATP, and 0.5 µM Hsp104 were spotted on the nitrocellulose membrane and were probed using the A11 antibody.

oligomer formation. As anticipated, the signal for oligomers reduced after the introduction of ATP, validating no generation of oligomers from mature fibrils upon disaggregation (Figure 4.3c-e). Taken together, our results showed that ATP can act as a unique, non-canonical disaggregating agent that non-stoichiometrically fragments matured fibrils without yielding

oligomers. This was distinct from the case of the disaggregases that generated oligomers that are crucial for prion-like propagation.

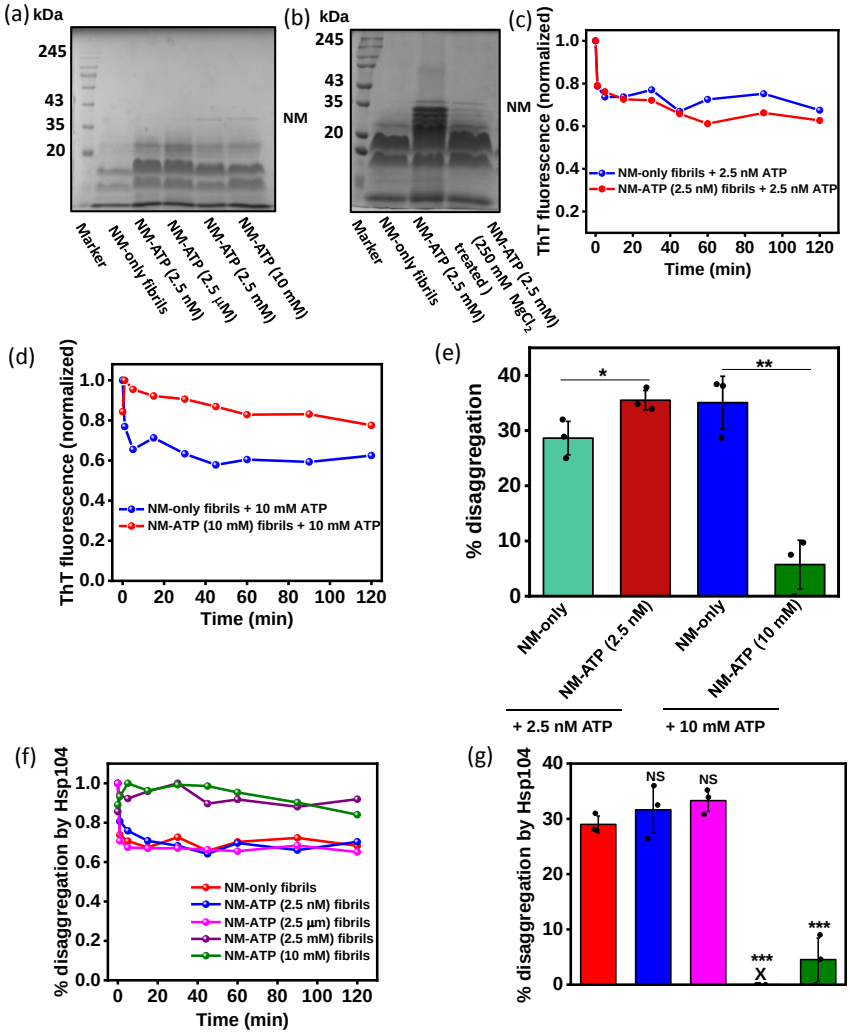

Figure 4.4. The stability and fragility of NM-ATP amyloids. (a) The concentrated fibrils formed from monomeric NM (2.5 μM) without or with ATP were incubated at 37 ºC for 30 min with proteinase K (PK) (NM: PK 1000:1), followed by SDS-PAGE analysis.(b) The concentrated fibrils formed from monomeric NM (2.5 μM) in the absence or presence of 2.5 mM ATP were incubated at 37 ºC for 30 min with PK (NM: PK 1000:1). Also, the NM-ATP fibrils formed in the presence of 2.5 mM ATP were treated with 250 mM $MgCl_2$ and then incubated at 37 ºC for 30 min with PK (NM: PK 1000:1) followed by SDS-PAGE analysis.(c) Representative ThT fluorescence disaggregation kinetics of NM-only fibrils (2.5 μM monomers) or NM-ATP (2.5 nM) fibrils by 2.5 nM ATP at room temperature and 80 rpm. (d) Representative ThT fluorescence disaggregation kinetics of NM-only fibrils (2.5 μM monomers) or NM-ATP (10 mM) fibrils by 10 mM ATP at room temperature and 80 rpm. (e) Percentage disaggregation of NM-only fibrils and NM-ATP (2.5 nM) fibrils by 2.5 nM ATP or NM-only fibrils and NM-ATP (10 mM) fibrils by 10 mM ATP. Standard deviations were calculated from three independent replicates (n = 3), $P < 0.05$, $P < 0.01$ for percentage disaggregation by 2.5 nM ATP of NM-ATP (2.5 nM) fibrils compared to NM-only fibrils and by 10 mM ATP of NM-ATP (10 mM) fibrils compared to NM-only fibrils, respectively. (f) Representative ThT fluorescence disaggregation kinetics of NM-only fibrils (2.5 μM monomers) or NM-ATP fibrils by Hsp104 (0.5 μM), ATP (5 mM), and ATP regeneration system and (g) the percentage of disaggregation. Standard deviations were calculated from three independent replicates (n = 3), NS, NS, $P < 0.001$, $P < 0.001$ percentage disaggregation by

Hsp104 of NM-ATP fibrils formed in the presence of 2.5 nM, 2.5 μM, 2.5 mM, and 10 mM ATP compared to NM-only fibrils, respectively.

4.3.3 ATP generates compact and stable amyloids

Based on our results described above, we next asked whether ATP can also act as an amyloid disaggregating agent for NM-ATP amyloids similar to the NM-only amyloids assuming their encounter with the free ATP molecules in the cellular milieu. Although all amyloids exhibit a generic cross-β-sheet rich structure, the binding of ATP during aggregation might contribute to the altered packing and kinetic stability of amyloid cores. Hence, assessing the conformational compactness of amyloids is crucial as it may dictate its fragility that drives the prion-like spread by generating amyloid seeds. Accordingly, we intended to characterize the packing of ATP-mediated NM amyloids via its sensitivity against proteolytic digestion by proteinase K (PK). PK is a non-specific endoprotease that digests the constituent monomers of amyloids that are not recruited in the amyloid core[33]. Thus, the digestion pattern of amyloids by PK reveals the supramolecular packing and stability of amyloids. Subsequently, we incubated the NM-only or NM-ATP fibrils formed in the presence of different concentrations of ATP with PK and observed that NM-only fibrils were completely digested by it, resulting in lower molecular weight peptides. On the other hand, NM-ATP amyloids exhibited more resistance to PK digestion showing relatively intense monomeric and sub-monomeric bands in SDS-PAGE. Notably, the NM-ATP fibrils formed in the presence of higher concentrations of ATP exhibited the most resistant amyloid cores demonstrating a prominent, undigested NM monomeric band at ~35 kDa (Figure 4.4a). Since NM is rich in positively charged amino acids, we suspected that the electrostatic association between ATP and such residues was crucial for the remarkable kinetic stability of NM-ATP fibrils. To test this hypothesis, the NM-ATP fibrils were treated with the high $MgCl_2$ buffer to disrupt the electrostatic interactions between aggregates and ATP prior to the protease digestion. However, in this case, an intermediate protease resistance pattern was observed compared to the NM-only fibrils and the salt-untreated NM-ATP fibrils (Figure 4.4b) .These observations indicated that the electrostatic interactions between the ATP and proteins were only partially responsible for generating stable and compact amyloids. Based on this set of data, we were next interested in deciphering how the stability of NM-ATP fibrils impacted their fragility. Accordingly, we used two different disaggregating agent such as Hsap104 and free ATP. Intriguingly, the NM-ATP fibrils formed in the presence of higher ATP concentrations showed much less fragmentation propensity,

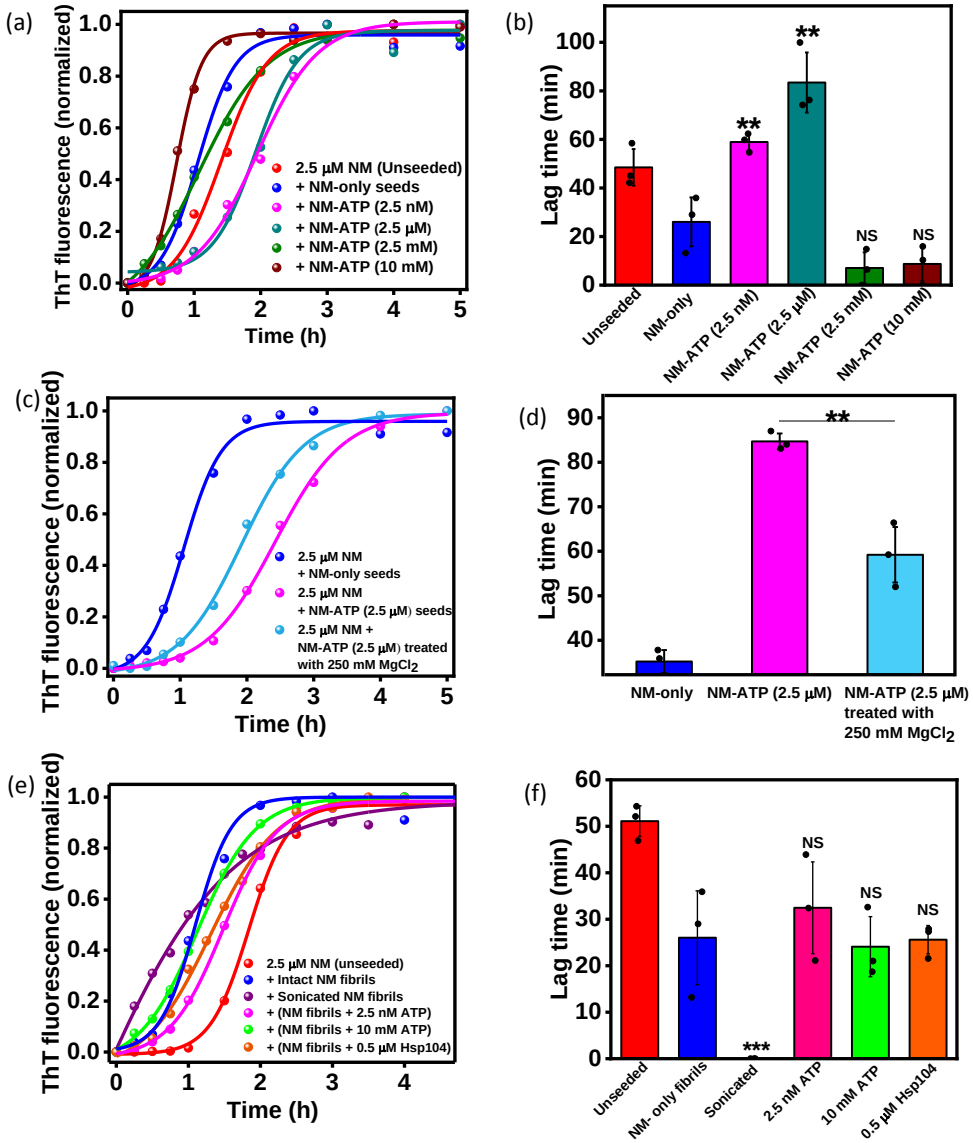

Figure 4.5. Seeding by NM-ATP amyloids. (a) Representative normalized ThT fluorescence kinetics of rotated (80 rpm) NM aggregation seeded without or with 10 % (w/w) NM-only fibrils (2.5 μM monomers) or NM-ATP fibrils aggregated in the presence of ATP. (b) Lag times estimated from the fitting. Standard deviations were calculated from three independent replicates (n = 3), $P < 0.01$, $P < 0.01$, NS, and NS for lag times in the case of NM-ATP fibrils formed in the presence of 2.5 nM, 2.5 μM, 2.5 mM, and 10 mM ATP compared to NM-only fibrils. (c) Representative normalized ThT fluorescence kinetics of NM aggregation rotated at 80 rpm at room temperature seeded with 10 % (w/w) NM-only fibrils (2.5 μM monomers) or NM-ATP (2.5 μM) fibrils. Also, NM-ATP (2.5 μM) fibrils treated with 250 mM $MgCl_2$ were used as seeds. (d) Lag times for seeded aggregation reactions, as mentioned in Figure 4.5c. Standard deviations were calculated from three independent replicates (n = 3), $P < 0.01$ for the lag time of seeded aggregation with 250 mM $MgCl_2$-treated NM-ATP fibrils compared to 250 mM $MgCl_2$-untreated NM-ATP fibrils. (e) Representative normalized ThT fluorescence kinetics of NM aggregation reaction rotated at 80 rpm and room temperature in the absence or presence of 10 % (w/w) seeds of intact NM-only fibrils (2.5 μM monomers), sonicated NM fibrils, NM-only fibrils disaggregated by 2.5 nM,10 mM ATP or 0.5 μM Hsp104. (f) Lag times estimated from the fitting. Standard deviations were calculated from three independent replicates (n = 3), $P < 0.001$, NS, NS, NS for seeded aggregation reactions seeded by sonicated NM fibrils, disaggregated NM-only

fibrils by 2.5 nM ATP, and 10 mM ATP, 0.5 μM Hsp104, respectively, compared to intact NM-only fibrillar seeds. The trace (blue) in 4.5a, 4.5c, and 4.5e are from the same dataset (10 % intact NM-only seeds, total [NM] = 2.5 μM) shown for comparison.

regardless of the disaggregating agent. However, the NM-ATP fibrils created in the presence of a trace amount of ATP demonstrated fragility similar to the NM-only fibrils (Figure 4.4c-g). In summary, these results indicated that the presence of high concentrations of ATP during the assembly of NM might give rise to stable and compact amyloids that displayed minimal fragmentation and may restrict the prion-like propagation of amyloids by limiting the formation of lower-order seeds.

4.3.4 ATP at low concentrations creates seeding-inefficient amyloids

Apart from the fragility of amyloids that regulate the number of seeds, the seeding efficiency accessed by their ability to accelerate a fresh aggregation reaction is a critical factor in prion-like amyloid transmission. Hence, we introduced them in the fresh aggregation reactions to elucidate the seeding potential of NM particles aggregated in the presence of ATP. The NM-ATP fibrils polymerized in the presence of millimolar concentrations of ATP exhibited seeding capability similar to the NM-only fibrils. On the contrary, the fibrils aggregated in the presence of low concentrations of ATP failed to accelerate the fresh aggregation reactions, as evident by similar lag times of unseeded and seeded aggregation kinetics (Figure 4.5a,b). We then intended to reverse the seeding inefficiency of NM-ATP fibrils generated in the presence of very low concentrations of ATP by treating them with a high $MgCl_2$ buffer to dissociate the electrostatically attached ATP molecules to amyloids. However, we were only able to partially recover the seeding capability with respect to the NM-only fibrillar seeds validating that amyloid-ATP interaction was not the sole factor that controlled the seeding inability of NM-ATP amyloids (Figure 4.5c,d). Next, we hypothesized that the fibrils disaggregated by ATP might also efficiently seed the fresh aggregation reaction due to the increase in the number of growth-competent amyloid ends and might facilitate the prion-like propagation. Therefore, we performed seeded aggregation with ATP-disaggregated NM fibrils, and, as the control, the seeds obtained from the disaggregation of NM fibrils by ultrasonic sound pulses and Hsp104. On careful inspection of the seeded aggregation kinetics, we found that the amyloids derived upon disaggregation of fibrils by ATP displayed a seeding ability similar to the intact fibrils. This data revalidated our previous observations in AFM and immunoblots that suggested a minimal change in the number and molecular weight of amyloids upon disaggregation by ATP. Moreover, the seeds created by Hsp104-induced disaggregation of NM fibrils exhibited

minimal seeding ability possibly due to the conversion of a major fraction of the fibrils to the non-self-templating entities. In contrast, a much greater seeding ability for sonicated fibrils was observed, indicating a considerable increase in the number of particles upon sonication that eliminated the lag time in seeded aggregation (Figure 4.5e,f) . Taken together, these data indicated that in the millimolar concentration regime, the presence of ATP during aggregation hardly impacted the seeding potential of the NM-ATP fibrils. On the contrary, the trace amount of ATP may lead to the formation of seeding-inefficient amyloids, which can impair their amplification cascade. In addition, unlike other disaggregating agents, the disaggregation of fibrils by ATP did not translate into an improved seeding, unmasking a propagation-neutral attribute of molecular ATP.

4.3.5 Conformational characterizations of ATP-mediated amyloids

The presence of molecular ATP during the polymerization of NM altered the stability and seeding potential of the amyloids. However, our PK sensitivity assay or seeded aggregation kinetics of NM-ATP amyloids indicated that the dissociation of electrostatically attached ATP could not completely reverse the consequences of ATP binding. These observations lead to the assumption that some changes may have occurred in the amyloid structure upon binding of ATP to the building blocks of these aggregates, which governed their conformational stability and seeding ability. To capture these plausible conformational remodeling of NM amyloids in the presence of various ATP concentrations, we employed circular dichroism spectroscopy and site-specific fluorescence spectroscopy, which is widely used to gain structural insights into several amyloids. We also performed circular dichroism (CD) spectroscopy to reconfirm the secondary structural content of NM-ATP amyloids. We noticed a drop in ratiometric mean residue ellipticity ($\theta_{218}/\theta_{200}$), representing the propensity to form β-sheet at the expense of random coil in the case of NM-ATP fibrils corresponding to nanomolar and micromolar ATP[34]. Contrastingly, in the presence of 10 mM ATP, $\theta_{218}/\theta_{200}$ was more for NM-ATP fibrils compared to the NM-only fibrils indicating a greater extent of β-sheet structure in these fibrils (Figure 4.6a,b). We also observed an increase in the fluorescence steady-state anisotropy with increasing ATP concentrations indicating more restricted rotation of the fluorophore fluorescein-5-maleimide-Cys150-NM amyloid fibrils in the M-domain due to the more ordered

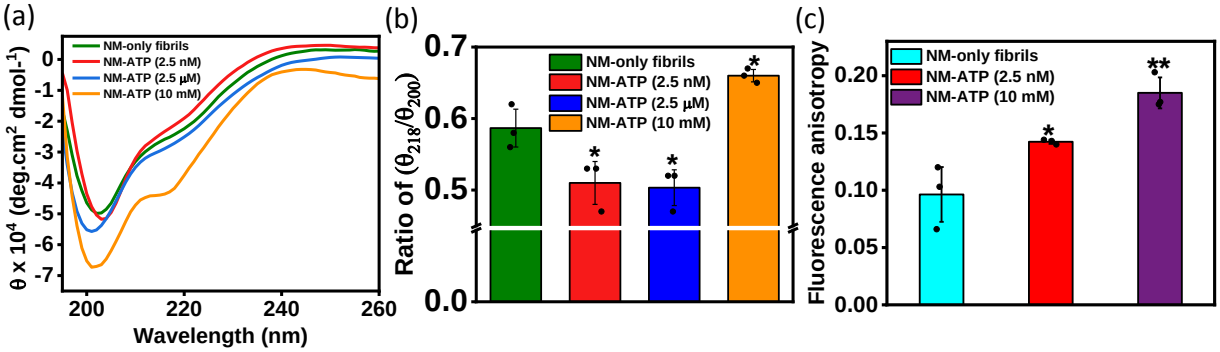

Figure 4.6. (a) Representative Far-UV CD spectra of NM-only fibrils (2.5 µM monomers) and NM-ATP fibrils in the presence of different concentrations of ATP. (b) Plot shows a of ratiometric ellipticity ($\theta_{218}/\theta_{200}$) for NM-only and NM-ATP fibrils. Standard deviations were calculated from three independent replicates (n = 3); $P < 0.05$, $P < 0.05$, and $P < 0.05$ for NM-ATP amyloids formed in the presence of 2.5 nM, 2.5 µM and 10 mM ATP, respectively, as compared to NM-only fibrils. (c) Steady-state fluorescence anisotropy of fluorescein-5-maleimide-Cys150-NM amyloid fibrils formed in the absence or presence of different concentrations of ATP. Standard deviations were calculated from three independent replicates (n = 3), $P < 0.05$ in the presence of 2.5 nM and $P < 0.01$ in the presence of 10 mM ATP compared to NM-only fibrils.

conformation validating our CD, and proteinase K sensitivity assay results (Figure 4.6c). Taken together CD, and fluorescence anisotropy results provided evidence of the Mg^{2+}-dependent conformational remodeling of NM amyloids by ATP, giving rise to altered secondary structures that can potentially govern several biologically important aspects.

4.4 Discussion

ATP is well-known for its role as cellular energy currency to fuel various physiological processes. In this current study, we were able to delineate a unique role of ATP in amyloid formation and disaggregation that may regulate the prion-like transmission of self-replicable amyloid entities. Our aggregation kinetics revealed that physiologically high concentrations of ATP facilitated the aggregation of NM. Further, Mg^{2+} was found to be indispensable with ATP in modulating both of these aggregation kinetics. Our aggregation kinetics data suggested that Mg^{2+} strengthened the electrostatic association between the anionic triphosphate moiety of ATP and positively charged amino acid residues in proteins such as lysine as suggested in previous reports[14,11, 35]. Interestingly, the electrostatic binding was weaker in the case of ADP due to lack of a phosphate moiety in these molecules. Moreover, Mg^{2+} ions also possibly extended the interaction of ATP by acting as a bridge between negatively charged amino acids and triphosphates by minimizing their electrostatic repulsion[36]. In order to gain more mechanistic insight into Mg^{2+}-ATP dependent kinetic acceleration, we polymerized NM

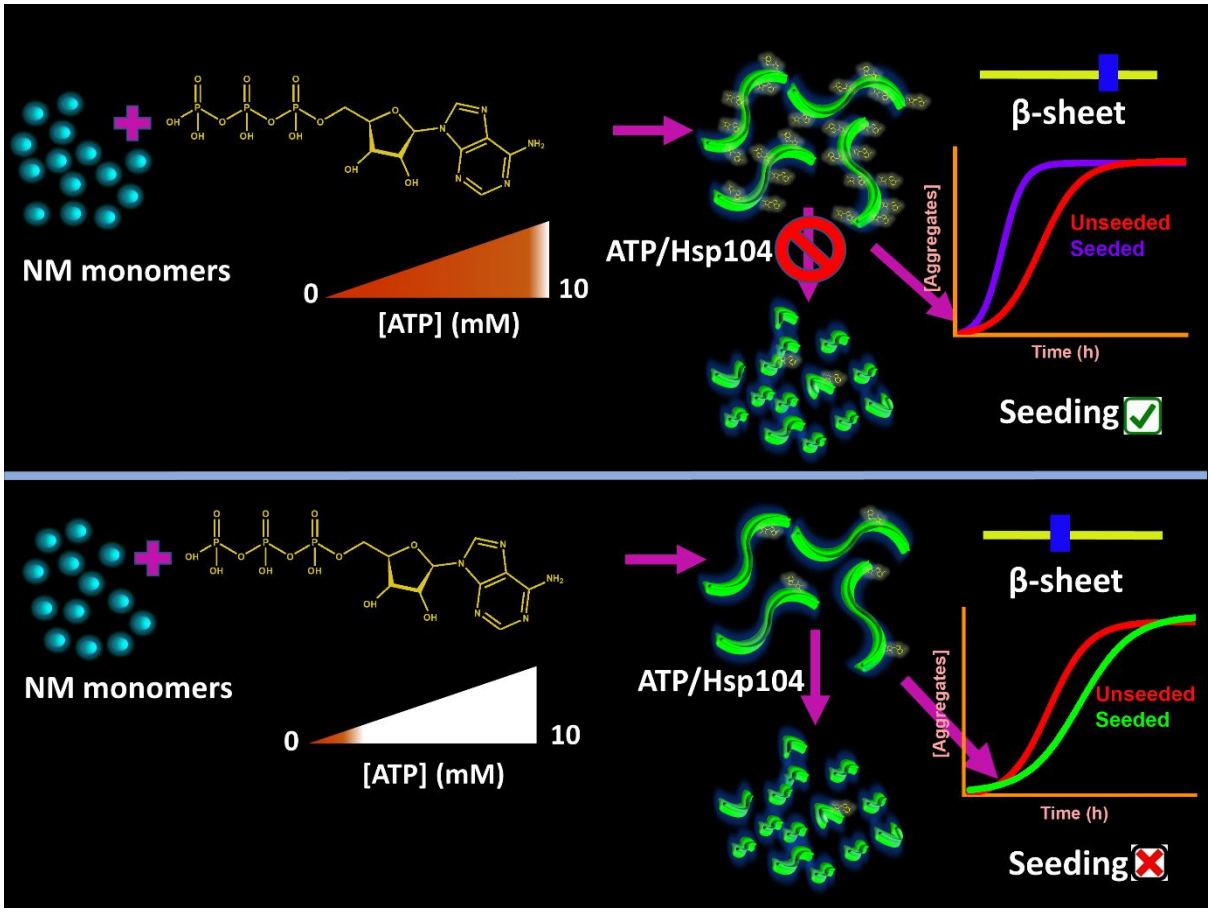

Figure 7. ATP may restrict the prion-like amyloid transmission by creating ATP-bound, robust amyloids at physiologically high concentrations that cannot further fragment to generate seeds or by generating seeding-inefficient amyloids having reduced β-sheet content at trace concentrations.

without ATP in the presence of high concentrations of $MgCl_2$ to screen the repulsion between building blocks, which might promote the aggregation. However, a much higher Mg^{2+}concentration was required to obtain a similar kinetic acceleration than ATP. Therefore, it possibly indicated the electrostatic crosslinking using lysine and multidentate triphosphate part of ATP that facilitated the critical nucleus formation, like in the case of the TauK18 aggregation[11].

Additionally, the amphipathic nature of ATP allowed it to participate in different chemical interactions, similar to the industrial hydrotropes, utilizing its hydrophobic aromatic part to solubilize NM fibrils, as reported in a previous study. Interestingly, this dissolution of NM fibrils was found to be Mg^{2+}-independent. Further, in agreement with the previous report, the extent of disaggregation was comparable, regardless of the ATP concentrations[5]. In addition to these observations, we were also able to elucidate critical anti-prion-like attributes of molecular ATP, as represented in Figure 4.7. For example, ATP could not disaggregate NM-ATP amyloids polymerized in the presence of physiologically high concentrations of ATP, delimiting the number of autocatalytic amyloid seeds for the prion-like transmission. The trace

ATP concentrations, reminiscent of oxidative stress or aging, gave rise to the seeding-incompetent NM amyloids that can impair the prion-like amplification cycles in recipient cells[37]. Two principal factors of ATP governed these phenomena. Firstly, the extensive binding of ATP in the lysine-rich M-domain of NM reinforced an extensive crosslinking through ATP molecules, especially in high concentrations, that resulted in a protease-resistant core. This remarkable conformational compactness probably made these amyloids inaccessible to disaggregating factors such as free ATP or Hsp104 that target the M-domain. Secondly, a remodeling in amyloid conformations in NM-ATP amyloids due to the binding of ATP during aggregation. Intriguingly, these nanoscale structural alterations in NM-ATP amyloids were dependent on the concentrations of ATP as per our CD data. Our detailed analysis indicated that the seeding-competent NM-only and NM-ATP fibrils formed in the presence of 10 mM ATP had a higher ratio of β-sheet to the random coil as opposed to the other NM-ATP fibrils that showed a greater extent of a random coil. This reduction in the β-sheet content probably was the reason for their seeding inefficiency[38,39]. Moreover, the detailed profiling of ATP-disaggregated fibrils by AFM and immunoblots revealed that ATP did not promote fibril to oligomer formation, unlike the canonical disaggregase Hsp104. This pointed toward the fact that the disaggregation by ATP may have a limited effect on the transmission and pathology as oligomers are considered as the predominant particles for infection and toxicity in amyloid-associated diseases[40].

In summary, our results provided key insights into ATP as a small chemical chaperone, that regulates the number and efficiency of seeds that may limit the spread of amyloids. Our findings on the modulation of amyloidogenesis covering orders of magnitude of the concentration range of ATP indicated some of the previously unexplored roles of this polyanion as an anti-propagation factor, in addition to its role in suppressing aggregation or dissolving preformed aggregates. Collectively, our study revealed a direct participation of molecular ATP to maintain proteostasis in addition to being the energy currency for chaperones. Considering generic nature of ATP-protein interactions, our results can have broad implications in functional non-Mendelian inheritance traits and transmissible neurodegenerative diseases associated with a diverse range of prions and prion-like domains.

4.5 References

(1) Chiti, F., and Dobson, C. M. (2017) Protein misfolding, amyloid formation, and human disease: A summary of progress over the last decade. *Annu. Rev. Biochem. 86*, 27–68.

(2) Ke, P. C., Zhou, R., Serpell, L. C., Riek, R., Knowles, T. P. J., Lashuel, H. A., Gazit, E., Hamley, I. W., Davis, T. P., Fändrich, M., Otzen, D. E., Chapman, M. R., Dobson, C. M., Eisenberg, D. S., and Mezzenga, R. (2020) Half a century of amyloids: Past, present and future. *Chem. Soc. Rev. 49*, 5473–5509.

(3) Iadanza, M. G., Jackson, M. P., Hewitt, E. W., Ranson, N. A., and Radford, S. E. (2018) A new era for understanding amyloid structures and disease. *Nat. Rev. Mol. Cell Biol. 19*, 755–773.

(4) Hipp, M. S. (2019) The proteostasis network and its decline in ageing. *Nat. Rev. Mol. Cell Biol.*

(5) Patel, A., Malinovska, L., Saha, S., Wang, J., Alberti, S., Krishnan, Y., and Hyman, A. A. (2017) Biochemistry: ATP as a biological hydrotrope. *Science 356*, 753–756.

(6) Moran, U., Phillips, R., and Milo, R. (2010) SnapShot: Key numbers in biology. *Cell 141*, 1–2.

(7) Snow, A. D., Kisilevsky, R., Willmer, J., Prusiner, S. B., and DeArmond, S. J. (1989) Sulfated glycosaminoglycans in amyloid plaques of prion diseases. *Acta Neuropathol. 77*, 337–342.

(8) Roy, E. R., Wang, B., Wan, Y. W., Chiu, G., Cole, A., Yin, Z., Propson, N. E., Xu, Y., Jankowsky, J. L., Liu, Z., Lee, V. M. Y., Trojanowski, J. Q., Ginsberg, S. D., Butovsky, O., Zheng, H., and Cao, W. (2020) Type I interferon response drives neuroinflammation and synapse loss in Alzheimer disease. *J. Clin. Invest. 130*, 1912–1930.

(9) Liu, C. C., Zhao, N., Yamaguchi, Y., Cirrito, J. R., Kanekiyo, T., Holtzman, D. M., and Bu, G. (2016) Neuronal heparan sulfates promote amyloid pathology by modulating brain amyloid-β clearance and aggregation in Alzheimer's disease. *Sci. Transl. Med. 8*, 1–12.

(10) Calamai, M., Kumita, J. R., Mifsud, J., Parrini, C., Ramazzotti, M., Ramponi, G., Taddei, N., Chiti, F., and Dobson, C. M. (2006) Nature and significance of the interactions between amyloid fibrils and biological polyelectrolytes. *Biochemistry 45*, 12806–12815.

(11) Kim, H. I., Heo, C. E., Han, J. Y., Lim, S., Lee, J., Im, D., Lee, M. J., and Kim, Y. K. (2020) ATP kinetically modulates pathogenic tau fibrillations. *ACS Chem. Neurosci. 11*, 3144–3152.

(12) Exley, C., and Korchazhkina, O. V. (2001) Promotion of formation of amyloid fibrils by

aluminium adenosine triphosphate (A1ATP). *J. Inorg. Biochem. 84*, 215–224.

(13) Greiner, J. V., and Glonek, T. (2020) Hydrotropic function of ATP in the crystalline lens. *Exp. Eye Res. 190*, 107862.

(14) Mehringer, J., Do, T. M., Touraud, D., Hohenschutz, M., Khoshsima, A., Horinek, D., and Kunz, W. (2021) Hofmeister versus Neuberg: is ATP really a biological hydrotrope? *Cell Reports Phys. Sci. 2*, 100343.

(15) Babinchak, W. M., Haider, R., Dumm, B. K., Sarkar, P., Surewicz, K., Choi, J. K., and Surewicz, W. K. (2019) The role of liquid-liquid phase separation in aggregation of the TDP-43 low-complexity domain. *J. Biol. Chem. 294*, 6306–6317.

(16) Polymenidou, M., and Cleveland, D. W. (2011) The seeds of neurodegeneration: Prion-like spreading in ALS. *Cell 147*, 498–508.

(17) Pearce, M. M. P., Spartz, E. J., Hong, W., Luo, L., and Kopito, R. R. (2015) Prion-like transmission of neuronal huntingtin aggregates to phagocytic glia in the Drosophila brain. *Nat. Commun. 6*.

(18) Brundin, P., and Melki, R. (2017) Prying into the prion hypothesis for parkinson's disease. *J. Neurosci. 37*, 9808–9818.

(19) Mehra, S., Ahlawat, S., Kumar, H., Datta, D., Navalkar, A., Singh, N., Patel, K., Gadhe, L., Kadu, P., Kumar, R., Jha, N. N., Sakunthala, A., Sawner, A. S., Padinhateeri, R., Udgaonkar, J. B., Agarwal, V., and Maji, S. K. (2022) α-Synuclein Aggregation Intermediates form Fibril Polymorphs with Distinct Prion-like Properties. *J. Mol. Biol. 434*, 167761.

(20) Costa, D. C. F., de Oliveira, G. A. P., Cino, E. A., Soares, I. N., Rangel, L. P., and Silva, J. L. (2016) Aggregation and prion-like properties of misfolded tumor suppressors: Is cancer a prion disease? *Cold Spring Harb. Perspect. Biol. 8*, 1–22.

(21) Goedert, M., Masuda-Suzukake, M., and Falcon, B. (2017) Like prions: The propagation of aggregated tau and α-synuclein in neurodegeneration. *Brain 140*, 266–278.

(22) Nakagawa, Y., Shen, H. C. H., Komi, Y., Sugiyama, S., Kurinomaru, T., Tomabechi, Y., Krayukhina, E., Okamoto, K., Yokoyama, T., Shirouzu, M., Uchiyama, S., Inaba, M., Niwa, T., Sako, Y., Taguchi, H., and Tanaka, M. (2022) Amyloid conformation-dependent disaggregation in a reconstituted yeast prion system. *Nat. Chem. Biol. 18*, 321–331.

(23) Desantis, M. E., and Shorter, J. (2012) Hsp104 drives "protein-only" positive selection of sup35 prion strains encoding strong [PSI+]. *Chem. Biol. 19*, 1400–1410.

(24) Figueira, A. J., Moreira, G. G., Saavedra, J., Cardoso, I., and Gomes, C. M. (2022) Tetramerization of the S100B Chaperone Spawns a Ca2+ Independent Regulatory Surface that Enhances Anti-aggregation Activity and Client Specificity. *J. Mol. Biol. 434*.

(25) Mahapatra, S., Sarbahi, A., Madhu, P., Swasthi, H. M., Sharma, A., Singh, P., and Mukhopadhyay, S. (2022) Sub-stoichiometric Hsp104 regulates the genesis and persistence of self-replicable amyloid seeds of Sup35 prion domain. *J. Biol. Chem.* 102143.

(26) Xue, W., Hellewell, A. L., Hewitt, E. W., Radford, S. E., Hellewell, A. L., Hewitt, E. W., Radford, S. E., Xue, W., Hellewell, A. L., Hewitt, E. W., and Radford, S. E. (2010) When size matters *6896*.

(27) Marchante, R., Beal, D. M., Koloteva-Levine, N., Purton, T. J., Tuite, M. F., and Xue, W. F. (2017) The physical dimensions of amyloid aggregates control their infective potential as prion particles. *Elife 6*, 1–20.

(28) Breydo, L., and Uversky, V. N. (2015) Structural, morphological, and functional diversity of amyloid oligomers. *FEBS Lett. 589*, 2640–2648.

(29) Chernova, T. A., Chernoff, Y. O., and Wilkinson, K. D. (2019) Yeast models for amyloids and prions: Environmental modulation and drug discovery. *Molecules 24*, 1–23.

(30) Uptain, S. M., Sawicki, G. J., Caughey, B., and Lindquist, S. (2001) Strains of [PSI+] are distinguished by their efficiencies of prion-mediated conformational conversion. *EMBO J. 20*, 6236–6245.

(31) Adamcik, J., and Mezzenga, R. (2018) Amyloid Polymorphism in the Protein Folding and Aggregation Energy Landscape. *Angew. Chemie - Int. Ed. 57*, 8370–8382.

(32) Williams, N. H. (2000) Magnesium ion catalyzed ATP hydrolysis [15]. *J. Am. Chem. Soc. 122*, 12023–12024.

(33) Kushnirov, V. V., Dergalev, A. A., and Alexandrov, A. I. (2020) Proteinase K resistant cores of prions and amyloids. *Prion 14*, 11–19.

(34) Dogra, P., Roy, S. S., Joshi, A., and Mukhopadhyay, S. (2020) Hofmeister Ions Modulate the Autocatalytic Amyloidogenesis of an Intrinsically Disordered Functional Amyloid Domain via Unusual Biphasic Kinetics. *J. Mol. Biol. 432*, 6173–6186.

(35) Sarkar, S., and Mondal, J. (2021) Mechanistic Insights on ATP's Role as a Hydrotrope. *J. Phys. Chem. B 125*, 7717–7731.

(36) Nishizawa, M., Walinda, E., Morimoto, D., Kohn, B., Scheler, U., Shirakawa, M., and Sugase, K. (2021) Effects of Weak Nonspecific Interactions with ATP on Proteins. *J. Am. Chem. Soc. 143*, 11982–11993.

(37) Panel, M., Ghaleh, B., and Morin, D. (2018) Mitochondria and aging: A role for the mitochondrial transition pore? *Aging Cell 17*, 1–15.

(38) Dasari, A. K. R., Hughes, R. M., Wi, S., Hung, I., Gan, Z., Kelly, J. W., and Lim, K. H. (2019) Transthyretin Aggregation Pathway toward the Formation of Distinct Cytotoxic

Oligomers. *Sci. Rep. 9*, 1–10.
(39) Wiglenda, T., Groenke, N., Hoffmann, W., Manz, C., Diez, L., Buntru, A., Brusendorf, L., Neuendorf, N., Schnoegl, S., Haenig, C., Schmieder, P., Pagel, K., and Wanker, E. E. (2020) Sclerotiorin Stabilizes the Assembly of Nonfibrillar Abeta42 Oligomers with Low Toxicity , Seeding Activity , and Beta-sheet Content. *J. Mol. Biol. 432*, 2080–2098.
(40) Cascella, R., Chen, S. W., Bigi, A., Camino, J. D., Xu, C. K., Dobson, C. M., Chiti, F., Cremades, N., and Cecchi, C. (2021) The release of toxic oligomers from α-synuclein fibrils induces dysfunction in neuronal cells. *Nat. Commun. 12*, 1–16.
(41) Narang, D., Swasthi, H. M., Mahapatra, S., and Mukhopadhyay, S. (2017) Site-Speci fi c Fluorescence Depolarization Kinetics Distinguishes the Amyloid Folds Responsible for Distinct Yeast Prion Strains.
(42) Sweeny, E. A., Desantis, M. E., and Shorter, J. (2011) Purification of Hsp104, a protein disaggregase. *J. Vis. Exp.* 2–9.
(43) Horcas, I., Fernández, R., Gómez-Rodríguez, J. M., Colchero, J., Gómez-Herrero, J., and Baro, A. M. (2007) WSXM: A software for scanning probe microscopy and a tool for nanotechnology. *Rev. Sci. Instrum. 78*.
(44) Schneider, C. A., Rasband, W. S., and Eliceiri, K. W. (2012) HISTORICAL commentary NIH Image to ImageJ : 25 years of image analysis. *Nat. Methods 9*, 671–675.
(45) Avni, A., Joshi, A., Walimbe, A., Pattanashetty, S. G., and Mukhopadhyay, S. (2022) Single-droplet surface-enhanced Raman scattering decodes the molecular determinants of liquid-liquid phase separation. *Nat. Commun. 13*, 1–13.

Optimum seed size generates amyloids that ensures uninterrupted seeding cycles of yeast prion amyloids

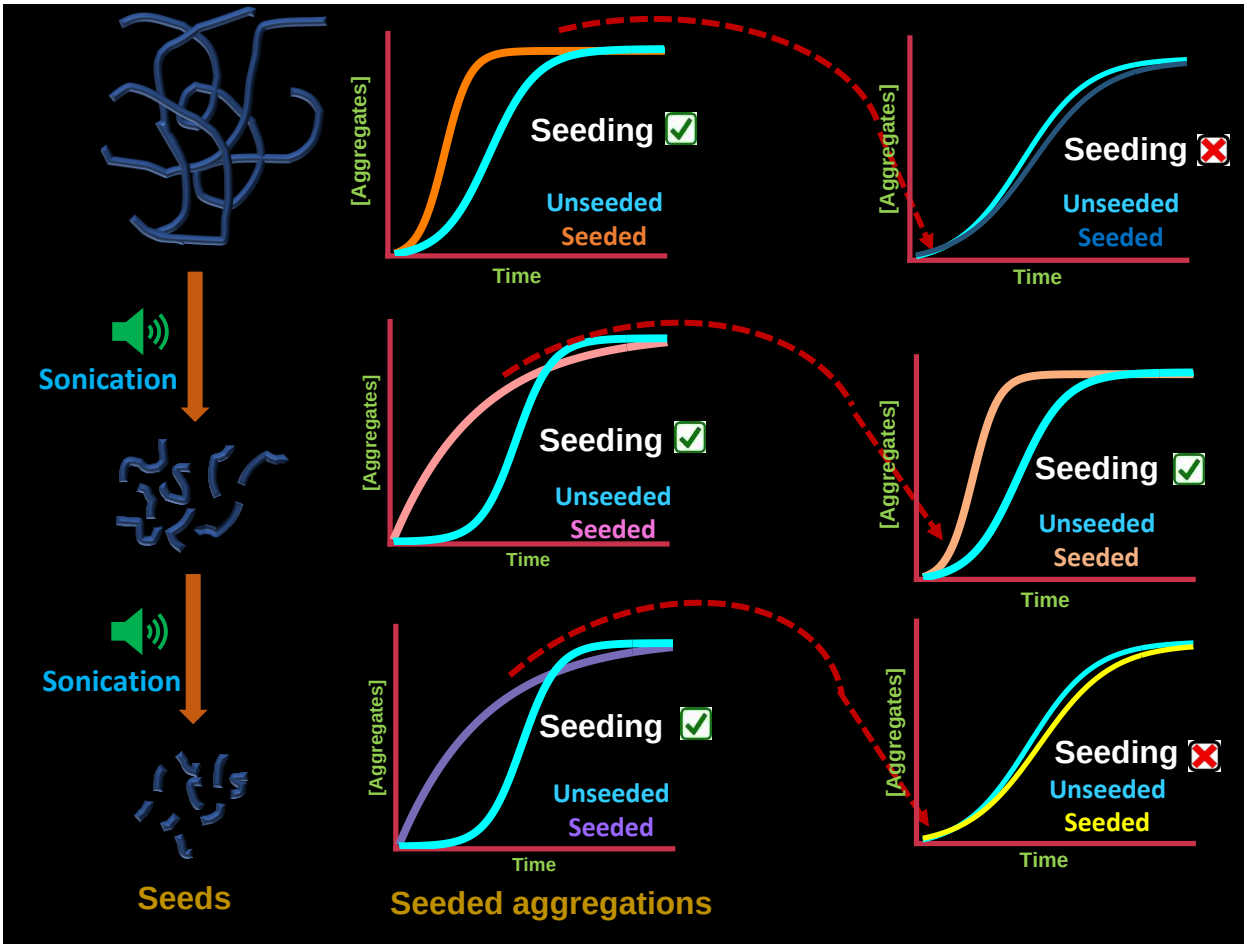

Reference: **Mahapatra, S.*,** Sarbahi, A., Avni, A., Mukhopadhyay, S*. (2023) Optimum seed size generates amyloids that ensures uninterrupted seeding cycles of yeast prion amyloids. *Co-corresponding authors. *(Manuscript in preparation)*

5.1 Introduction

Amyloids are β-sheet rich proteinaceous assemblies that arise from misfolded or unfolded proteins associated with various pathological and functional consequences[1,2]. Prions are the sub-class of amyloids that show self-propagating behaviour[3]. Mounting evidence of prion-like attributes exhibited by several non-prion amyloids pinpoints this mechanism as the consensus mechanism of transmission across the amyloidogenic proteins[4,5,6,7]. Central to the prion-like propagation is the nucleated formation of amyloids and their fragmentation to create highly transmissible lower molecular weight species for the next rounds of self-replication[8,9]. Inheritance of preformed amyloid particles, popularly known as seeds, is pivotal for the continued transmission of amyloids. A seminal kinetic investigation on seeded aggregations revealed that the presence of seeds during aggregation increases the rate of amyloid formation, which is otherwise a slow process. The extent of seeding depends on the size or molecular weight of the seeds. Higher molecular weight seeds, such as fibrils, has limited capability to accelerate fresh aggregation reactions. Whereas the lower molecular weight seeds exhibit greater seeding potential due to having a greater number of growth-competent ends for recruiting monomers in seeded aggregations. Moreover, higher order aggregates such as fibrils demonstrate limited permeability through lipid bilayers compared to lower order aggregates[10]. Therefore, it is critical to generate lower-order seeds of optimal molecular weight, which is suitable for accelerating seeded aggregation in prion-like propagation.

From unicellular bacteria to multicellular mammals, cells have chaperone machinery called disaggregases that depolymerize the amyloids with the help of the energy provided by ATP hydrolysis[11,12,13]. Sem inal *in vivo* and *in vitro* studies using *Saccharomyces cerevisiae* prion Sup35 as a model amyloid-forming proteins, the concentration-dependent role of yeast disaggregase Hsp104 in prion propagation has been elucidated. Intriguingly, at very high concentrations, Hsp104 may extensively disaggregate amyloids yielding very low molecular weight non-self-templating entities. On the other hand, genetic or chemical inactivation of Hsp104 in yeasts impairs the prion spread, as revealed by the phenotypic assay due to hindered seed genesis upon fibril fragmentation[14,15,16,17]. Thus, disaggregases are vital to generating seeds of a particular molecular weight or size critical to accelerating a fresh aggregation reaction.

Successful cross-generational inheritance of amyloids relies on uninterrupted seeding cascades for successive generations. Apart from the kinetic comparison between the seeded and *de novo* aggregation, the characterization of the amyloids generated in seeded aggregations in terms of their ability to accelerate the next rounds of the seeding cycle has remained elusive. In this work, we performed *in vitro* sequential seeding with amyloids generated from the seeded aggregation of the prion determinant of *Saccharomyces cerevisiae* Sup35 (Sup35NM), in the presence of seeds of different sizes. We observed an intriguing variation in the seeding capability of the amyloids generated in seeded aggregations, depending on the size of the seeds used during polymerization. Our results unveiled the importance of seed size in prion-like amyloid transmission

5.2 Experimental procedures

5.2.1 Materials

Sodium phosphate dibasic dihydrate, magnesium chloride hexahydrate, Thioflavin-T (ThT), adenosine-5'-triphosphate disodium salt hydrate (ATP), dimethyl sulfoxide (DMSO), guanidinium hydrochloride (GdmCl), β-mercaptoethanol and HEPES [4-(2-hydroxyethyl)-1-piperazineethanesulfonic acid] were procured from Sigma (St. Louis, MO, USA). Urea was bought from Amresco. Sodium dodecyl sulfate (SDS), imidazole, ammonium sulfate, potassium chloride, and ethylenediaminetetraacetic acid (EDTA) were purchased from HIMEDIA. Sodium hydroxide, potassium hydroxide, glycerol, methanol and sodium chloride were bought from Merck. Antibiotics (ampicillin and chloramphenicol) and Isopropyl-β-thiogalactopyranoside (IPTG) were procured from Gold Biocom (USA). Q-sepharose and Ni-NTA columns were bought from GE Healthcare Lifesciences, USA.

5.2.2 Expression and purification of Sup35NM

The detailed protocol is described in chapter 2 of this thesis (Page 32).

5.2.3 Amyloid aggregation reactions

Methanol-precipitated NM was first dissolved in 8 M urea (20 mM Tris-HCl buffer, pH 7.4) for 3 h at RT to set up aggregation reactions. Monomeric NM was then passed through a 100 kDa filter to remove any preexisting aggregates if present, and subsequently, the filtrate was concentrated using a 3 kDa filter. The concentrated monomers of NM were further centrifuged at 13,000 rpm for 15 min at RT, after which the supernatant was added such that its final concentration was 2.5 μM in assembly buffer (40 mM HEPES–KOH pH 7.4, 150 mM KCl, 20

mM $MgCl_2$, 1 mM DTT, 10 μM ThT) at RT under stirring at 80 rpm using magnetic beads. ThT fluorescence was monitored RT by exciting at 450 nm, and the fluorescence emission was recorded at 480 nm.

5.2.4 Seeded aggregation reactions

NM seeds were generated by incubating monomerized NM (2.5 μM) protein in assembly buffer (40 mM HEPES–KOH pH 7.4, 150 mM KCl, 20 mM $MgCl_2$, 1 mM DTT) at RT under stirring at 80 rpm using magnetic beads. On saturation, the resulting mature NM fibrils were introduced as it is or were sonicated either for 1 min or for 2 min before adding them to fresh aggregation reactions of NM monomers (2.5 μM) in a 10% (w/w) ratio in assembly buffer. The seeded aggregation reactions were kept at RT under stirring at 80 rpm using magnetic beads, and the ThT fluorescence was recorded with time. Alternatively, the NM amyloids generated in the above-mentioned seeded aggregation reactions (2^{nd} generation) were further introduced in the fresh aggregation reactions of NM in the assembly buffer, and ThT fluorescence was monitored.

5.2.5 Sedimentation assay

2.5 μM monomeric NM was aggregated in the assembly buffer (40 mM HEPES-KOH pH 7.4, 150 mM KCl, 1 mM DTT, 20 mM $MgCl_2$) at room temperature with stirring at 80 rpm. Next, amyloid species were pelleted before and after sonication of NM amyloids at 16,400 rpm for 30 min. These pellets were resuspended in 8 M urea (20 mM Tris-HCl pH 7.4) and incubated overnight to monomerize the amyloids. SDS-PAGE was performed, and band intensities were estimated using ImageJ software[18]. Also, monomeric NM (2.5 μM) was aggregated in the absence or presence of intact or sonicated NM fibrils in the assembly buffer (40 mM HEPES-KOH pH 7.4, 150 mM KCl, 1 mM DTT, 20 mM $MgCl_2$) at room temperature with stirring at 80 rpm. Later, upon saturation, we pelleted amyloid species at 16,400 rpm for 30 min. These pellets were resuspended in 8 M urea (20 mM Tris-HCl pH 7.4) and incubated overnight to monomerize the amyloids, followed by SDS-PAGE analysis.

5.2.6 Raman spectroscopy

NM monomers were aggregated in assembly buffer (40 mM HEPES-KOH pH 7.4, 150 mM KCl, 1 mM DTT, 20 mM $MgCl_2$) in the absence or the presence of intact NM fibrils or sonicated NM fibrils (both for 1 min or 2 min) at room temperature with stirring at 80 rpm for 6 h. Next, the amyloid species were pelleted after 6 h at 16,400 rpm for 30 min and resuspended

in 5 mM Na_2PO_4, 150 mM NaCl pH 7.4 buffer. Three µL of the pelleted sample was deposited onto a glass slide covered with aluminum foil and dried under a gentle stream of nitrogen gas. This step was repeated thrice. The sample was focused on using a 50x objective lens (Nikon, Japan). A NIR laser, 785 nm with an exposure time of 10 sec and 250 mW laser power, was used to excite the samples. All the spectra were averaged over 20 scans. Rayleigh scattered light was removed using an edge filter, while the Raman scattered light was dispersed using a 1200 lines/mm diffraction grating and was further detected using an air-cooled CCD detector. Wire 3.4 software provided with the instrument was used for data acquisition, and the recorded Raman spectra were baseline corrected using the cubic spline interpolation method and smoothened in the same software. Spectra were finally plotted using Origin

5.2.8 Statistical analysis

All the experiments were performed three times, and the data are represented as mean ± SD indicated by scattered data points from independent experimental replicates. The statistical significance analysis was performed using one-way ANOVA tests, and the *p*-values were indicated in the figure legends. All the data analysis, data fitting (adjusted $R^2 > 0.95$), and data plotting were performed with the help of Origin.

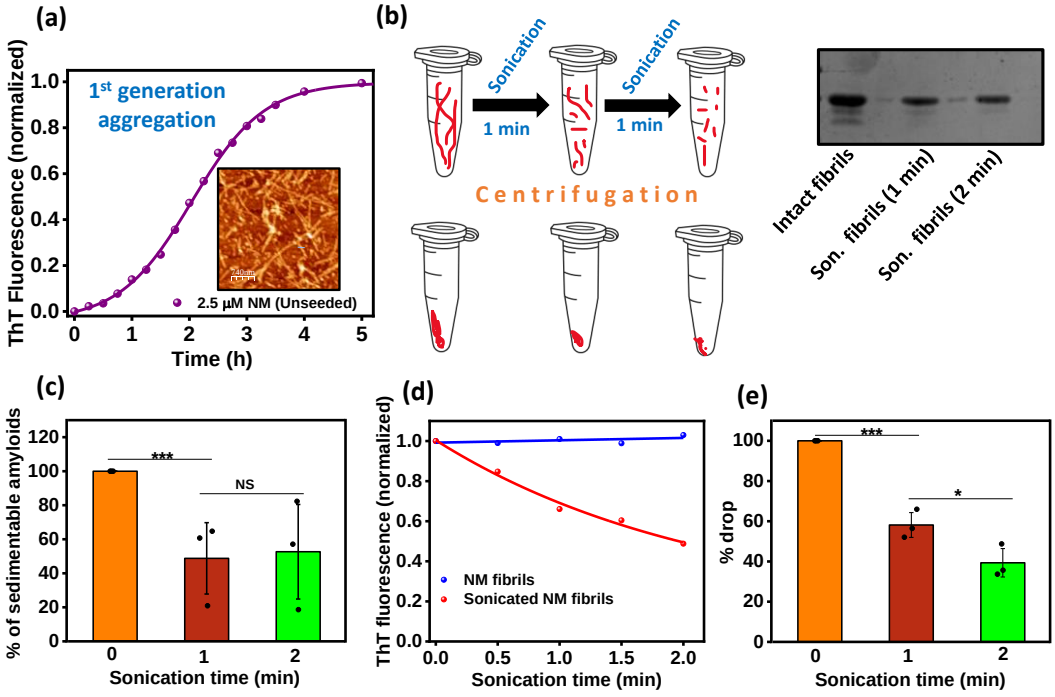

Figure 5.1. (a) Normalized ThT fluorescence kinetics of rotated (80 rpm) NM (2.5 µM) aggregation at room temperature showing the fibrils formed in atomic force microscope (inset). (b) Sedimentation of intact or sonicated (1 min or 2 min) NM fibrils at 16,400 rpm for 30 min. The retrieved pellets were monomerized by 8 M urea (20 mM Tris-HCl pH 7.4) before SDS-PAGE analysis. (c) The relative quantification by ImageJ software of NM monomers retrieved from the sonicated or intact fibrils. (d)

Representative disaggregation kinetics using the ultrasonic sound pulse of amplitude 5 for several pulses of 30 s and the drop in the ThT fluorescence was recorded after each pulse. The ThT fluorescence intensities were normalized with respect to the initial ThT fluorescence intensity. (e) The extent of disaggregation at 80 rpm was estimated from three experimental replicates to calculate the SD (n = 3).

5.3 Results

We aggregated 2.5 μM of NM at room temperature that followed a typical nucleation polymerization pathway with a lag time of ~55 min[19]. The progress of the aggregation reaction was monitored by the increase in the fluorescence intensity of an amyloid-marker dye Thioflavin-T (ThT) in amyloid-rich environments[20]. To visualize the nanoscale

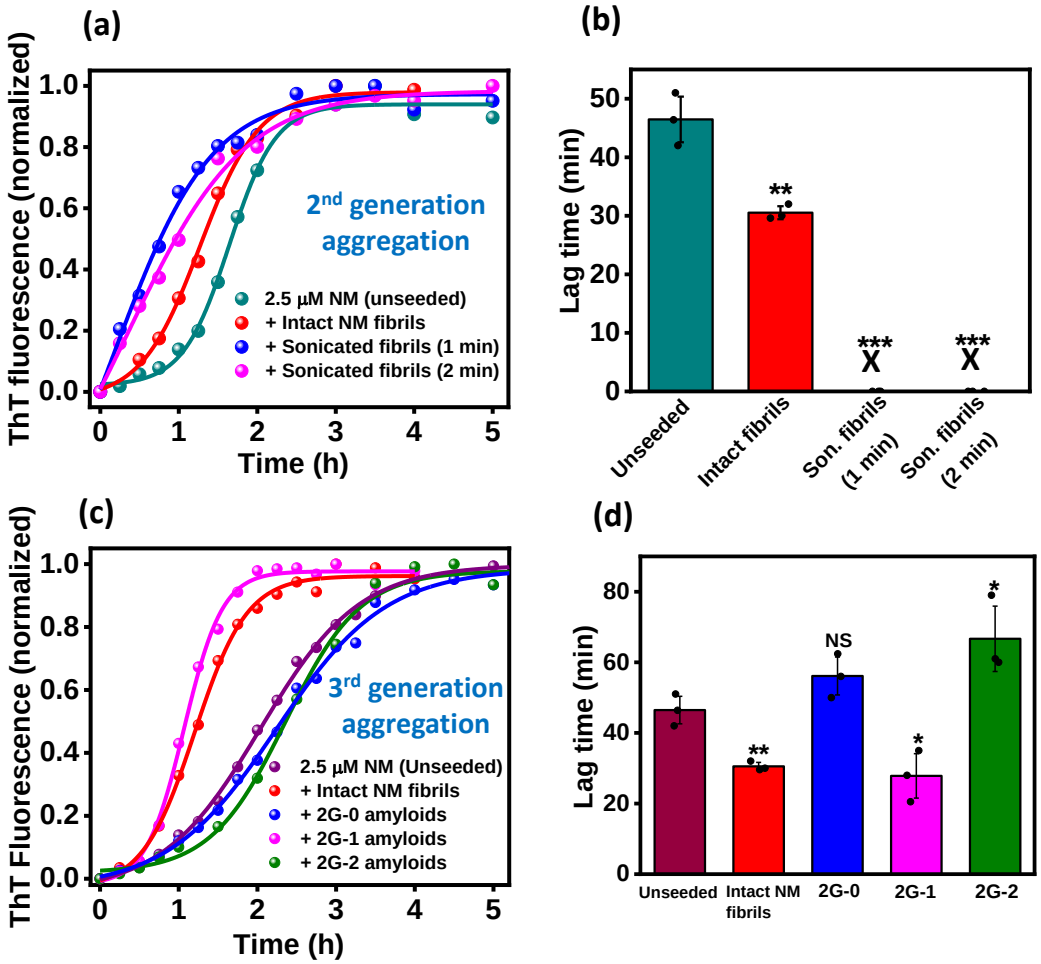

Figure 5.2. (a) Normalized ThT fluorescence kinetics of rotated (80 rpm) NM (2.5 μM) aggregation without or with intact NM fibrils, fibrils sonicated for 1 min or 2 min. (b) The lag times of the same were retrieved from three independent experimental replicates (n = 3), $**p < 0.01$, $***p < 0.001$, and $***p < 0.001$, respectively, compared to the unseeded NM aggregation. (One-way ANOVA). (c) Normalized ThT fluorescence kinetics of rotated (80 rpm) NM (2.5 μM) aggregation without or with intact NM fibrils, 2G-0, 2G-1, and 2G-2 amyloids. 2G-1 amyloids represent the amyloids formed during 2nd generation aggregation (2G) that were seeded with NM fibrils sonicated for 1 min. 2G-0 and 2G-2 amyloids represent amyloids formed from aggregations with intact and 2 min sonicated fibrils, respectively. (d) The lag times were retrieved from three independent experimental replicates (n = 3),

$**p < 0.01$, NS, $*p < 0.05$, and $*p < 0.05$, respectively, compared to the NM-only aggregation. (One-way ANOVA).

morphology of amyloids yielded in the saturation phase of aggregation, we performed atomic force microscopy and observed long fibrils of NM (Figure 5.1a). Next, to create seeds of different sizes, we sonicated these fibrils for 1 min or 2 min, which is reported to fragment amyloids as reported by us and others. To confirm that sonication indeed reduced the size of seeds, we sedimented sonicated fibrils after each sonication cycle of 1 min and monomerized the pellet using a denaturant. We observed a drastic drop in the fraction of pelletable amyloids upon sonication in SDS-PAGE, suggesting an increase in the fraction of lower molecular weight species resulting from fibrils (Figure 5.1b,c). However, we could not detect much change in the species profile in terms of their ability to get sedimented between fibrils sonicated for 1 min or 2 min. Therefore, as an indicator of amyloid fragmentation, we monitored the drop in ThT fluorescence after each ultrasonic pulse of 30 sec. The drop in ThT fluorescence is a convenient marker for *in vitro* NM disaggregation, as reported by us and other groups using disaggregase Hsp104 or chemical chaperone ATP as disaggregating agents[21]. As anticipated, there was a drastic drop in ThT fluorescence after 1 min of sonication, indicating fragmentation. Furthermore, ThT intensity dropped after one more minute of sonication, indicating further fragmentation. Taken together, this set of results points to the formation of seeds of varying sizes by consecutive sonication for the subsequent seeding reactions (Figure 5.1d,e).

In a cellular scenario, the rate of *de novo* amyloid formation is very slow unless cells inherit preformed seeds from preceding generations of yeast. Therefore, self-templated conformational conversion to amyloids is critical for continued prion propagation in daughter yeast cells. To determine the seeding efficiency of intact and sonicated fibrils, we introduced these particles to the fresh aggregation of NM. All kinds of amyloids, irrespective of their size, accelerated amyloid formation in the second generation. However, upon a careful comparison between the lag times of seeded and *de novo* aggregations, we found that the seeding efficiency of sonicated seeds was greater than the intact fibrillar seeds, regardless of the extent of sonication. Sonicated fibrils as seeds completely bypassed the lag phase of aggregation, possibly due to having plenty of polymerizing ends as opposed to fibrils that possess limited ends for further polymerization (Figure 5.2a,b). Altogether, this set of data indicates the fact that seeds of varied sizes were capable of promoting the genesis of amyloids with their differential seeding efficiency. However, the cascade of seeded amplification of amyloids should continue for successive generations where the N^{th} generation of aggregation should be

efficiently promoted by the amyloids formed in (N-1)th generation.

To decipher the role of amyloids generated in the second-generation aggregation in the next self-templating cycle, we set up aggregations with the amyloids aliquoted from saturated seeded aggregation as seeds. As a control for seeding, we used the intact fibrillar seeds derived from unseeded aggregation reactions. However, not all the particles from the second-generation aggregation displayed seeding behavior. Intriguingly, except for amyloids formed from the aggregation seeded with 1 min sonicated fibrils, other seeds failed to produce seeding-competent amyloids for third-generation aggregation (Figure 5.2c,d). We hypothesized that in seeded aggregations, there could be a substantial drop in the amount of amyloids compared to

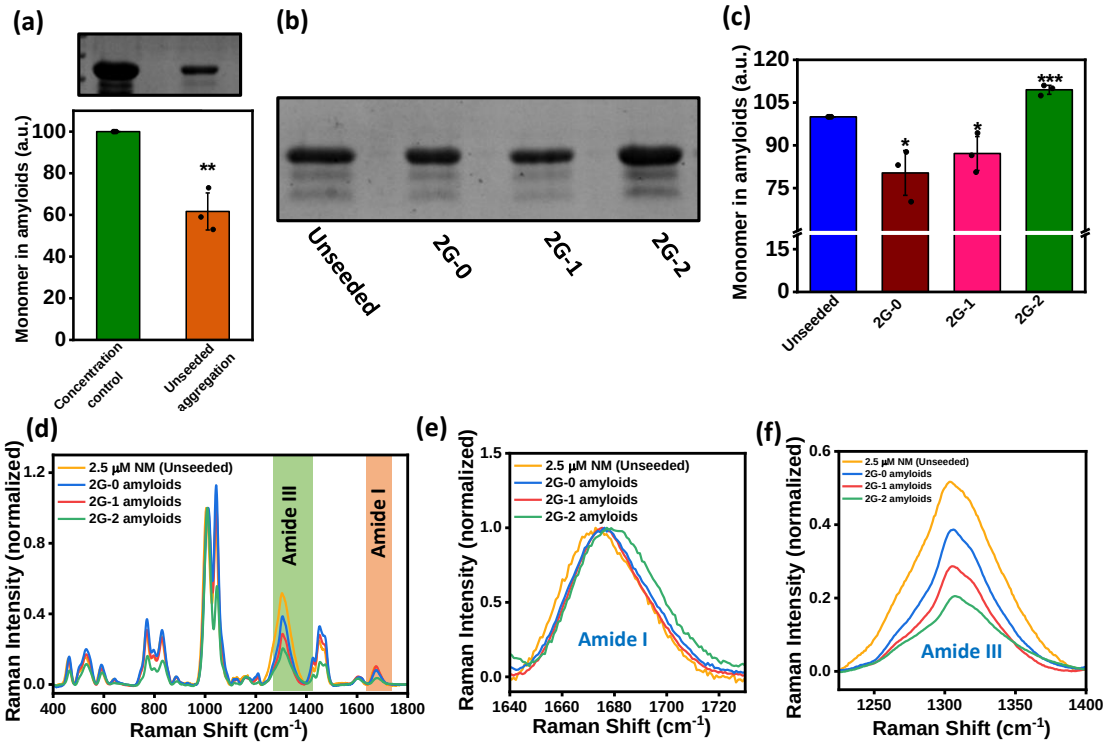

Figure 5.3. (a) The relative quantification by ImageJ software of NM monomers retrieved from the amyloids formed from the rotated (80 rpm) unseeded polymerization of NM (2.5 μM) with respect to the concentration control in SDS-PAGE. SDs were estimated from three independent replicates (n = 3), ∗∗p < 0.01 compared to concentration control (One-way ANOVA). (b) The relative quantification by ImageJ software of NM monomers retrieved from the amyloids formed from the rotated (80 rpm) unseeded polymerization of NM (2.5 μM) or seeded polymerization of NM with 10% (w/w) second-generation amyloids (2G-0, 2G-1, 2G-2). (c) Relative band intensities in SDS-PAGE corresponding to Figure 5.2b are shown. SDs were estimated from three independent replicates (n = 3), ∗p < 0.05, ∗p < 0.05, and ∗∗∗p < 0.001 for 2G-0, 2G-1, and 2G-2 amyloids, respectively, compared to unseeded aggregation (One-way ANOVA).

the *de novo* aggregation. Therefore, due to the drastic reduction in the fraction of amyloids in seed aliquots, amyloids derived during seeding with intact fibrils or 2 min sonicated fibrils could not show seeding potential. To test this hypothesis, as a prelude, we estimated that 60 %

of the monomers were recruited to form pelletable amyloids in *de novo* aggregation (Figure 5.3a). The rest of the monomers probably remained unrecruited or formed soluble lower-order aggregates and co-existed in equilibrium with the higher-order amyloids, such as fibrils, in saturated aggregation reactions. To probe the compositional change in the amount of pelletable amyloids over soluble particles, we sedimented saturated seeded reactions aggregated with different sizes of seeds. However, even the pellet corresponding to the seed aliquots that did not demonstrate seeding ability in the third generation consisted of sedimentable amyloids (Figure 5.3b). These results pointed out that the reduction in the amyloid amount in seeded aggregations via certain seeds may not be the reason for their seeding inefficiency in the subsequent generation. Therefore, we speculated that there must be a conformational difference in amyloids generated in seeded aggregation with respect to amyloids of unseeded aggregations. Despite having a generic β-sheet rich structure in all amyloids, there could be nanoscale variations in the amyloid architecture that may alter its properties, such as seeding efficiency. Several studies that include our work on binding partner induced conformational change in the NM amyloids suggests a link between amyloid conformational and their seeding efficiency. Therefore, we speculated that the seeding competent conformation of *de novo* amyloids is not exactly replicating during seeded polymerization where these amyloids were used as seeds. The generation-wise conformational variation of amyloids might translate into dissimilar seeding ability in the subsequent seeding cycles. We employed vibrational Raman spectroscopy to discern the conformational characteristics of amyloids, such as secondary structure elements. Raman spectroscopy has been widely used to distinguish between amyloid conformers for various amyloids, including the ATP-concentration-dependent conformational diversity of NM amyloids that we reported in the previous chapter. However, the similar spectra in amide I and amide III for all the amyloids formed in the unseeded and seeded aggregation indicated no conformational difference despite having dissimilar seeding efficiency (Figure 5.3d-f). Upon careful densiometric analysis of monomeric bands derived from pellets of *de novo* and seeded aggregations suggested a compositional change in amyloids resulted from seeded reactions. We noticed a drop in sedimentable amyloid fraction in the case of seeded aggregations with intact or 1 min sonicated fibrils. On the other hand, in the case of 2 min sonicated fibrils as seeds, the aggregation yielded amyloids that gave rise to more intense monomeric bands upon denaturation of pelleted amyloids. This indicated an increase in the supramolecular weight of amyloids that resulted from this aggregation reaction (Figure 5.3c).

5.4 Discussion

The size of the seeds is thought to be critical as it controls their transmissibility and number of growth-competent ends[22,10]. In this study, we were able to conjecture one more critical aspect of seeds that determines the seeding abilities of amyloids generated from them via seeded aggregation. The variation in seeding capability varied with the size of the seeds used during polymerization. Neither the intact, unsonicated fibrils nor the extensively sonicated fibrils that were sonicated for 2 min gave rise to seeding competent amyloids for the subsequent generation. However, only seeds created by sonication of fibrils for 1 min, generated amyloids in the saturated seeded reactions that displayed further seeding ability as represented in Figure 5.4. Conformational characterization of the amyloids by Raman unraveled that there were no significant structural changes in the amyloids formed in seeded assembly, regardless of the seeds used. Therefore, conformational alterations might not be the reason for the dissimilar seeding potential. However, upon a careful compositional comparison between amyloids

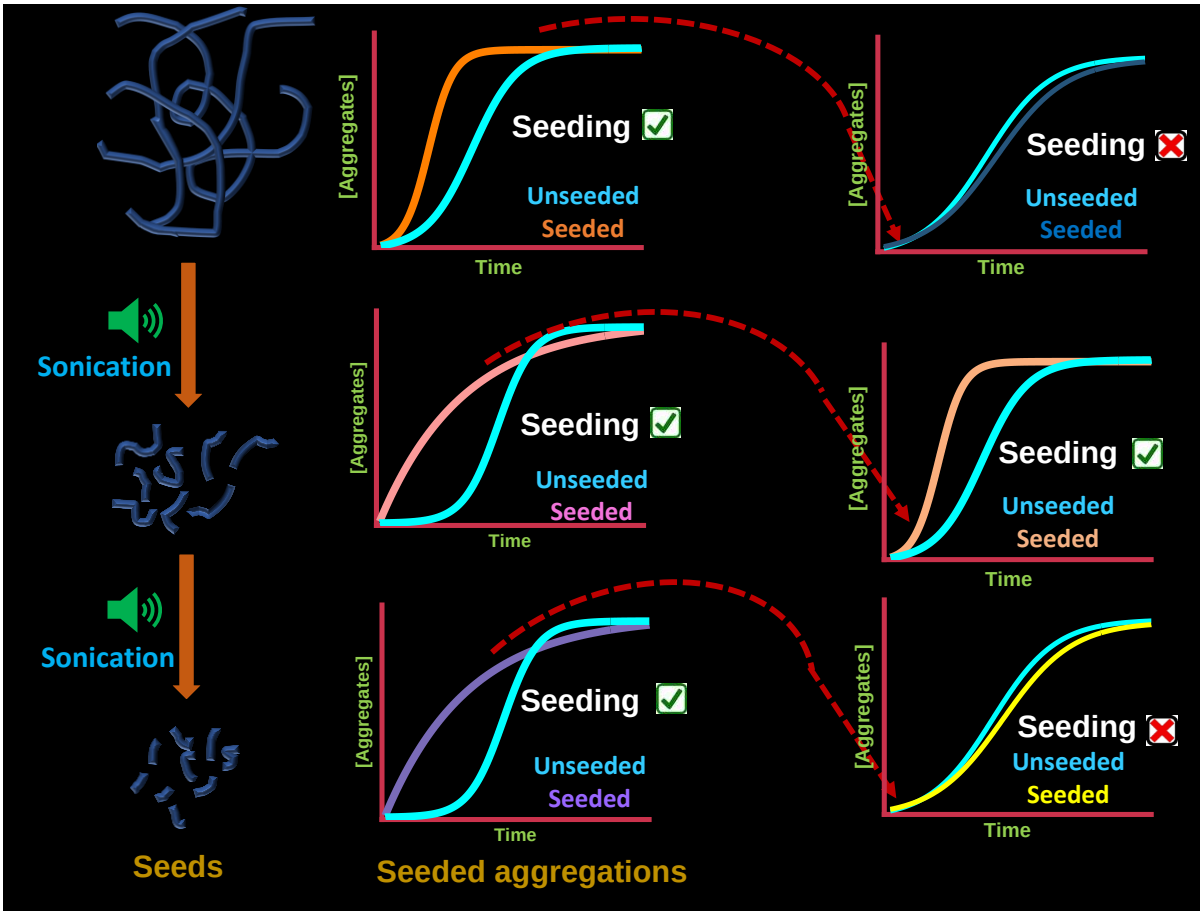

Figure 5.4. Model showing sequential seeding for three consecutive generations. Only amyloids generated in the presence of seeds of an optimum size exhibited seeding ability in the subsequent generation.

produced in *de novo* and seeded assembly, it was found that the species profile changes in seeded aggregation. These alterations were governed by the size of the seeds used during polymerization. There was a drop in the fraction of sedimentable amyloids after aggregation regulated by intact or 1 min sonicated fibrillar seeds. In contrast, there was an increase in the amount of sedimentable amyloids in the aggregation seeded by 2 min sonicated fibrils. However, how the species composition in the seed aliquots directs their seeding potential is not sufficiently clear to us and needs further attention. Nevertheless, the number and supramolecular weight of amyloids are inversely proportional. So, in the aggregation with 2 min sonicated seeds, we can speculate that the increase in the fraction of sedimentable amyloids resulted in a drop in the number of seeds that impaired further seeding.

Taken together, our results point to a protective mechanism in cells that create a barrier in the self-templated amplification of amyloids in successive seeding cycles by blocking sequential seeding. Except for the seeds of optimum size, other seeds failed to form seeding-competent amyloids and might disrupt the chain of seeding to impair [*PSI*$^{+}$] prion propagation. Although our observations were based on the amyloids formed from yeast prion Sup35, due to the generic nature of self-templated conformational conversion to amyloids of several amyloids, our results uncovered a consensus protective mechanism in cells for controlling amyloid transmission by introducing inert seeds in the seeding cascades.

5.5 References

(1) Greenwald, J., and Riek, R. (2010) Biology of amyloid: Structure, function, and regulation. *Structure 18*, 1244–1260.

(2) Otzen, D., and Riek, R. (2019) Functional amyloids. *Cold Spring Harb. Perspect. Biol. 11*.

(3) Si, K. (2015) Prions: What Are They Good For? *Annu. Rev. Cell Dev. Biol. 31*, 149–169.

(4) Brundin, P., Melki, R., and Kopito, R. (2010) Prion-like transmission of protein aggregates in neurodegenerative diseases. *Nat. Rev. Mol. Cell Biol. 11*, 301–307.

(5) Jucker, M., and Walker, L. C. (2018) Propagation and spread of pathogenic protein assemblies in neurodegenerative diseases. *Nat. Neurosci. 21*, 1341–1349.

(6) Costa, D. C. F., de Oliveira, G. A. P., Cino, E. A., Soares, I. N., Rangel, L. P., and Silva, J. L. (2016) Aggregation and prion-like properties of misfolded tumor suppressors: Is cancer a prion disease? *Cold Spring Harb. Perspect. Biol. 8*, 1–22.

(7) Heilbronner, G., Eisele, Y. S., Langer, F., Kaeser, S. A., Novotny, R., Nagarathinam, A., Åslund, A., Hammarström, P., Nilsson, K. P. R., and Jucker, M. (2013) Seeded strain-like transmission of β-amyloid morphotypes in APP transgenic mice. *EMBO Rep. 14*, 1017–1022.

(8) Brundin, P., and Melki, R. (2017) Prying into the prion hypothesis for parkinson's disease. *J. Neurosci. 37*, 9808–9818.

(9) Scheckel, C., and Aguzzi, A. (2018) Prions, prionoids and protein misfolding disorders. *Nat. Rev. Genet. 19*, 405–418.

(10) Marchante, R., Beal, D. M., Koloteva-Levine, N., Purton, T. J., Tuite, M. F., and Xue, W. F. (2017) The physical dimensions of amyloid aggregates control their infective potential as prion particles. *Elife 6*, 1–20.

(11) Klaips, C. L., Jayaraj, G. G., and Hartl, F. U. (2018) Pathways of cellular proteostasis in aging and disease. *J. Cell Biol. 217*, 51–63.

(12) Barnett, M. E., Zolkiewska, A., and Zolkiewski, M. (2000) Structure and activity of ClpB from Escherichia coli. Role of the amino- and carboxyl-terminal domains. *J. Biol. Chem. 275*, 37565–37571.

(13) Taguchi, Y. V., Gorenberg, E. L., Nagy, M., Thrasher, D., Fenton, W. A., Volpicelli-Daley, L., Horwich, A. L., and Chandra, S. S. (2019) Hsp110 mitigates α-synuclein pathology in vivo. *Proc. Natl. Acad. Sci. U. S. A. 116*, 24310–24316.

(14) Paushkin, S. V., Kushnirov, V. V., Smirnov, V. N., and Ter-Avanesyan, M. D. (1996) Propagation of the yeast prion-like [psi+] determinant is mediated by oligomerization of the SUP35-encoded polypeptide chain release factor. *EMBO J. 15*, 3127–3134.

(15) Shorter, J., and Lindquist, S. (2008) Hsp104, Hsp70 and Hsp40 interplay regulates formation, growth and elimination of Sup35 prions. *EMBO J. 27*, 2712–2724.

(16) Shorter, J., and Lindquist, S. (2004) Hsp104 catalyzes formation and elimination of self-replicating Sup35 prion conformers. *Science 304*, 1793–1797.

(17) Ness, F., Cox, B. S., Wongwigkarn, J., Naeimi, W. R., and Tuite, M. F. (2017) Over-expression of the molecular chaperone Hsp104 in Saccharomyces cerevisiae results in the malpartition of [PSI+] propagons. *Mol. Microbiol. 104*, 125–143.

(18) Schneider, C. A., Rasband, W. S., and Eliceiri, K. W. (2012) HISTORICAL commentary

NIH Image to ImageJ : 25 years of image analysis. *Nat. Methods 9*, 671–675.

(19) Adamcik, J., and Mezzenga, R. (2018) Amyloid Polymorphism in the Protein Folding and Aggregation Energy Landscape. *Angew. Chemie - Int. Ed. 57*, 8370–8382.

(20) Lakowicz, J. R. (2006) Principles of fluorescence spectroscopy. *Princ. Fluoresc. Spectrosc.*

(21) Desantis, M. E., and Shorter, J. (2012) Hsp104 drives "protein-only" positive selection of sup35 prion strains encoding strong [PSI+]. *Chem. Biol. 19*, 1400–1410.

(22) Xue, W., Hellewell, A. L., Hewitt, E. W., Radford, S. E., Hellewell, A. L., Hewitt, E. W., Radford, S. E., Xue, W., Hellewell, A. L., Hewitt, E. W., and Radford, S. E. (2010) When size matters *6896*.

Conclusions and future directions

The boundary between amyloids and prions is blurring with passing days, with mounting reports where classical non-prion amyloids show prion-like transmission. The prion-like transmission in amyloids is governed by the already-formed aggregates termed seeds. Seeds are considered the minimum unit of amyloid transmission in both pathological amyloids and amyloids connected with biological roles. There are several regulators in cells that govern the amount and ability of seeds during self-templating cycles. The regulation of prion-like propagation is dependent on two principal characteristics of amyloids. First, the fragility of amyloids by disaggregating factors that ensure the formation of adequate, highly transmissible lower-order amyloids as seeds for amyloid spread. Second, the efficiency of the seeds to accelerate fresh aggregation reactions, which is critical for autocatalytic amplification of amyloids. In this thesis, we tried to decipher the role of two molecular regulators of prion-like propagation that influence the properties of amyloids, such as fragility and seeding efficiency.

We used the yeast prion determinant of Saccharomyces cerevisiae prion Sup35 as the model amyloid-forming protein for our entire work. Our work on sub-stoichiometric disaggregase Hsp104 uncovered the previously unexplored role of Hsp104 in promoting amyloid formation but retarding their maturation into fibrils that exhibit limited transmissibility and seeding potential. In addition, we also reported a structural heterogeneity in Hsp104-created amyloids compared to the amyloids aggregated in their absence via an amalgamation of biochemical techniques and biophysical tools. Our results, primarily based on *in vitro* recapitulation, indicated the structural diversity in amyloids that are also reflected in their seeding potential. The Hsp104-created amyloids showed a greater seeding potential during amyloidogenesis. In the future, it will be interesting to explore the phenotypic outcome in red-white colony colour assay of this *in vitro* prepared sub-stoichiometric Hsp104-regulated conformers of Sup35NM amyloids via injecting them inside the prion-negative yeast cells. Moreover, due to the widespread presence of disaggregases in the proteome of bacteria to mammals, the dose-dependent remodeling by disaggregases can be extended to a host of proteins, especially the neuropathological amyloids, that may regulate several facets of their transmission and cytotoxicity. Discerning the role of critical co-chaperones in fine-tuning the substrate processing of disaggregases via liquid-liquid phase separation will be fascinating to study in the future, which remains largely unexplored currently.

In this thesis, efforts were made to understand the chemical chaperoning by ATP that is present in our cells in abundance. In previous studies on different proteins, the role of ATP in the formation of amyloids and the disassembly of existing aggregates were reported. Our study was a unique attempt to shed light on several amyloid-modulating effects on

aggregates formed from a single protein. As the formation of amyloids and the disaggregation of amyloids leading to the genesis of lower-order seeds are an integral part of the prion-like cascade of amyloid transmission, our results shed light on ATP as a small molecule regulator of amyloid transmission.Our dose-dependent studies uncovered the anti-propagation role of ATP in a wide range of concentrations relevant to cellular pathology and physiology either by enhancing the stability of amyloids (at high concentrations of ATP) or by giving rise to seeding incompetent amyloids (at low concentrations of ATP). The study can be extended further to other biologically relevant polyanions that could have an intriguing impact on prion-like propagation by involving in the process of amyloid making or amyloid braking. Deciphering the concentration-dependent role of ATP in controlling the phase behavior of the molecular chaperones during substrate processing will also be fascinating.

In this thesis, we also performed sequential seeding and unveiled the role of optimum seed size for continued consecutive prion propagation. We carried out the conformational and compositional profiling of amyloids generated in seeded aggregations compared to those formed in *de novo* aggregation. Our results suggested no conformational distinctness between *de novo*-formed aggregates and aggregates formed in seeded aggregation with different sizes of seeds. However, a variation in amyloid composition was observed depending on the size of the seeds used during aggregation. The change in the fraction of sedimentable amyloids in seeded aggregations controlled their ability to accelerate the next seeding cycles due to the inversely proportional relationship between the supramolecular weight of amyloids and their number. In the future, this study can be extended to the aggregation reactions that are controlled by other factors, such as molecular chaperones or small molecules. We can speculate that apart from modulating the *de novo* aggregation, the presence of these molecules can have interesting impacts on sequential seeding, which might govern prion-like transmission.

Taken together, in this thesis, we were able to dissect several facets of a molecular chaperone and a small chemical chaperone in determining the quality and quantity of seeds by forming amyloids or disassembling preformed aggregates. Moreover, our work unmasked the generation-wise change in the amyloid composition, having interesting impacts on their successive self-templated replication cycles. Our results contribute to understanding the fundamental mechanistic underpinning of the complex cascade of prion-like transmission across the amyloidogenic proteins.